U.S. Department
of Transportation

**Federal Railroad
Administration**
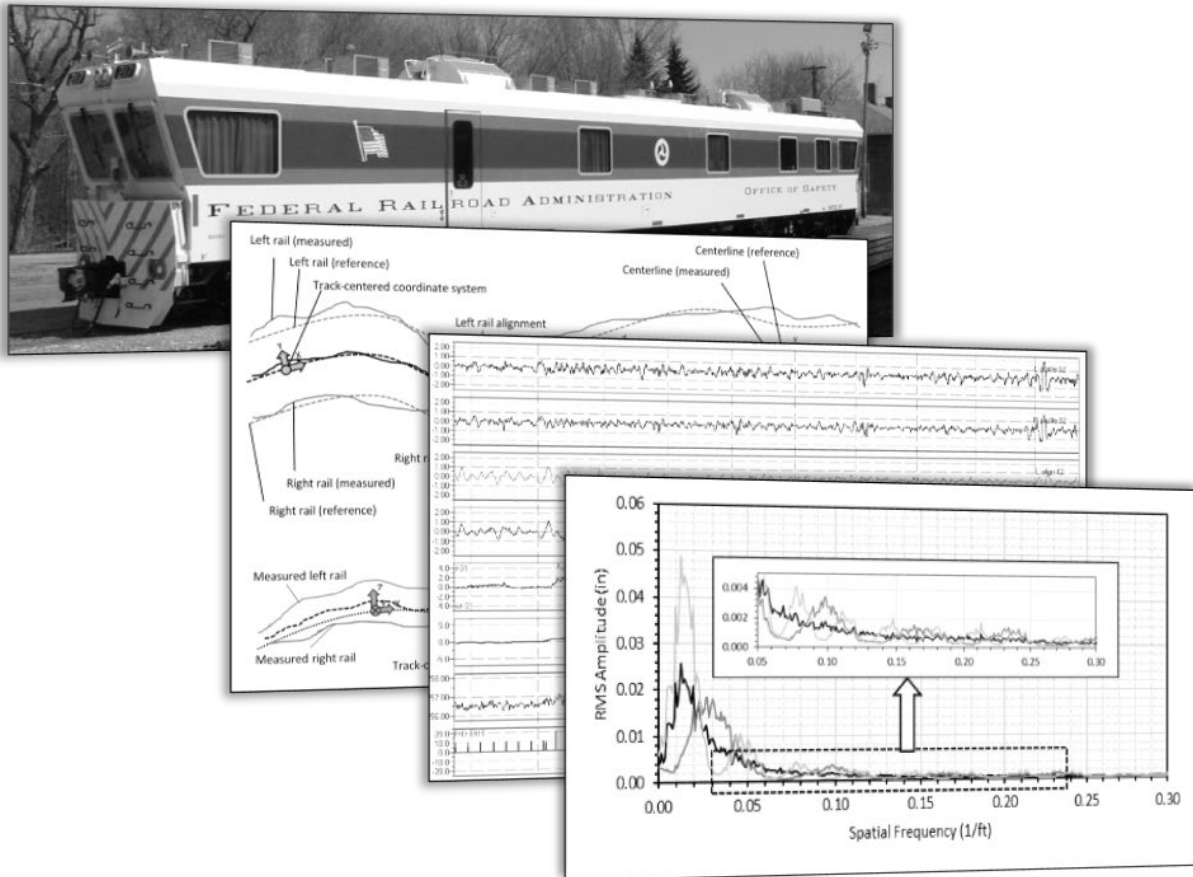
Office of Research,
Development and Technology
Washington, DC 20590

Measurement and Characterization of Track Geometry Data: Literature Review and Recommendations for Processing FRA ATIP Program Data

1. AGENCY USE ONLY (Leave blank)	2. REPORT DATE **March 2019**	3. REPORT TYPE AND DATES COVERED Technical Report, 10/2018 – 03/2019

4. TITLE AND SUBTITLE Measurement and Characterization of Track Geometry Data: Literature Review and Recommendations for Processing FRA ATIP Program Data	5. FUNDING NUMBERS
6. AUTHOR(S) Alexander Keylin: ORCID 0000-0003-2786-3992	Task Order 86

6. AUTHOR(S)
Alexander Keylin: ORCID 0000-0003-2786-3992

7. PERFORMING ORGANIZATION NAME(S) AND ADDRESS(ES) Transportation Technology Center, Inc. (TTCI) 55500 DOT Rd. Pueblo, CO 81001	8. PERFORMING ORGANIZATION REPORT NUMBER

9. SPONSORING/MONITORING AGENCY NAME(S) AND ADDRESS(ES) U.S. Department of Transportation Federal Railroad Administration Office of Railroad Policy and Development Office of Research, Development, and Technology (RD&T) Washington, DC 20590	10. SPONSORING/MONITORING AGENCY REPORT NUMBER DOT/FRA/ORD-23/21

11. SUPPLEMENTARY NOTES
COR: Ali Tajaddini

12a. DISTRIBUTION/AVAILABILITY STATEMENT This document is available to the public through the FRA web site.	12b. DISTRIBUTION CODE

13. ABSTRACT (Maximum 200 words)

From October 2018 to March 2019, the Federal Railroad Administration sponsored Transportation Technology Center, Inc. to conduct a literature review on the methods of measurement and characterization of track geometry. The goal of the review was to summarize the current state of track geometry measurement and to provide recommendations on methods for processing and characterizing track geometry data collected under FRA's Automated Track Inspection Program.

14. SUBJECT TERMS Track geometry, track quality, track irregularities, space curve, Track Quality Index, TQI, Track Geometry Measurement System, TGMS, Automated Track Inspection Program, ATIP, Power Spectral Density, PSD.	15. NUMBER OF PAGES 106
	16. PRICE CODE

17. SECURITY CLASSIFICATION OF REPORT Unclassified	18. SECURITY CLASSIFICATION OF THIS PAGE Unclassified	19. SECURITY CLASSIFICATION OF ABSTRACT Unclassified	20. LIMITATION OF ABSTRACT

METRIC/ENGLISH CONVERSION FACTORS

ENGLISH TO METRIC

LENGTH (APPROXIMATE)

1 inch (in)	=	2.5 centimeters (cm)
1 foot (ft)	=	30 centimeters (cm)
1 yard (yd)	=	0.9 meter (m)
1 mile (mi)	=	1.6 kilometers (km)

AREA (APPROXIMATE)

1 square inch (sq in, in^2)	=	6.5 square centimeters (cm^2)
1 square foot (sq ft, ft^2)	=	0.09 square meter (m^2)
1 square yard (sq yd, yd^2)	=	0.8 square meter (m^2)
1 square mile (sq mi, mi^2)	=	2.6 square kilometers (km^2)
1 acre = 0.4 hectare (he)	=	4,000 square meters (m^2)

MASS - WEIGHT (APPROXIMATE)

1 ounce (oz)	=	28 grams (gm)
1 pound (lb)	=	0.45 kilogram (kg)
1 short ton = 2,000 pounds (lb)	=	0.9 tonne (t)

VOLUME (APPROXIMATE)

1 teaspoon (tsp)	=	5 milliliters (ml)
1 tablespoon (tbsp)	=	15 milliliters (ml)
1 fluid ounce (fl oz)	=	30 milliliters (ml)
1 cup (c)	=	0.24 liter (l)
1 pint (pt)	=	0.47 liter (l)
1 quart (qt)	=	0.96 liter (l)
1 gallon (gal)	=	3.8 liters (l)
1 cubic foot (cu ft, ft^3)	=	0.03 cubic meter (m^3)
1 cubic yard (cu yd, yd^3)	=	0.76 cubic meter (m^3)

TEMPERATURE (EXACT)

$[(x-32)(5/9)]$ °F = y °C

METRIC TO ENGLISH

LENGTH (APPROXIMATE)

1 millimeter (mm)	=	0.04 inch (in)
1 centimeter (cm)	=	0.4 inch (in)
1 meter (m)	=	3.3 feet (ft)
1 meter (m)	=	1.1 yards (yd)
1 kilometer (km)	=	0.6 mile (mi)

AREA (APPROXIMATE)

1 square centimeter (cm^2)	=	0.16 square inch (sq in, in^2)
1 square meter (m^2)	=	1.2 square yards (sq yd, yd^2)
1 square kilometer (km^2)	=	0.4 square mile (sq mi, mi^2)
10,000 square meters (m^2)	=	1 hectare (ha) = 2.5 acres

MASS - WEIGHT (APPROXIMATE)

1 gram (gm)	=	0.036 ounce (oz)
1 kilogram (kg)	=	2.2 pounds (lb)
1 tonne (t)	=	1,000 kilograms (kg)
	=	1.1 short tons

VOLUME (APPROXIMATE)

1 milliliter (ml)	=	0.03 fluid ounce (fl oz)
1 liter (l)	=	2.1 pints (pt)
1 liter (l)	=	1.06 quarts (qt)
1 liter (l)	=	0.26 gallon (gal)
1 cubic meter (m^3)	=	36 cubic feet (cu ft, ft^3)
1 cubic meter (m^3)	=	1.3 cubic yards (cu yd, yd^3)

TEMPERATURE (EXACT)

$[(9/5) y + 32]$ °C = x °F

QUICK INCH - CENTIMETER LENGTH CONVERSION

Inches: 0 1 2 3 4 5

Centimeters: 0 1 2 3 4 5 6 7 8 9 10 11 12 13
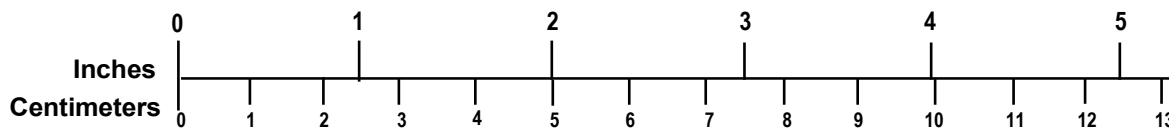
QUICK FAHRENHEIT - CELSIUS TEMPERATURE CONVERSIO

°F	-40°	-22°	-4°	14°	32°	50°	68°	86°	104°	122°	140°	158°	176°	194°	212°
°C	-40°	-30°	-20°	-10°	0°	10°	20°	30°	40°	50°	60°	70°	80°	90°	100°
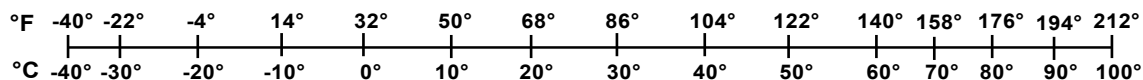
For more exact and or other conversion factors, see NIST Miscellaneous Publication 286, Units of Weights and Measures. Price $2.50 SD Catalog No. C13 10286

Updated 6/17/98

ii

Acknowledgements

Contents

Illustrations

Tables

Executive Summary

From October 2018 to March 2019, the Federal Railroad Administration (FRA) sponsored Transportation Technology Center, Inc. (TTCI) to conduct a literature review on the methods of measurement and characterization of track geometry. The goal of the review was to summarize the current state of track geometry measurement and to provide recommendations on methods for processing and characterizing track geometry data collected under FRA's Automated Track Inspection Program (ATIP).

The key findings of the literature review are summarized below.

1. Railroads around the world use many different methods to process and characterize track geometry data. Even within Western Europe, where operators generally follow Euronorms and Technical Specifications for Interoperability (TSI), there are significant differences between countries and rail operators.

2. Track geometry data can be represented in two broad forms: distance domain (i.e., using time histories of track irregularities as functions of the distance along the track) and frequency or wavelength domain (i.e., amplitude and phase or power spectral density of track irregularities as functions of signal wavelengths). Distance domain is the format used to assess track compliance with safety and quality norms. The majority of methods described in the literature are applicable to the distance domain.

3. Some flexibility is required for analyzing track geometry data from various track classes. In particular, filters with different cutoff frequencies may need to be used to process data from different classes of track.

4. Although experts have proposed or are using several alternative methods for track geometry characterization, the most common methods by far are those which extract simple statistical features from track geometry variables (e.g., alignment, cross level, etc.). These methods are *maximum values* and *standard deviations*. Railroad agencies/companies use maximum values to assess the safety of operations and use standard deviations to assess the overall track quality and to prioritize track maintenance.

5. Alternative methods of track geometry characterization are not conclusively proven to be superior to standard deviation-based statistics in terms of predicting the response of rail vehicles to track geometry. Different studies on the topic give conflicting or inconclusive results.

6. For track geometry analysis, track data should preferably be segmented based on track layout, special trackwork, and other features. For agencies using constant length segments, the most common length suggested is between 1/8 mile and 1/10 mile.

7. Track irregularities generally should not be assumed to be described by a stationary, random process. Thus, standard deviation values do not provide a definite description of track geometry condition and should not be relied upon to predict the number or severity of track class defects, even though there is a correlation between class defects and standard deviation values.

8. Characterization of track geometry in wavelength (i.e., frequency) domain is widely used to generalize about overall characteristics of track classes, railroad systems, etc. The most

widely used method of wavelength characterization is power spectral density (PSD) functions calculated with different varieties of Fast Fourier Transform (FFT) algorithms.

9. Studies show strong coherence between left and right rail alignment, as well as between left and right profile signals. However, mean alignment, mean profile, gauge, and cross level signals have low coherence (i.e., are relatively independent).

Overall, the most widely used methods for track geometry characterization are refined versions of methods which were used in an FRA-sponsored study of track geometry in the 1970s-1980s.

1. Introduction

1.1 Overview

Track geometry is the position of rails in horizontal and vertical planes. It includes design features (e.g., tangents, curves, transition curves, superelevation) as well as irregularities (i.e., defects).

Track geometry defects are the second-most common cause of derailments on Class I main line track in the United States (Liu, 2012). Accurate and timely measurement of track geometry is critical for maintaining the safety of rail transportation, as well as for passenger comfort and the prevention of damage to rolling stock and lading.

Track geometry measurement has evolved from relying on manual and visual methods, to early track geometry cars equipped with analog instrumentation and strip chart recorders, and finally to modern Track Geometry Measurement Systems (TGMS), which record a wide range of parameters and use advanced digital instrumentation (Figure 1).

Figure 1. FRA DOTX 217 Track Geometry Car (FRA, 2019)

Processing and characterizing track geometry measurement involves a series of complex steps and a variety of methods, some of which are widely used and some of which are experimental. The selection of the method depends on the goal of the processing (e.g., planning for maintenance, preparation of data for computer simulations, etc.) and the type of data available.

From October 2018 to March 2019, the Federal Railroad Administration (FRA) sponsored Transportation Technology Center, Inc. (TTCI) to conduct a literature review on the methods of measurement and characterization of track geometry.

1.2 Objectives and Scope

This report reviews the current state of track geometry measurement and characterization methods and provides an overview of:

- Basic definitions related to track geometry, including design elements and irregularities
- Causes of track irregularities and their effect on vehicle performance

- Various forms of track geometry, including absolute track geometry, space curve, chordal offsets, power spectral density (PSD) functions, and mathematical methods of transitioning between these forms

- Modern methods of track geometry measurement, including surveying, inertial and chord-based systems, and vehicle response measurement methods

- Methods of characterizing track irregularities, such as track quality indices

- Process of preparing track geometry measurement for use with multi-body dynamics simulations

The report concludes with recommendations for processing the track geometry data collected under FRA's Automated Track Inspection Program (ATIP).

1.3 Sources

The sources used in this literature review were identified using:

- The Transport Research International Documentation database by the Transportation Research Board of the United States National Academies of Sciences, Engineering, and Medicine

- Google Scholar search engine

- FRA's eLibrary system

- Association of American Railroads (AAR) internal report database

- TTCI's collection of technical literature

- Personal communication with researchers active in the field of track geometry and manufacturers and users of track geometry measurement systems

Many sources were identified through the literature reviews in these publications:

- (Haigermoser et al., 2015), (Karis, 2018), and (Lewis, 2011): comprehensive information on characterization of track geometry

- (Haigermoser et al., 2013): comparative assessment of track irregularity characterization methods

- (Nielsen et al., 2013), (Moskal and Pastucha, 2016), and (Lewis, 2011): information about methods of measurement of track geometry

- (Berawi, 2013): characterization of irregularities in the wavelength domain

- (Sadeghi, 2010) and (Liu et al., 2015): track quality indices

Readers looking for additional information about specific topics are encouraged to review these papers.

The following sources contain additional information on topics that are closely related but outside the scope of this document:

- (Nielsen et al., 2013): short-wavelength irregularities, such as rail corrugation

- (Berawi, 2013), (Soleimanmeigouni et al., 2018a and 2018b), (Higgins and Liu, 2018), (Elkhoury et al., 2018): track geometry degradation
- (Lindahl, 2001): design elements of track geometry

1.4   Organization of the Report

Section 2 describes the basics of track geometry, including terminology, track layout (i.e., design) elements, and different formats of recording track geometry data, including space curve, chordal offsets, and PSD data.

Section 3 provides a broad overview of the track geometry measurement and characterization process.

Section 4 describes the current state of TGMS.

Section 5 describes the initial steps in processing track geometry data, such as filtering and segmentation.

Section 6 describes various methods used to characterize track irregularities in distance domain, including standard deviations and track quality indices.

Section 7 describes methods to characterize track geometry in wavelength domain, such as PSD functions.

Section 8 outlines the steps necessary to prepare track geometry for use as input in multi-body dynamics simulations.

Section 9 summarizes the findings of the literature review.

Section 10 makes recommendations on the use of various characterization methods in the Track Geometry Characterization Study.

2. The Basics of Track Geometry

The term "track geometry" refers to both **track design (i.e., layout) elements** and **track irregularities** (i.e., deviations from design).

2.1 Track Geometry Design Elements

The design elements of **horizontal track geometry** are **tangents** (straight sections), **simple curves**, and **transition curves**. A layout of a simple curve is shown in Figure 2.
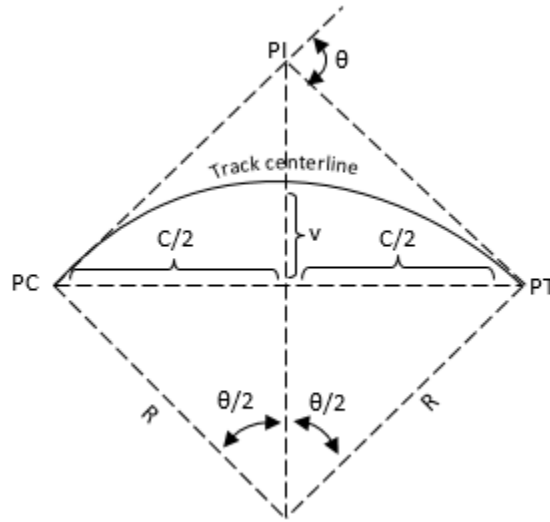
Figure 2. A simple curve

Track curvature usually is expressed in one of the four formats:

a. As a radius of curvature R – This form is rarely used in track geometry measurement systems because tangent track has infinitely large radius of curvature.

b. As an inverse of a radius of curvature $(1/R)$

c. As the magnitude of the arc angle subtended by a chord of a specified length (generally 100 feet or 20 meters), also known as degree of curvature – Note that this is different from the typical practice of highway engineering in North America, where the 100-foot figure refers to the arc length and not chord length.

The relationship between radius of curvature, chord length, and degree of curvature is described by the formula:

$$\sin\left(\frac{\theta}{2}\right) = \frac{C}{2} \tag{1}$$

where R is curve radius, θ is the arc angle in radians, and C is chord length. Using a small angle approximation, for a 100-foot chord the formula is simplified to:

$$R\ [\text{ft}] \cong \frac{100\ [\text{ft}] \times \frac{180}{\pi} [\frac{\text{degrees}}{\text{radian}}]}{\theta\ [\text{degrees}]} \cong \frac{5729.65\ [\text{ft}]}{\theta\ [\text{degrees}]} \tag{2}$$

6

d. As a **versine** measured at a middle point of a chord of a specified length, also known as a **mid-chord offset (MCO)**:

$$v = R - \sqrt{R^2 - \frac{C^2}{4}} = R\left(1 - \cos\frac{\theta}{2}\right) \tag{3}$$

where v is versine, R is curve radius, and C is chord length (all length dimensions in feet or meters; θ in radians).

By using the small angle approximation and combining Equations (1) and (3), the following relationship is obtained (Ciobanu, 2016):

$$v \cong \frac{C^2}{8R} \cong \frac{C\theta}{8} \tag{4}$$

If a 62-foot chord is used, mid-chord offset per one degree of curvature is close to 1 inch, i.e., a one-degree curve will have a MCO of 1 inch, a 2-degree curve will have a 2-inch MCO, etc. (Figure 3).
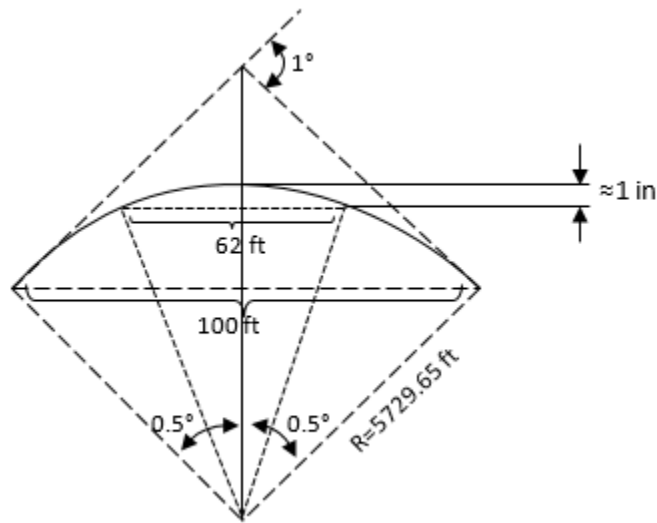
Figure 3. MCO measurement with a 62-foot chord

$$v_{62ft}[\text{in}] \cong \frac{C^2}{8R_{1^\circ}} \cong \frac{62^2\,[\text{ft}^2]}{\frac{1}{1[\text{deg}]}\times 8\times 100\,[\text{ft}]\times\frac{180}{\pi}\left[\frac{\text{deg}}{\text{rad}}\right]} \times 12\left[\frac{\text{in}}{\text{ft}}\right] = 1.006\ \text{in} \tag{5}$$

Transition curves, also called **easement curves** or **spirals**, are sections of track between tangents and simple curves (Figure 4). They are introduced to avoid abrupt changes of superelevation and centripetal acceleration when vehicles are transitioning between tangents and curves or between curves of different radii. Transition curves are sometimes omitted on low-speed track, in cases of shallow curves, in turnouts, on old rail lines, and in cases when space is limited due to terrain features or structures around the track route.

The most common type of transition curve in North America is a cubic parabola. In Western Europe, transition curves are often based on a clothoid, in which curvature changes linearly with respect to curve length.
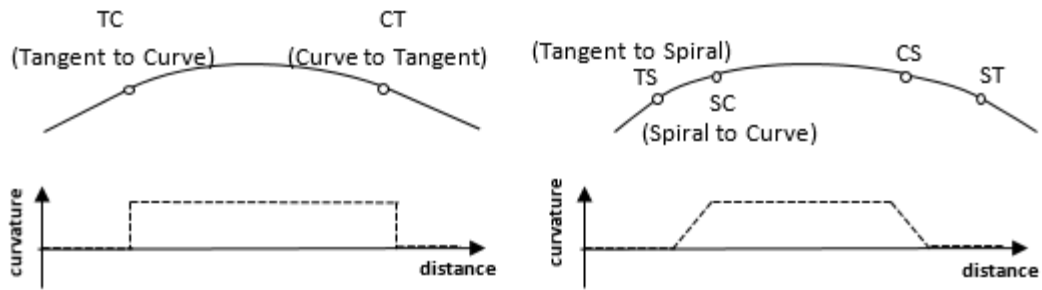
Figure 4. Curves without (left) and with (right) transition curves

Multicentered curves (Figure 5) are adjacent simple curves with either no tangent section or a short section of tangent track separating them. Transition curves may or may not be present. Compound curves (i.e., adjacent curves with the same sign of curvature), reverse curves (i.e., opposite signs) and broken back curves (i.e., curves in the same sign with a short tangent separating them) are special cases of multicentered curves (Hay, 1982).
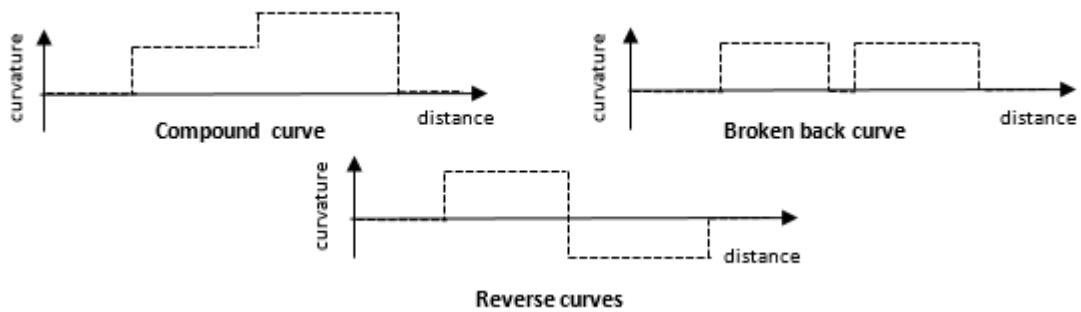
Figure 5. Multicentered curves

Vertical track geometry consists of constant grade sections and vertical curves, which are usually designed as quadratic parabolas. **Grade** is the change in elevation (i.e., rise) over horizontal distance (i.e., run), often closely approximated as rise over distance traveled. Grade is usually expressed as a percentage (% or ‰).

Track gauge (Figure 6) is the distance between the inner sides of rail heads measured at a certain height below the top of the rail (5/8-inch in North America, 14 mm in Europe). Standard gauge, which is used is most countries, is 56 1/2 inches, or 1435 mm. In tight curves, gauge may be intentionally made slightly wider than nominal to improve vehicle steering.
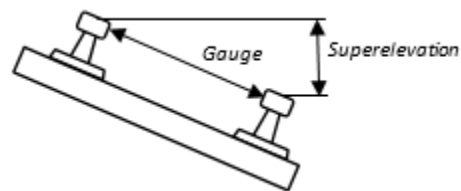
Figure 6. Track gauge and superelevation

8

Superelevation is an intentionally introduced elevation of the outer (i.e., high) rail in a curve over the inner (i.e., lower) rail to compensate for centrifugal acceleration experienced by the vehicle negotiating the curve. **Balance speed** in a curve is a speed at which the lateral component of centrifugal acceleration and the lateral component of gravitational acceleration cancel out, thus a vehicle experiences no net lateral force, and the wheel loads on left and right wheels are equal (Figure 7).
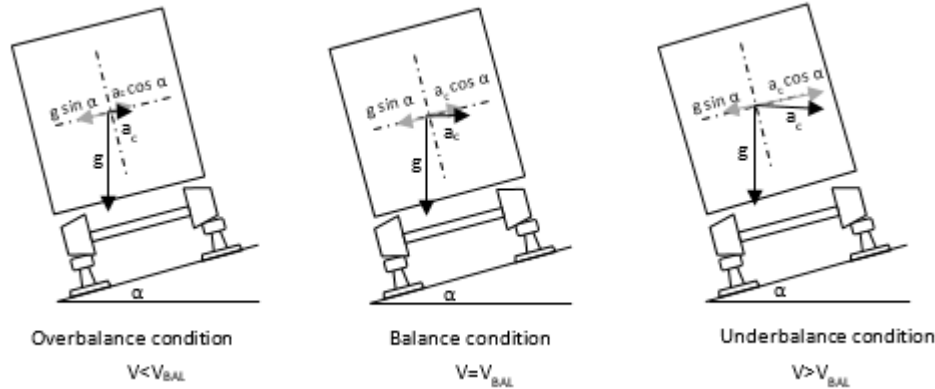
Figure 7. Balance conditions

In U.S. units, balance speed is calculated by:

$$V_{bal} = \sqrt{\frac{E_a}{0.00069\,\theta}} \tag{6}$$

Where V_{bal} is balance speed in miles per hour, E_a is track superelevation in inches, and θ is track curvature in degrees.

When a vehicle negotiates a curve at a higher speed than balance speed, it is said to be operating at a **cant deficiency**. Cant deficiency is the difference between the actual superelevation in a given curve and a superelevation which would result in a balance condition in a given curve at a given speed. When the vehicle operates at a lower speed than balance speed, it is said to be operating at a **cant excess**:

$$E_u = 0.00069\,\theta\,V^2 - E_a \tag{7}$$

where E_u is cant deficiency in inches and other variables are defined above.

2.2   Track Irregularities

With the passage of time, track geometry deteriorates, i.e., track position starts deviating from design geometry; these deviations are called **irregularities** or **excursions**. Their causes include (Puzavac et al., 2012; Haigermoser et al., 2015; Mariott and Ciobanu, 2018; Zarembski et al., 2015; Muinde, 2018):

- Manufacturing tolerances of track components, such as rail rolling defects

- Measurement errors during initial surveying, construction, and realignment of track

9

- Degradation of crossties and fasteners

- Poor weld geometry

- Rail surface wear

- Soil settlement

- Changes in ballast density and stiffness due to settlement, washout, scattering and tamping operations

- Vehicle-track interaction on small scale (e.g., rail corrugation, rail squats, etc.) and large scale (e.g., uneven ballast and soil settlement under vehicle loads); there is a significant positive feedback between increasing wheel-rail forces and degradation of track geometry (Elkhoury et al., 2018)

- Lateral track movement due to high lateral wheel forces and insufficient lateral stiffness of the track

- Track buckling due to thermal loads and insufficient restraint

The amplitude of track irregularities usually increases when they are measured under a vertical load (see Section 4.2).

The majority of modern TGMS sample data at intervals of about 1 ft, or 0.25 m, which means that even under ideal conditions they cannot measure irregularities with wavelengths less than 2 ft. Furthermore, many TGMS apply band-pass filters with lower cutoff wavelength of about 9-13 ft. Irregularities with shorter wavelengths, such as rail corrugation, require special equipment for measurement and are subject to standards and regulations that are separate from track geometry standards (Bracciali et al., 2009; Nielsen et al., 2013). These short irregularities are not covered in this report.

2.3   Absolute vs. Relative Track Geometry; Distance and Wavelength Domains

Track geometry measurements are often separated into two broad categories: absolute and relative geometry.

Absolute (i.e., **outer geometry**) refers to the position of the track with respect to an absolute reference point. It allows establishing track location with respect to other structures, which is especially important for maintaining clearances around the track.

Absolute track geometry is measured using traditional or automated surveying methods and is recorded in a surveying coordinate system (i.e., northings, eastings, and elevation). The origin of the coordinate system can be at any point on or off the track; XY surface is parallel to the surface of the geoid, and Z axis is perpendicular to this surface (i.e., parallel to the direction of Earth's gravitational force).

While absolute track geometry is important for track construction (and, in some cases, maintenance), it is not well-suited for evaluating the track's compliance with track safety standards or for predicting rail vehicles' responses to track irregularities.

Relative (i.e., **inner geometry**) is recorded in a track-centered coordinate system, with design geometry variables (i.e., curvature, superelevation, grade) and track irregularity variables (e.g., alignment, profile, gauge, cross level, etc.) being plotted as functions of distance along the track

(i.e., chainage). Such data is sometimes also described as being in **distance domain** and its graphical representation is referred to as a **strip chart** (Figure 8). Relative track geometry contains no information on the position or heading of the track with respect to absolute references, but it describes curves and perturbations in the track which affect vehicle behavior. Relative track geometry is what is being measured by most TGMS. It is well-suited for verifying track quality and compliance with track safety standards, as well as for predicting a vehicle's response using **multibody dynamics (MBD)** simulation.
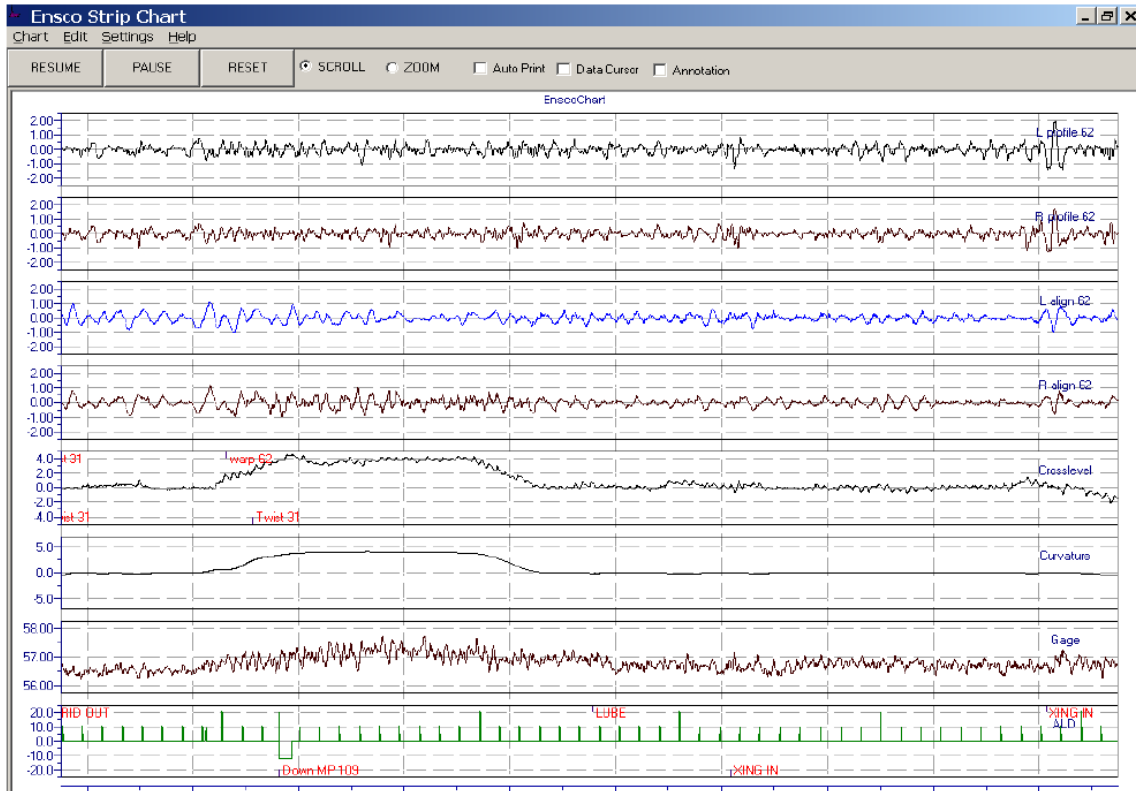
Figure 8. An example of relative track geometry (i.e., profile, alignment, cross level, curvature, and gauge) displayed in a strip chart (FRA, 2017)

Relative track geometry can be calculated from absolute track geometry easily and accurately (see Section 5.1). The reverse process can, in theory, be performed by integration, but the accuracy is low due to rapidly accumulating integration error, unless the relative track geometry measurements are combined with engineering survey measurements (Reedman, 2014).

Relative track geometry is recorded in one of two formats: the **space curve** format and the **chordal offset** (i.e., **versine**) format.

The space curve format is directly related to vehicle performance and is therefore used for MBD simulations and for assessment of track quality (Zhang et al., 2004; El-Sibaie and Zhang, 2004; Li et al., 2016). In many countries, track safety standards are based on space curve measurements (EN 13848-1,5,6). However, space curve is relatively complex to measure and process, and as a result, many agencies are either unfamiliar with it or avoid using it (Malone, 2007).

Chordal offset measurements do not directly relate to vehicle performance, although a recent large study showed that statistics based on chordal measurements perform similarly to statistics

based on space curve measurements in terms of predicting vehicle response to track geometry (see Section 6.7). Chordal measurements are intuitive and can be taken with simple hand tools. In many countries, including the United States, track safety standards are based on chordal measurements.

Space curve and chordal measurements are described in detail in Sections 2.4 and Section 2.5.

Distance domain is useful for, among other things, examining individual track geometry defects and making safety-critical decisions, such as setting speed restrictions and prioritizing repairs. For this reason, most characterization methods and assessment criteria, such as **track quality indices (TQIs)**, are designed for distance domain. These methods are described in Section 6.

In **wavelength domain**, track geometry variables are presented in terms of amplitudes, phase, and/or signal power densities. These variables are plotted as functions of wavelengths or spatial frequencies (i.e., inverse wavelengths) of their signal. A plot of power spectral density vs. wavelength or spatial frequency is called **a PSD plot**, and a heat map of power spectral density as a function of wavelength and distance along the track is called a **spectrogram** (Figure 9).
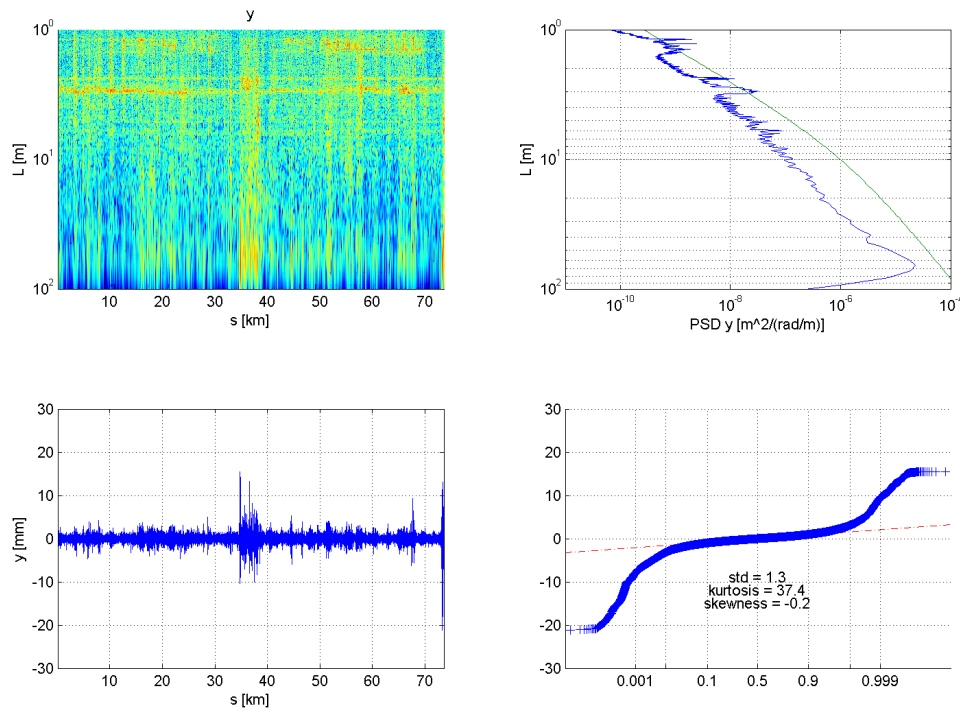
Figure 9. Track alignment data in distance and wavelength domain: space curve (bottom left), spectrogram (top left), PSD plot (top right) and normal probability plot (bottom right) – Data from DYNOTRAIN project (Haigermoser et al., 2013)

Presenting track geometry data in the wavelength domain is useful for:

- Identifying periodical patterns in irregularities, such as cyclical dips associated with rail joints or welds

- Looking at the big picture and making general conclusions about the condition of a large section of track or even an entire rail system

- Making qualitative comparisons between different sections of track, categories of track, or rail systems

- Describing the properties of filters and transfer functions

- Exploring relationships and correlations between different track geometry variables (e.g., alignment and gauge, gauge and cross level, etc.)

- Verifying measured track geometry and identifying problems in track geometry measurement systems

- Making general predictions about long-term vehicle behavior, for instance, by identifying cyclical track defects which can excite suspension oscillations (see Section 2.8)

- Generating artificial stochastic track irregularities for computer simulations

Wavelength domain analysis, as well as methods of transitioning between distance and wavelength domain, are discussed in detail in Section 7.

2.4 Space Curve

The principle behind the space curve is the separation of long length features of the track geometry, such as curvature and gradient, from short length features, such as alignment and profile deviations. This separation is achieved by defining a reference track trajectory. Space curve is a description of the deviations of measured track from the reference trajectory combined with the description of the gross geometry of the reference trajectory. The reference trajectory is not necessarily the same as design geometry (see Sections 5.1 – Section 5.2).

Figure 10 shows a plane view of a rail track. Solid lines represent the actual positions of the rails and of track centerline, dashed lines represent the reference trajectory of the track, and the distance between solid and dashed lines represents the space curve (shown in Figure 11). Note: chainage is defined as the measured distance along the track centerline. Typically, one chain is equal to 100 feet in length.
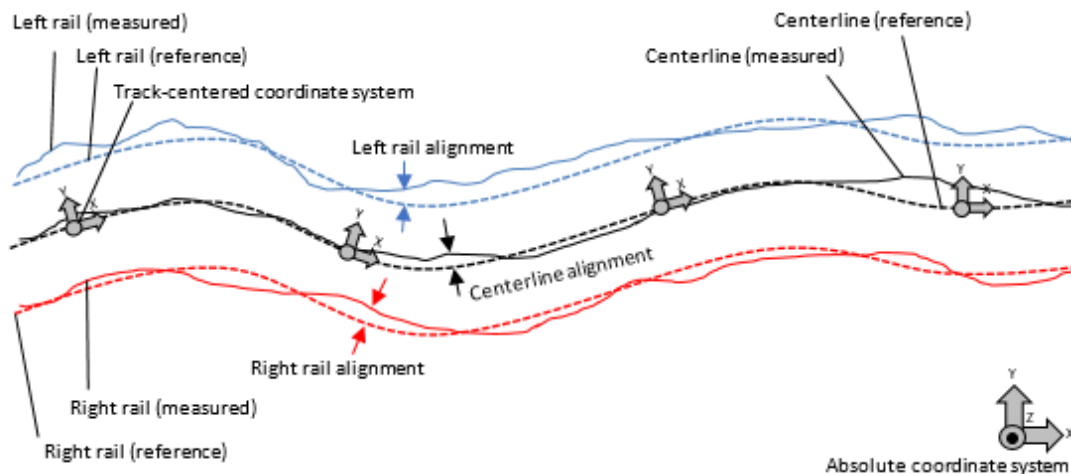
Figure 10. The relationship between absolute track geometry and alignment

13
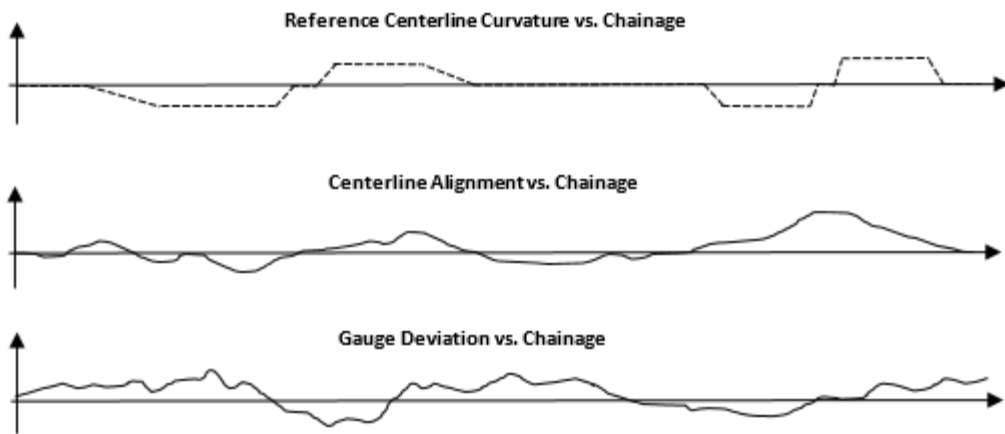
Figure 11. Space curve corresponding to the track in Figure 10

Track geometry in the vertical plane is described similarly (Figure 12). The geometry of the reference centerline is described in terms of grade or vertical curvature and the geometry of measured track is described in terms of profile and cross level (or, alternatively, in terms of left and right rail profiles).
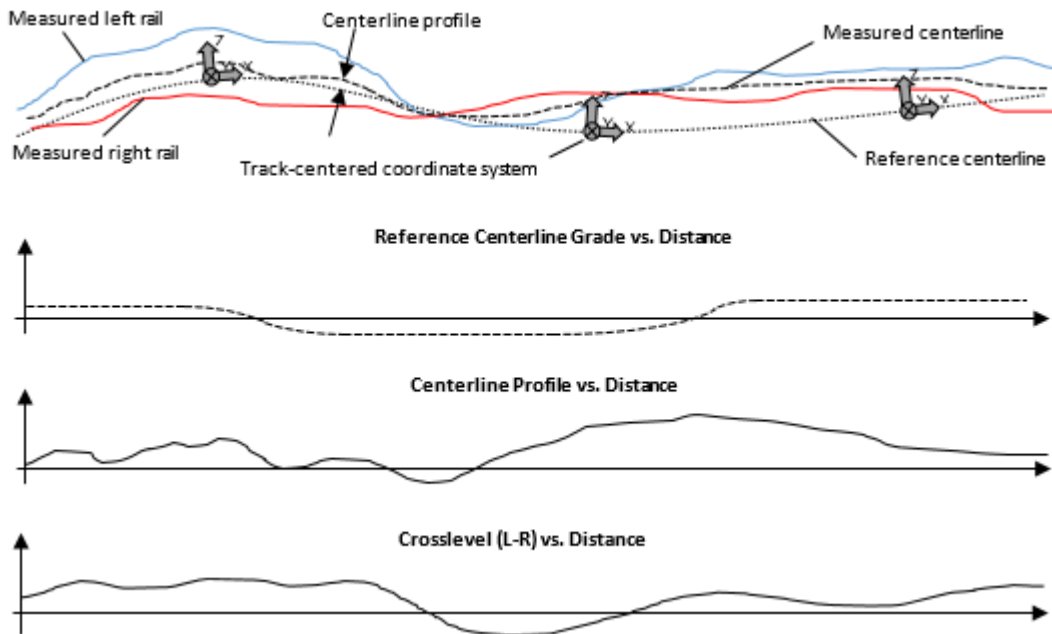
Figure 12. Absolute and relative vertical track geometry

Space curve data is recorded in a track-centered coordinate system. There is no universally agreed-upon coordinate system, but one possible option is described below.

The origin of the system is located on the reference centerline trajectory. The X axis is in the direction of heading of the track, the Y axis points from the origin toward the nominal left rail position, and the Z axis points from the origin up. This coordinate system can be either tilting or non-tilting (Figure 13). In a non-tilting coordinate system, the Z axis always remains parallel to the Earth's gravity. In a tilting coordinate system, the Z axis is always perpendicular to the plane

14

of the reference track (defined by the nominal positions of left and right rails) or the measured track (defined by the measured positions of left and right rails) (Lewis, 2011). This distinction plays a role when defining space curve variables.
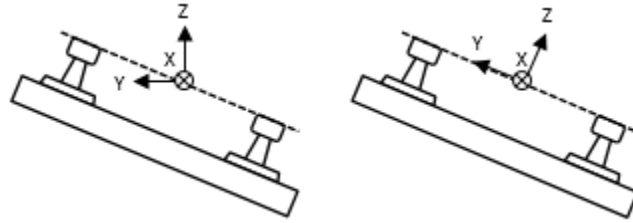
Figure 13. Non-tilting (left) and tilting (right) track-centered coordinate systems

In its basic form, space curve data consists of **chainage**, **curvature**, **gauge**, **cross level**, **alignment**, **gradient, superelevation**, and **profile**.

Chainage is the distance along the centerline of the measured track.

Curvature usually refers to the localized curvature of the reference centerline trajectory in the horizontal plane. It can be expressed as an inverse of radius of curvature, as MCO, or as an angle subtended by a 100-foot chord (Figure 2).

Gauge in this context refers to the measured track gauge (Figure 6) at a particular location on the track. Deviation from nominal gauge is produced by out-of-phase lateral deviations of left and right rails from their nominal positions.

Cross level (**cant** in European terminology) is usually defined as the unintended difference in elevation between the top of the left and right rail (Figure 6). Designed difference, e.g., elevation of the outer rail in curves, is called **superelevation**. Note that in some literature and TGMS software, the term "superelevation" is used to designate both the intended and unintended difference in elevation.

Cross level is measured as:

$$\Delta z_{XLV} = W \sin \alpha_{XLV} - \Delta z_{SE} \tag{8}$$

Where Δz_{XLV} is the crosslevel, Δz_{SE} is the superelevation, α_{XLV} is the crosslevel angle measured with an inclinometer, and W is the nominal track width, or center to center rail distance (also known as "cant base"), typically 1,500 mm (59.055 in) for standard gauge track (1435 mm, or 56.5 in). When the measured gauge deviates from the nominal gauge, Δz_{XLV} is not exactly equal to the difference in height between the tops of the rails.

Centerline alignment (**slew** in European terminology) is the lateral distance between the measured track centerline and the reference track centerline, measured perpendicular to the reference track centerline. It represents the in-phase lateral deviation of left and right rails from their nominal positions.

Gradient, or **grade,** is the rate of change of elevation of reference track centerline with respect to chainage.

Centerline profile, (**longitudinal level** or **lift** in European terminology), is the vertical distance between the measured and the reference centerline, measured perpendicular to the reference

centerline. It represents the in-phase vertical deviation of left and right rail from their nominal positions. The reference centerline has the gradient and vertical curves.

In most cases, TGMS outputs the alignments and profiles for left and right rails separately instead of centerline alignment and profile.

In a tilting reference system, the following relationships hold true:

$$y_L \cong y_C + \frac{1}{2}\Delta g, y_R \cong y_C - \frac{1}{2}\Delta g \tag{9}$$

$$z_L \cong z_C + \frac{1}{2}\Delta z_{XLV}, z_R \cong z_C - \frac{1}{2}\Delta z_{XLV} \tag{10}$$

where y_L, y_R, and y_C are left rail, right rail, and centerline alignments; z_L, z_R, and z_C are left rail, right rail and centerline profiles, respectively; Δg is gauge deviation and Δz_{XLV} is cross level. The reasons these relationships are not exact are:

1. Depending on the cross level, the plane is which gauge is measured may not be horizontal.

2. Cross level does not exactly equal the difference in elevation between the tops of the rails, as explained earlier.

Some of these space curve variables are illustrated in Figure 14. Note the effect of the reference system (tilting vs. non-tilting); when processing data from TGMS for use in MBD software, it is important to know which of the two reference systems is used by both TGMS and the software to ensure a correct conversion.
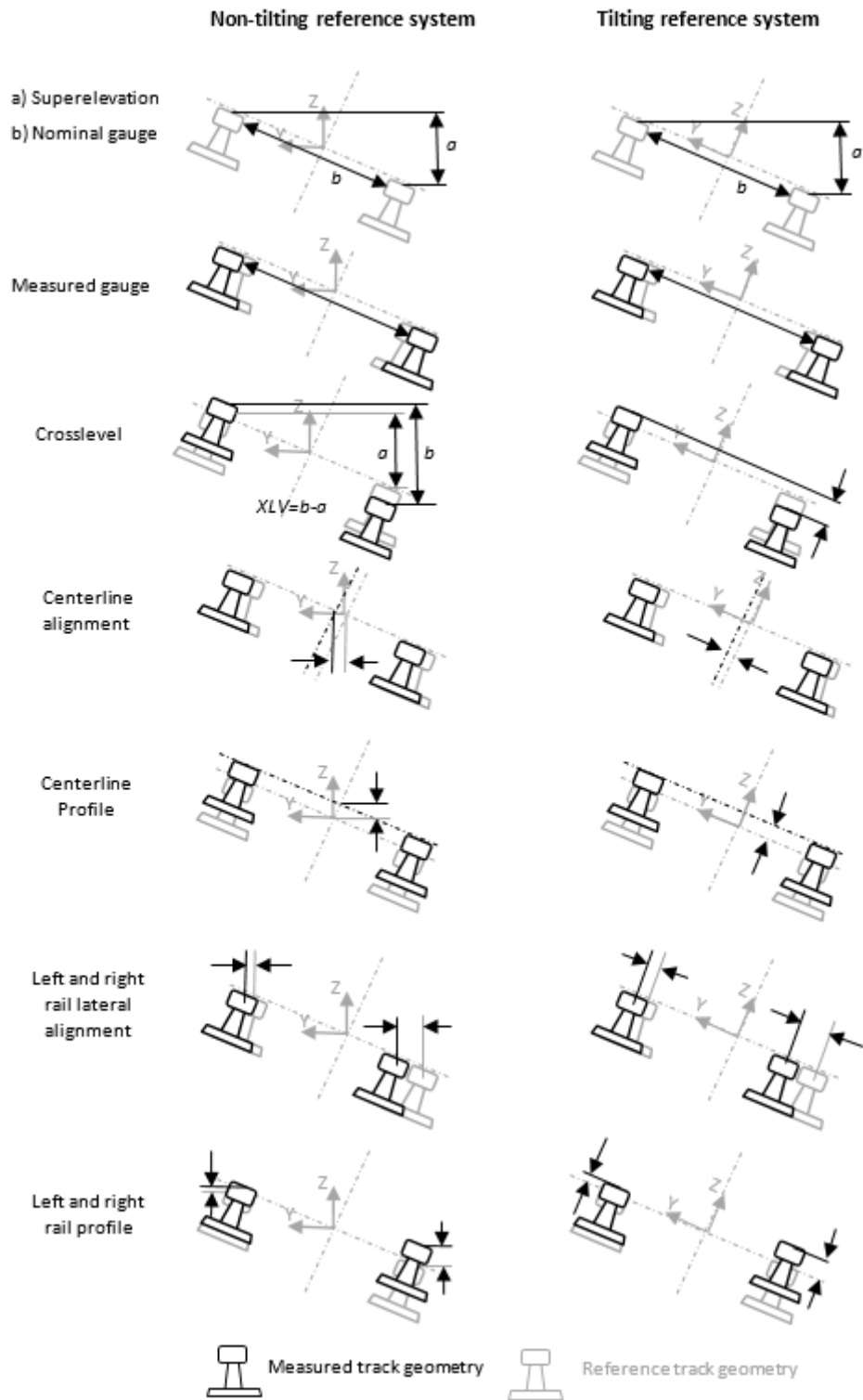
Figure 14. Space curve variable definitions

2.5 Chordal (Versine) Measurements

In many countries, including United States (49 CFR §213 Subpart C) and Canada (TC E-54 Subpart C), track safety standards are defined not in terms of space curve but rather in terms of chordal measurements, also called versines (Figure 15, Figure 16). Versine with ratio (α) of 0.5 is known as a symmetric versine, also called a mid-chord offset (MCO).

The convenience of chordal measurements is that they can be taken easily in the field with simple hand tools.
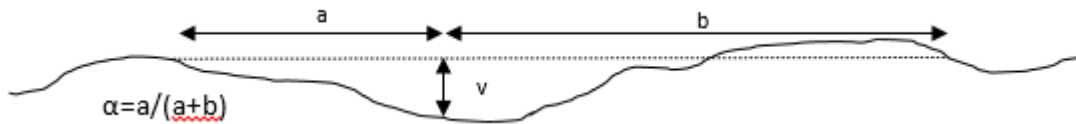
Figure 15. Versine (chordal) measurement
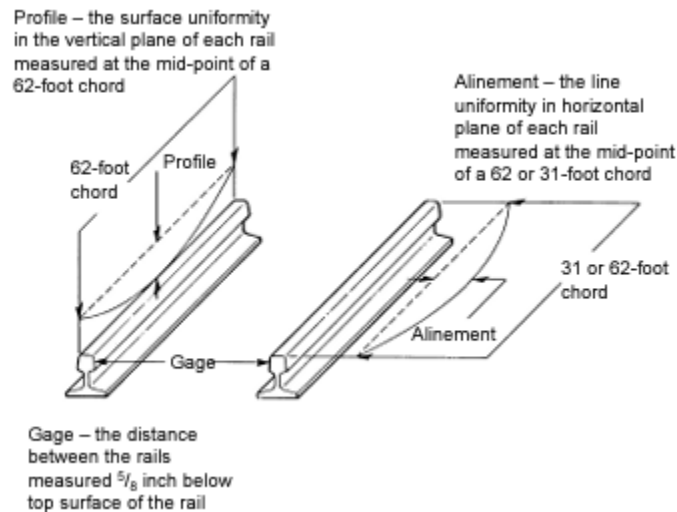
Figure 16. Mid-chord offsets (2017 FRA Compliance Manual, Vol. 2, Ch.1, p.2.1.29)

Chordal offset is a function of both alignment irregularity (Figure 15) and track design curvature (Figure 3). For example, a point in the body of a 10-degree curve has an MCO value of 10 inches for a 62-foot chord length if the rail at that point is perfectly aligned with its reference trajectory. For this reason, track geometry exceptions are defined not in terms of raw chordal values, but in terms of the deviation of chordal values from their localized averages. The FRA Compliance Manual specifies that for manual chordal measurements in curves, the averaging must be performed as follows:

- For Track Classes 1 through 5:
  - Alignment (2017 FRA Compliance Manual Vol. II Ch. 1, §213.55):
    - On tangent track: no averaging
    - In a body of a curve: averaging is performed over measurements taken at 9 or 17 overlapping uniformly spaced points over a total curve length of 248 feet, regardless of chord length

18

- In transition curves: MCO deviation from projected values must be calculated, i.e., projected MCO values must be calculated based on the assumption that in the transition curve track curvature changes linearly with distance
  - Profile/Surface: no averaging (2017 FRA Compliance Manual Vol. II Ch. 1, §213.63)
- For Track Classes 6 through 9:
  - Alignment (2017 FRA Compliance Manual Vol. II Ch. 2, §213.327):
    - Over measurements taken at 9 points over a total track length of 2 times chord length (62 ft. for 31-ft. chord, 124 ft. for 62-ft. chord, and 248 ft. for 124-ft. chord)
  - Profile/surface: no averaging (2017 FRA Compliance Manual Vol. II Ch. 2, §213.331)

The procedure specified for track Classes 6-9 is easily adaptable to track geometry vehicles (moving average filter with a window width of two times chord length), while the procedure specified for Classes 1-5 is not. Therefore, FRA's automated track inspection vehicles use a moving average filter with a window width of two times chord length on all track classes (Sherrock, 2018). This may result in differences between hand measurements and automated measurements.

2.6   Additional Track Geometry Variables

Sometimes, additional track geometry parameters can be calculated from basic track geometry variables.

Vertical curvature, i.e., curvature of reference track centerline in the vertical plane, can be used to calculate centrifugal acceleration of a rail vehicle negotiating a vertical curve.

Twist and **warp** are measures of cross level rate of change. **Twist** is the difference in cross level between two points a specified distance apart, and **warp** is the maximum difference in cross level between any two points less than a specified distance apart. If x is chainage and L is base distance, then:

$$Twist(x) = \Delta z_{XLV}\left(x + \frac{L}{2}\right) - \Delta z_{XLV}\left(x - \frac{L}{2}\right) \tag{11}$$

$$Warp(x) = \max\left(\Delta z_{XLV}(x_1)\right) - \min\left(\Delta z_{XLV}(x_2)\right); \quad x - \frac{L}{2} \le (x_1, x_2) \le x + \frac{L}{2} \tag{12}$$

Maximum change of gauge is calculated within a specified distance (i.e., between any two points less than a specified distance apart).

Runoff (ramp) is defined as a change in elevation of a rail "*in any 31-foot segment at the end of a raise where the track is elevated as a result of automatic or manual surfacing or bridge work*" (49 CFR §213.63). Track geometry recording vehicles typically interpret it as a peak-to-peak amplitude within a 31-foot space curve window (Clouse, 2018).

Dip angle is a measure of a localized change in the rail's vertical gradient. It is usually most noticeable near rail joints. Dip angle is measured in degrees or milliradians and is calculated

from a change in vertical rail profile gradient over a short wavelength. Dip angle is directly related to the vertical impact wheel loads and is sometimes used as a pre-indication of an impending rail end break. Due to the elasticity of rails, the magnitude of dip angle depends on vehicle speed, wheel load, and direction of travel. (Mandal et al., 2016; RAIB, 2014; prEN 13848-1:2016).

Kink angle, or **entry angle**, can be described as a lateral equivalent of a dip angle, although it occurs for very different reasons. Kink angle is a design variable of turnouts and is not commonly measured by TGMS.
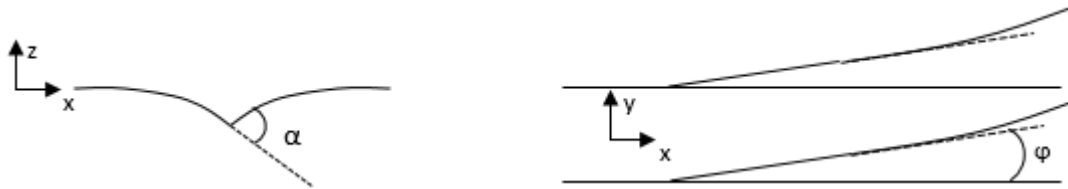
Figure 17. Rail dip angle (left); switch entry (i.e., kink) angle (right)

2.7   Relationship between Space Curve and Chordal Offset

Qualitatively, the relationship between space curve and chordal data can be described as follows: if a reference trajectory is a straight line, then space curve is a series of mid-chord offset measurement made with an infinitely long chord. For a curvilinear reference trajectory, the relationship is more complex (Figure 18).
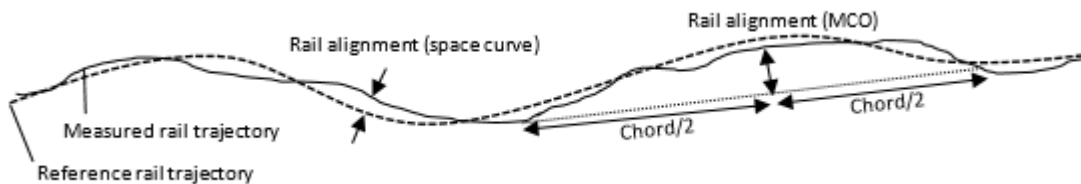
Figure 18. A comparison between rail alignment in space curve and mid-chord offset format

Figure 19 shows a dip in the track expressed in a space curve and chordal formats with different chord lengths. The distorting effect of chordal measurements can be seen clearly.
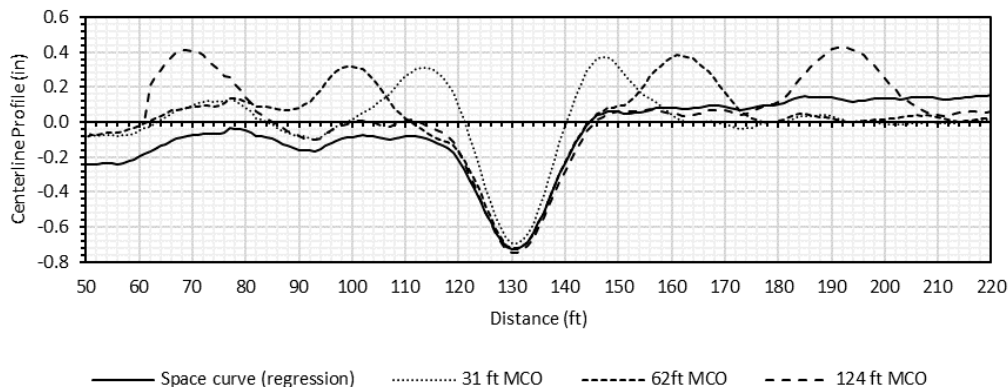
Figure 19. Vertical track irregularity recorded in space curve and mid-chord offset formats

20

The magnitude of the distortion is a function of the ratio of the wavelength of the track perturbation to the chord length (λ/C). Figure 20 demonstrates the relationship between space curve and chordal offsets for a sinusoidal track irregularity (see Section 7.2 for discussion of transfer functions). Mid-chord offset (i.e., chordal offset where $\alpha=0.5$) measurements distort the signal by magnifying amplitudes of waves whose wavelengths are odd submultiples of chord wavelength (e.g., C, C/3, C/5, C/7, etc.) and eliminate the waves whose wavelengths are even submultiples of chord wavelength (e.g., C/2, C/4, C/6, etc.). This is the reason Federal Track Safety Standards require making MCO measurements with multiple chord lengths.
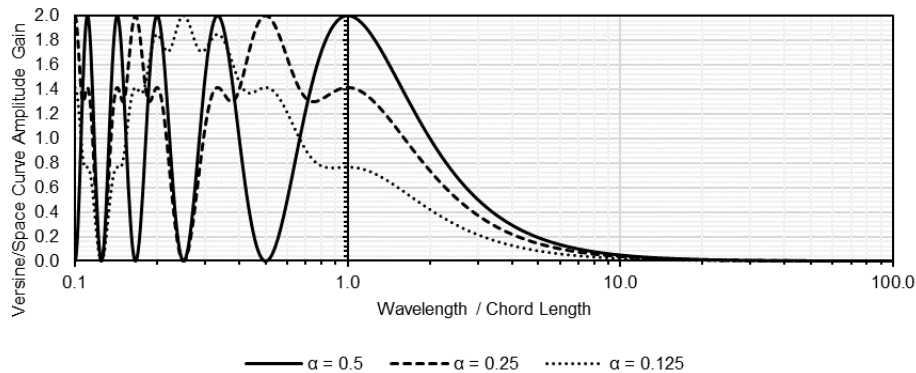
Figure 20. Magnitude of a space curve-to-versine transfer function vs. the ratio of irregularity wavelength to chord length; α=0.5 corresponds to a symmetric versine, also known as a mid-chord offset (Cohen and Hutchens, 1970; Ahmadian, 1999 and others)

Note that irregularities with 15.5-ft wavelengths are eliminated by all standard chord lengths used in the United States and Canada: 31 ft, 62 ft, and 124 ft (Figure 21). No information is available on whether track irregularities at this particular wavelength are a practical safety concern although several hypothetical scenarios could be envisioned where they could be a problem. This blind spot can be eliminated by using a chord length that is not a multiple of 31 ft or by using asymmetric chord measurements.
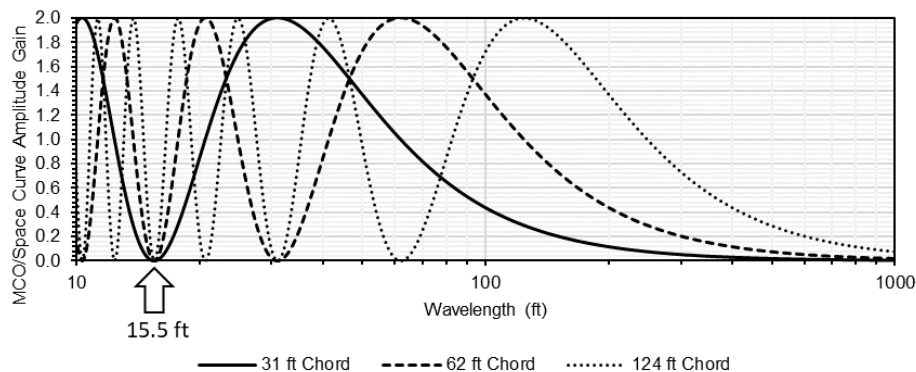
Figure 21. Magnitude of a space curve-to-chordal offset transfer function vs. irregularity wavelength, calculated for standard chord lengths (31, 62, and 124 ft)

The plots in Figure 20 and Figure 21 assume that the reference trajectory is linear. In curves, this relationship is complicated by the effects of filters used to calculate reference trajectory and to average MCO values over a distance. Figure 22 illustrates this effect by analyzing data recorded

21

with a track geometry car equipped with an inertial TGMS, which records track geometry data in MCO and space curve formats. Figure 22 shows the magnitude of three transfer functions for left rail alignment data:

1. Analytically calculated transfer function of a 62-ft MCO over space curve (same as the 62-ft. MCO plot in Figure 21)

2. Numerically calculated transfer function of synthetic 62-ft. MCO data over the space curve data recorded by the TGMS (Synthetic 62-ft. MCO data is calculated analytically from the space curve data recorded by the TGMS using the analytical equation for the transfer function)

3. Numerically calculated transfer function of 62-ft MCO data recorded by the TGMS over space curve data recorded by the TGMS
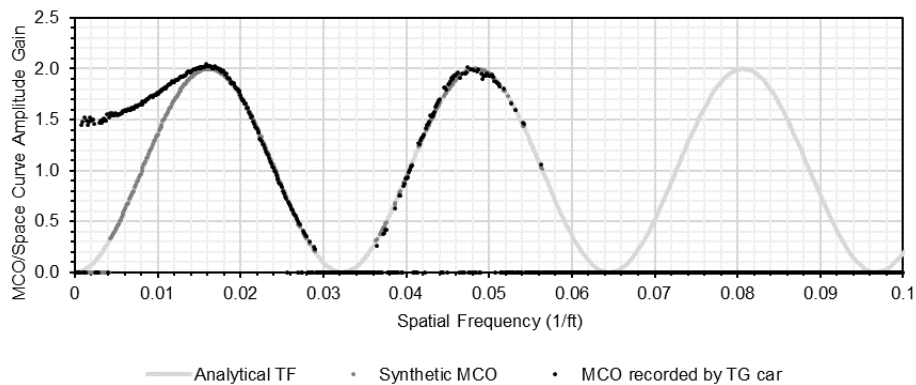
Figure 22. Magnitude of theoretical vs. measured transfer function of MCO over space curve

Comparison of these transfer functions shows that due to the filter effects described earlier, MCO data recorded by TGMS contains more low frequency components than predicted by an analytical transfer function equation.

Occasionally an engineer is presented with a set of track geometry data collected with an unknown chord length, or even data whose type (space curve or MCO) is unknown. In these cases, frequency analysis is especially useful. Figure 23 shows the FFT amplitude plot of space curve and mid-chord offset data for left rail alignment measured with a track recording vehicle. Note the characteristic periodic peaks and valleys in the space curve data, which allow easy identification of chord length.
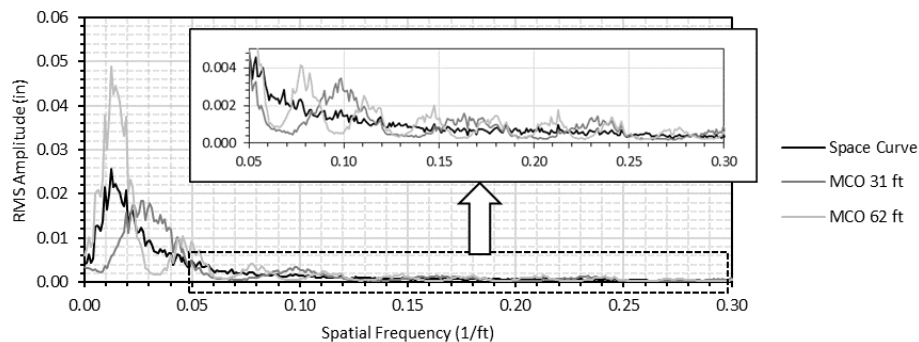
Figure 23. FFT amplitude plot of space curve and mid-chord offset data

Regardless of chord length and methods for curvature removal, track geometry data recorded in the MCO format should not be used as an input for MBD simulations. At a minimum, it must first undergo a restoration (i.e., decoloring) process to convert it into space curve format (see Section 5.3).

2.8 Effects of Track Irregularities on Rail Vehicles

Gauge deviation. Narrow gauge can lead to excessive lateral wheel-rail forces and cause excessive wheel and rail wear. Wide gauge can decrease lateral stability of the vehicle and, in extreme cases, lead to wheel drop derailment (Sun et al., 2013; Wolf, 2015).

Cross level. Cross level irregularities cause wheel unloading on the affected side, which under extreme conditions may lead to derailment, especially when high lateral wheel forces are also present. In some cases, vehicle suspension can bottom out (i.e., its range of motion is exceeded), resulting in shock loads to the vehicle and damage to the vehicle, occupants, and cargo. In less extreme cases, it is a ride quality issue, inducing roll motion of the carbody.

Warp and **twist** cause wheel unloading on the opposite corners of the truck (i.e., bogie) and of the vehicle, increasing the risk of flange climb derailment. The longer the wheel base and the less compliant the vehicle suspension, the more severe the wheel unloading due to track warp. This is one of the limiting factors for design length of transition curves.

Alignment irregularities cause excessive lateral wheel-rail forces, resulting in excessive wheel and rail profile wear and increasing the risk of flange climb derailment. They also may lead to excessive carbody lateral accelerations, resulting in poor ride quality. Out-of-phase alignment irregularities in left and right rail constitute gauge irregularities.

Profile (surface). When left and right rail profile irregularities occur in phase, they excite the pitch and bounce carbody modes (see explanation on cyclical irregularities below), resulting in cyclic wheel unloading, excessive vertical wheel-rail forces, and carbody accelerations. As with cross level defects, extreme cases may lead to the exceedance of suspension's range of motion and damage to the vehicle. Out-of-phase profile irregularities are equivalent to cross level irregularities.

Cyclical irregularities and resonance. Even relatively small excursions of alignment, profile, or cross level can have catastrophic effects if multiple irregularities are spaced at such distances that the vehicles' resonant frequencies are excited. As few as 2-3 irregularities, each of which below a safety threshold, may be enough to cause a derailment or damage track and vehicle components.

Table 1. Carbody resonant frequencies

Carbody vibration mode	Typical frequency range (Hz) by vehicle type				Track geometry excursion types likely to excite the mode
	Locomotives	Freight cars (empty)	Freight cars (loaded)	Passenger cars	
Bounce	1.2–1.8	4.2–5.0	1.8–2.5	0.8–1.2	Profile
Pitch	2.0–2.7	5.0–7.5	2.7–4.5	0.8–1.3	Profile
Yaw	1.2–1.8	3.5–5.0	1.5–3.0	1.0–1.3	Alignment
Roll (lower center)	0.4–1.0	1.5–3.0	0.7–1.2	0.5–0.8	Cross level, Alignment
Roll (upper center)	2.2–2.6	5.0–6.0	2.5–3.8	1.1–2.0	Cross level, Alignment

The body of a rail vehicle and its suspension elements can be modeled as a 3D mass-spring-damper system with multiple modes of vibration. The modes that are of the most interest are bounce, pitch, yaw, roll (i.e., upper center), and roll (i.e., lower center). Resonant frequencies of rail vehicles vary but generally range between 0.4 Hz and 8 Hz (Table 1). Figure 24 shows the vehicle suspension resonance modes.

Excitation of any of these modes at a frequency close to its resonant frequency can have catastrophic consequences.
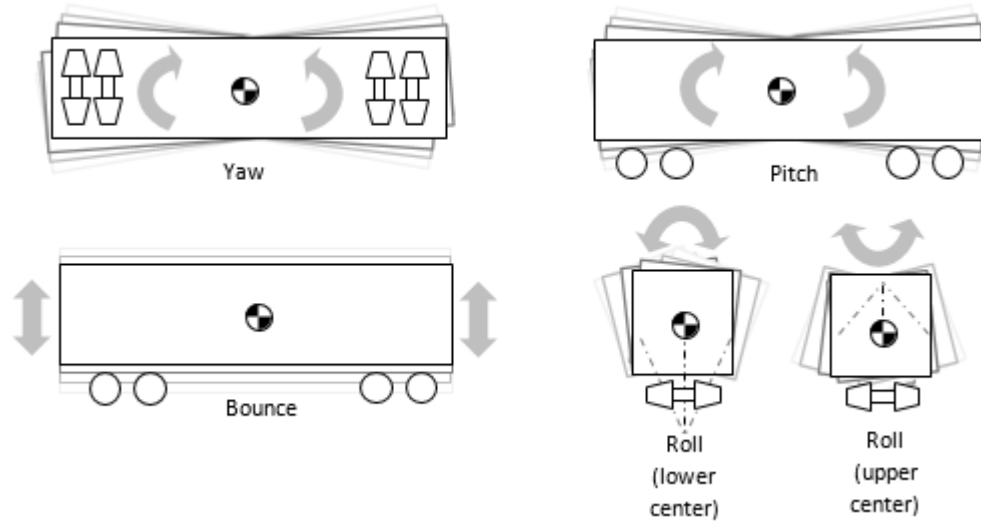
Figure 24. Vehicle suspension resonance modes

Figure 25 shows an example of the relationships between resonant frequencies, vehicle speed, and wavelength for a hypothetical loaded hopper car. For example, vertical irregularities associated with rail length (39 ft) and its second harmonic (19.5 ft) may excite this railcar's bounce frequency at speeds near 55 mph and 28 mph, respectively.
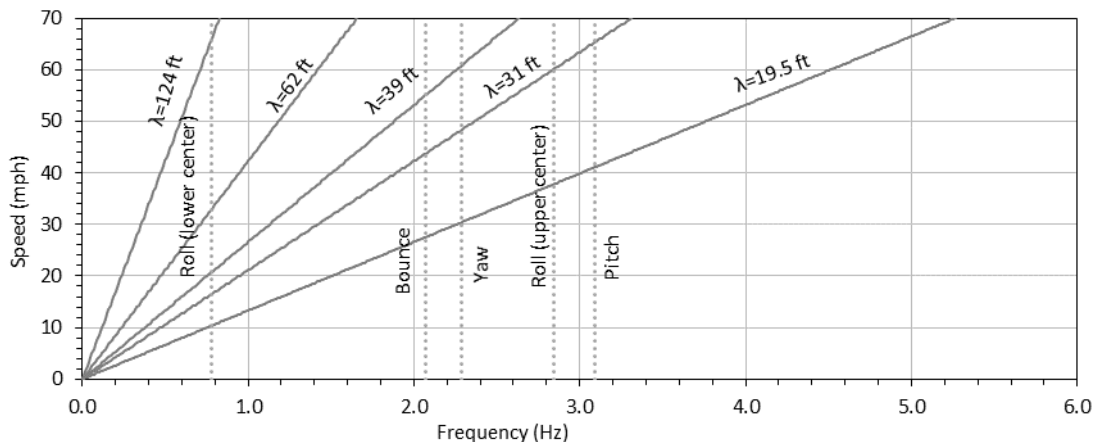
Figure 25. Example of a relationship between carbody resonant frequencies, vehicle speed, and track irregularity wavelength

3. Overview of Process of Track Geometry Measurement and Characterization

Figure 26 shows an overview of track geometry measurement, processing, and characterization cycle based on a classification proposed by Haigermoser et al. (2015). White rectangles designate data, grey rectangles designate processes, and dashed shapes designate optional steps.

The cycle may vary considerably depending on the hardware used to measure track geometry, end goals, and desired characterization methods. The next sections of this report focus on specific steps on this cycle.

The cycle begins with one of the types of TGMS: inertial, chordal, or surveying (Section 4.3). Alternatively, track geometry may be assessed indirectly by measuring vehicle reactions (e.g., wheel-rail forces, car body accelerations, etc.) using a **Vehicle Reaction Measurement System (VRMS)**.

In the case of an inertial system, the output of TGMS sensors is processed (usually by software aboard a track geometry vehicle) and the data from various sensors is combined to yield a raw space curve, which contains variables such as gauge, alignment, curvature, cross level, and surface (Section 2.4). Depending on the wavelength measurement range of the system, this space curve data may already have design elements (i.e., track layout) separated from track irregularities; if this is not the case, it must be performed in a separate step.

In the case of a chordal measurement system, the measured track geometry is output in chordal offset format. In this case, too, track irregularities must be separated from track layout.

Output of surveying track geometry measurement systems usually is in a form of absolute track geometry (Section 2.3), which must be converted into space curve or chordal format before proceeding to next steps. This process is generally combined with the process of separating track layout from irregularities.

Track quality assessment methods for chordal and space curve are not interchangeable. Therefore, in many cases, it is necessary to convert chordal data into space curve or vice versa. Some data is lost during space curve to chordal conversion, and space curve usually cannot be fully restored from chordal measurements (Section 5.3).

Track irregularity data may undergo additional, optional steps before track irregularity characterization is performed. These steps may include **filtering** (for example, under EN 13848 standards, track irregularities are separated into different wavelength ranges) and, in some cases, detection and extraction of **track anomalies** and **special features** (e.g., joints, turnouts, crossings).

Track characterization can be performed in the distance domain (i.e., space curve of chordal offset) or wavelength domain. Transition from the former to the latter is achieved by several different methods, most commonly by Fast Fourier Transform (FFT).
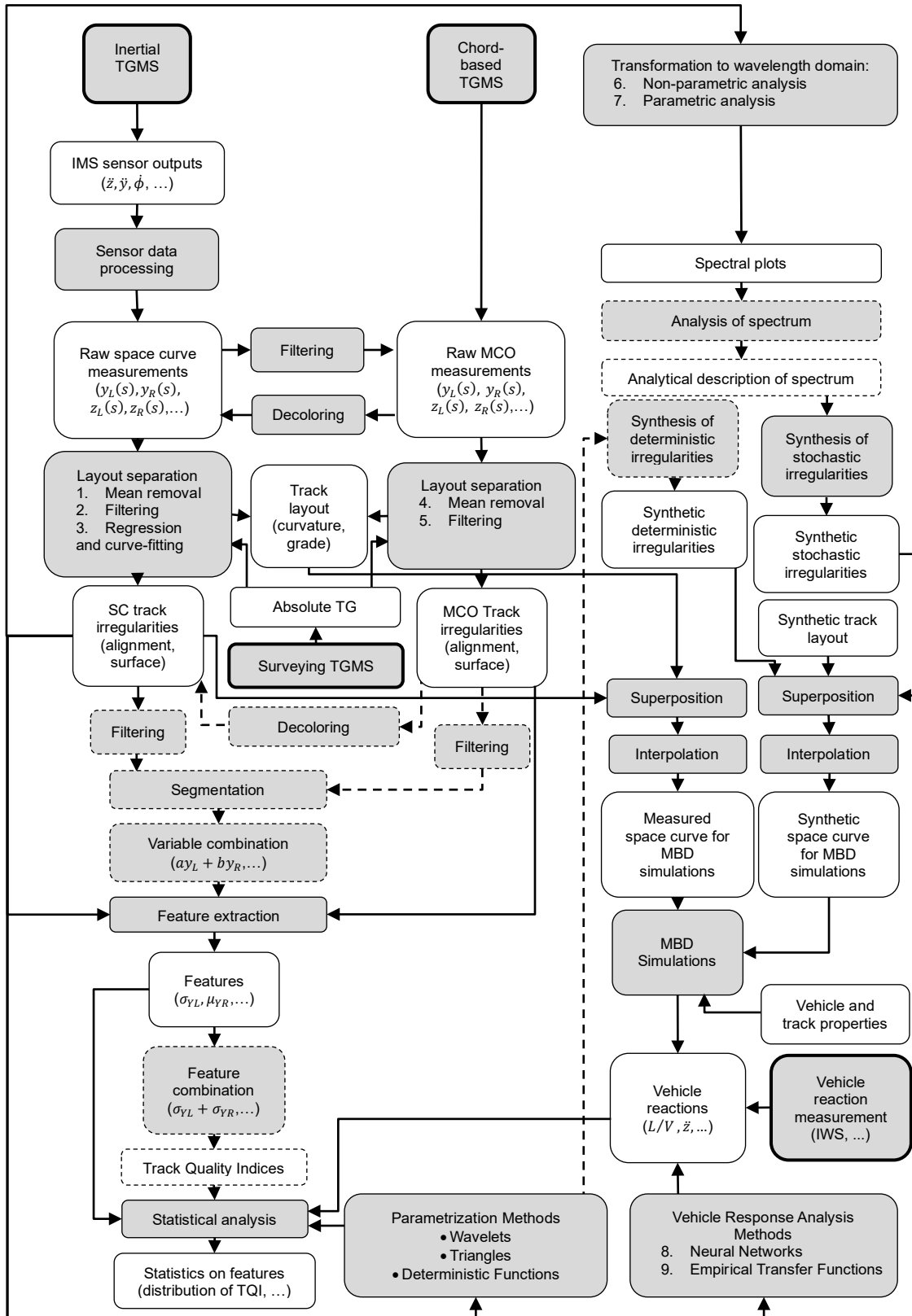
Figure 26. Overview of track geometry measurement and characterization process

In the distance domain, the characterization steps are:

1. **Segmentation** of track into sections; consecutive analysis can be performed on each segment

2. **Combining multiple track geometry variables** into a single variable (e.g., average of left and right rail alignment)

3. **Extraction of features** (e.g., mean, median, maximum, and standard deviation) from individual and/or combined track geometry variables

4. **Combining extracted features** (e.g., sum of standard deviations of gauge and cross level) into a single variable; this is how most **track quality indices (TQIs)** are calculated

5. **Performing statistical analysis of features** (e.g., calculating the distribution of track quality indices amongst track segments)

All the steps except Step 3 (extraction of features) are optional.

If track irregularity data is **transformed into wavelength domain** via parametric or non-parametric methods, the resulting spectral density functions can be described analytically.

Collected and processed track geometry data can be used to predict rail vehicles' response to track. It may be done directly via **vehicle response analysis (VRA) methods** such as point-mass-acceleration (PMA), neural networks (NN), or, after additional processing, via **MBD simulations**. As an alternative to using measured data for simulation, **synthetic track geometry data** can be created by combining synthetic track layout with stochastic and/or deterministic track irregularities.

4. Types of Track Geometry Measurement Systems

Below is a brief overview of the most common types of track geometry measurement systems. This section only discusses TGMS which collect comprehensive track geometry data, including curvature, grade, cross level, gauge, alignment, and profile. Simpler systems which only measure some of the track geometry variables (most often gauge and cross level) are outside of the scope of this section.

4.1 Relative and Absolute TGMS

Relative TGMS, which typically use either inertia-based or chordal methods, constitute the majority of both trolley-based and vehicle-mounted systems. Compared to absolute TGMS of similar accuracy and portability, they tend to be more affordable and simpler to use.

The majority of **absolute TGMS** rely on optical surveying methods (see Section 4.3). Some of the new TGMS avoid the limitations of optical surveying by using combinations of inertial measurement systems (IMS), high-accuracy global navigation satellite systems (GNSS), and/or machine vision (Engstrand, 2011; Pinter, 2012; Chen et al., 2015; Chen et al., 2018; Trimble, 2017). Almost all absolute TGMS systems are mounted on small trolleys, although track recording vehicles with absolute TGMS also exist (Vogelaar, 2017).

When users want to only measure relative track geometry, they may still benefit from using an absolute TGMS, which provide complete control over conversion of absolute track geometry into relative track geometry data, allowing the use of linear regression and curve fitting, customization of filters, etc.

4.2 Platform

TGMS can be mounted on hand-pushed trolleys, self-propelled carts, road-rail (i.e., hi-rail) vehicles, dedicated track geometry vehicles, and revenue service vehicles. Aside from the obvious logistical and financial considerations, it is important to recognize that track geometry measurements are affected by the stiffness of the track and the weight of the measuring vehicle. The relationship between wheel load and track geometry irregularities is not straightforward. It depends on the condition of ballast and soil, type of track structure, type of rail fasteners, etc. Furthermore, the extent to which a truck deflects rails (and therefore measured amplitudes of gauge and alignment irregularities) depends in part on its dynamic performance, such as curving characteristics.

In the United States, regulations require that in certain cases "*track geometry measurements shall be taken no more than 3 feet away from the contact point of wheels carrying a vertical load of no less than 10 kips per wheel, unless otherwise approved by FRA*" (49 CFR §213.333(b)).

If track geometry data is being used to evaluate track condition, then ideally it should be measured with a track geometry measurement car with an axle load representative of other vehicles on that line. If measured track geometry data collected in a loaded condition (i.e. loaded track geometry from a track geometry car) is being used as input (i.e. unloaded geometry) for MBD simulations, then using actual track stiffness parameters in the simulation may result in simulated loaded track geometry and wheel-rail forces that are somewhat different than reality (Section 8.1).

4.3   Principle of Operation

Manual measurements are simple in principle but time-consuming and labor-intensive.

Manual chord surveying measures relative track geometry in chordal offset format. It is performed using a chord of defined length and a ruler (Figure 15, Figure 16). This method often is used to verify track geometry defects measured by vehicle-mounted systems.

Manual optical surveying measures absolute track geometry. It is performed using a theodolite or an automated geodetic total station (Figure 27, top). Vertical and lateral coordinates of a point on one of the rails with respect to a global coordinate system are measured; vertical and lateral coordinates of a point on the opposing rail are estimated from the coordinates of the original rail, combined with gauge and cross level at that point, measured with a gauge bar (Stow and Andersson, 2006).
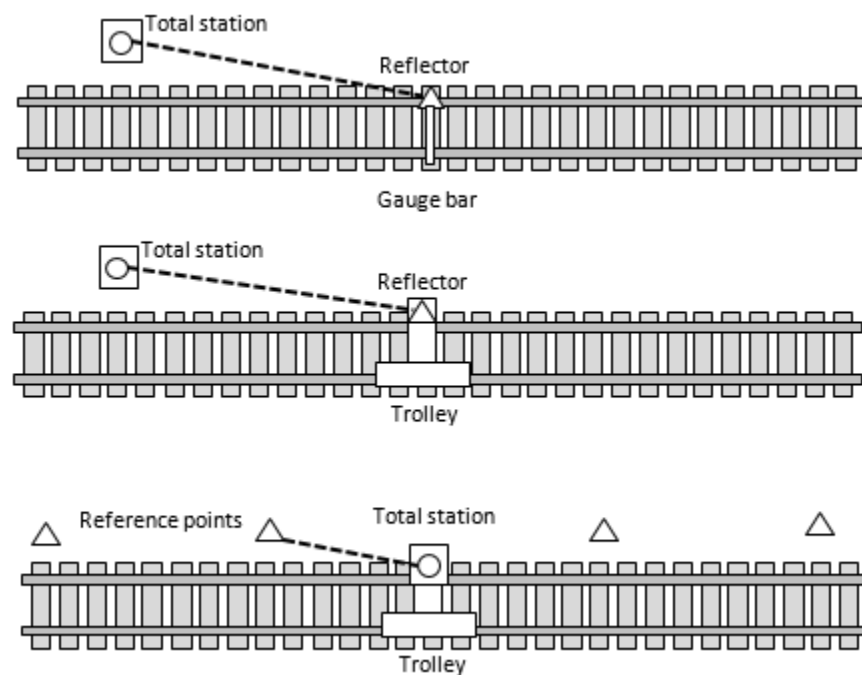
Figure 27. Manual and automated optical surveying

Automated optical surveying is performed using track surveying trolleys. A typical setup consists of a wayside total station and a reflective target mounted on a trolley, which also contains sensors for cross level and gauge measurement. Alternatively, a total station can be mounted on a trolley and use wayside reflectors (Figure 27).

The trolley can make measurements in either kinematic mode (i.e., at walking speed) or in a more accurate stop-and-go mode. The main disadvantages of these systems are their slow speed of measurement and short range (tens or hundreds of meters), which is further limited by topography and atmospheric conditions (higher air temperature and larger wind speeds decrease the useful range). Range and accuracy can be increased by relocating a total station and making sequential overlapping measurements, but this process is relatively cumbersome and time-consuming, limiting most absolute TGMS systems to use on trolleys intended for measuring

short sections of track. Some optical surveying systems combine surveying data with measurements from inertial measurement systems, as described below.

Inertial measurement systems (IMS) can be mounted on either the carbody or truck frame of a track recording vehicle, or, less often, on a portable trolley (Chen et al., 2015; Sundaram and Wilson, 2016; Trimble, 2017).

They combine the data from multiple sensors:

- An odometer to measure chainage

- Non-contact (usually optical) or contact sensors which determine the relative position of rails with respect to the sensor

- A combination of accelerometers and gyroscopes, which determines the relative acceleration and velocity of the measuring device with respect to ground and integrates these data to calculate the relative position

Traditional vehicle-mounted IMS have accelerometers and gyroscopes mounted on the truck frame or carbody, and displacement sensors (such as linear variable differential transformers (LVDTs)) mounted across vehicle suspension elements (Figure 28). Such systems are custom designed for each vehicle. On the other hand, many modern IMS are self-contained units mounted entirely to the carbody or truck frame and do not measure displacement across suspension. Each approach has advantages and disadvantages. Mounting sensors to an unsprung mass, such as an axle box, creates a more rigid coupling between sensor readings and track irregularities, but it places the sensors in a harsh vibration environment and requires measuring a very wide range of frequencies. TGMS with optical sensors mounted to the carbody may be limited to the maximum curvature of the track they are able to measure due to lateral offsets of the mounting location on the car body relative to the rails. Ultimately, there are systems of either type on the market that are capable of measuring space curve to EN 13848 specifications.
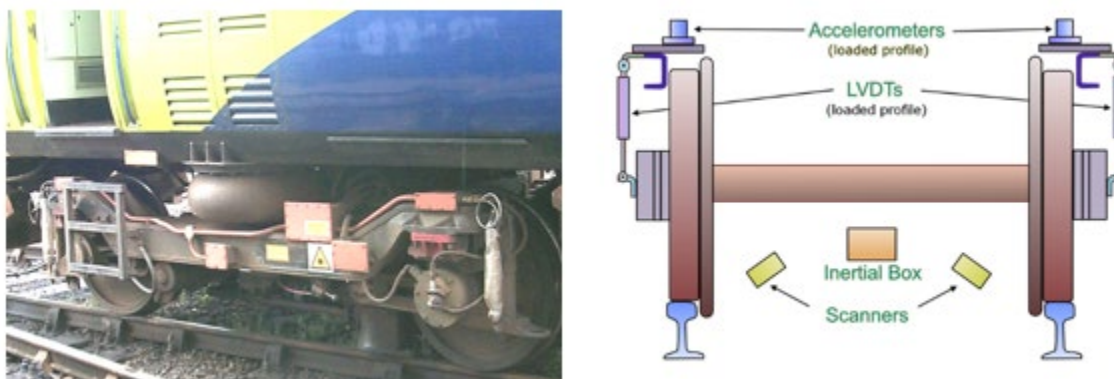
Figure 28. Traditional vehicle-mounted IMS and its schematic (Lewis, 2011)

One notable limitation of IMS is a minimum vehicle speed required for measurement. The lower the speed of the vehicle, the lower the magnitudes of the outputs of accelerometers and gyroscopic sensors, and below a certain speed signal to noise ratio it becomes too low for accurate measurements (Lewis, 2011). Therefore, the lower the speed of the vehicle, the shorter the maximum wavelength of a track irregularity that the IMS can measure accurately; measurement of long wavelengths usually requires much higher speeds than shorter wavelengths

(see discussion of wavelength domains in Section 5.2). However, due to recent improvements in sensor design and data processing, some of the newer IMS are capable of measuring track geometry at low speeds (i.e., ~5 mph) and/or can accommodate limited-duration stops. Such systems are often described as having "zero-speed" or "extended speed range" measurement capabilities.

Chordal systems are automated versions of manual chord survey (Figure 16). They measure lateral and vertical distances between each rail and the frame of the track recording vehicle or trolley at a minimum of three points (Figure 29). Where required, corrections can be made for the distortion resulting from the bending of the vehicle frame (Haigermoser et al., 2015). Resulting chordal measurements can be converted into space curve using a restoration process (Section 5.3). Asymmetric chordal systems have fewer zeros (i.e., wavelengths with zero gains that are impossible to restore) but introduce a phase distortion. Even for asymmetric systems, the larger the ratio of track defect wavelength to the chord length, the more difficult it is to accurately restore that wavelength due to decreasing signal/noise ratio (Figure 20). For this reason, small trolley-based chord systems are limited to short wavelengths, making them unsuitable for measuring high-speed rail tracks. Vehicle-mounted chord-based systems can measure longer wavelengths.

$$\alpha = a/(a+b)$$

$$versine = h_2-(h_1+ \alpha\ (h_3-h_1))$$
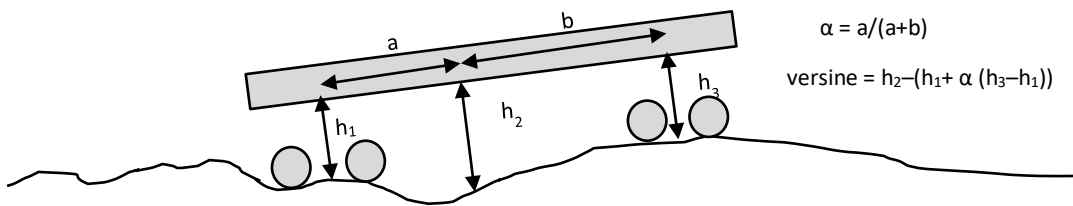
Figure 29. Vehicle-mounted chordal TGMS

Despite these limitations, chordal systems have several advantages over inertial systems. Chordal systems tend to be mechanically simpler and less costly than IMS. Their accuracy does not depend on vehicle speed and they can make static measurements. Nevertheless, because of the ongoing improvements to the design of IMS, vehicle-mounted chordal systems are becoming increasingly rare. Trolley-mounted chordal systems are still used widely.

Some chordal systems combine chordal measurements with other types of measurements to overcome the typical disadvantages of chordal systems. One of trolley-mounted systems uses a principle called "differential difference method," which combines versine and slope measurements (Naganuma and Yada, 2016) and other systems combine chordal and inertial measurements (Yazawa and Takeshita, 2002; Yada et al., 2017).

With proper data processing, both chordal and inertial systems can produce relative track geometry measurements of acceptable quality, but the limitations of each must be understood.

Global Navigation Satellite Systems/Global Positioning Systems (GNSS/GPS) by themselves do not have sufficient accuracy to be used for track geometry measurements, because even high-accuracy differential GNSS used in this application have an accuracy of 0.5-1.0 inch (Szwilski et al., 2003). Generally, GNSS mounted on a track recording vehicle are used to record the location of the track geometry defects, but not to measure their magnitude.

However, some recently designed TGMS blend the data from high-accuracy GNSS with inertial or chordal systems, which allows measurement of both absolute and relative track geometry while overcoming some of the problems of optical surveying systems (Luck et al., 2001; Kreye et al., 2004; Chen et al., 2015; Trimble, Inc., 2017). Other systems combine data from GNSS and optical surveying systems (Mahalakshmi and Joseph, 2013; Jiang et al., 2017).

The use of **Doppler Light Detection and Ranging (LIDAR)** systems to measure track chainage and curvature has been investigated. Their advantages over traditional methods of measurement of chainage (i.e., tachometers and encoders) and curvature (i.e., gyroscopes) include accuracy at low speeds and not being susceptible to wheel slip and wheel tread wear (Wrobel, 2013; Andani, 2016; Andani et al., 2018).

Additionally, more complex LIDAR-based **machine vision** systems have recently emerged on the TGMS market. They can create 3D point clouds, allowing the measurement of not only track geometry (absolute and relative) but also clearances between track and nearby structures. (Vogelaar, 2017; Burton, 2018). Non-LIDAR machine vision systems also are being developed (Gabara and Sawicki, 2018).

Position determination: One of the challenges in the design and operation of TGMS is determining the accurate absolute position of track geometry defects (i.e., milepost). Odometers often have insufficient accuracy and GNSS does not work in tunnels; furthermore, GNSS is not sufficiently accurate to identify the track number in multi-track territory. This may necessitate more complicated methods, such as installing radio-frequency identification (RFID) tags or special processing of accelerometer data (Broquetas et al., 2012).

4.4 Autonomous TGMS

In the last decade, advances in electronics and software development led to a development of autonomous track geometry measurement systems (ATGMS). These systems are mounted on revenue service trains and allowed to function unattended, which allows more frequent and less costly inspections than traditional manned TGMS. Collected track geometry data is transmitted wirelessly to a remote operator (Morant, 2016; Stuart, 2017; Higgins and Liu, 2018). Railroads, transit agencies, and regulatory bodies show great interest in ATGMS and have been conducting extensive tests. However, at this time, their widespread implementation is being impeded by issues (Morell, 2017) such as:

- Difficulties with precise location of the defects, especially distinguishing between tracks in multi-track territory

- Challenges with assuring data quality and preventing false positives without personnel examining data in real time (see Section 6.1)

- Logistical difficulties (procedures for hardware maintenance and data handling are not well established)

- Regulatory issues (unclear requirements as to remediation of defects revealed during automated inspections)

Additional technical challenges may arise depending on the specifics of vehicles on which ATGMS are installed. For example, placing an ATGMS on a freight railcar may subject it to a harsh load environment with high accelerations and natural frequencies that vary with loading

condition; the vehicle's weight and curving characteristics can cause ATGMS measurements to differ from those taken by a traditional track geometry vehicle on the same route (see Section 4.2).

It is expected that within the next few years use of ATGMS will become much more widespread.

4.5 Vehicle Response Measurement

The end goal of measuring track geometry is to ensure vehicle safety and ride comfort. Therefore, it is often beneficial to measure vehicle performance directly by recording wheel-rail forces and/or carbody and truck accelerations, and to make conclusions about track condition from these measurements.

Vehicle response measurement systems (VRMS) supplement traditional track geometry measuring systems, but do not replace them for these reasons:

- Vehicle response does not clearly differentiate between irregularity types or measures their magnitudes.

- Response is vehicle-specific. Lack of response by one vehicle to a track defect does not mean it is safe for other vehicle types or even for the same vehicle at a different speed; correlation is not straightforward.

Direct measurement of wheel-rail forces requires use of instrumented wheelsets, which are expensive and labor-intensive to design, use, and maintain. Accelerometers do not have those problems, but their readings do not directly describe wheel-rail forces.

In the United States, vehicle response measurement is mandated as a part of vehicle/track system qualification for Class 6 track speeds and above, or for any curving speed producing cant deficiency of more than 5 inch (49 CFR §213.333, §213.345). An overview of American and International Vehicle-Track Interaction (VTI) safety standards is given in Marquis et al. (2014).

Vehicle response measurements can be used to calculate vertical track irregularities. Accelerometers are mounted onto axle boxes or carbodies, and the resulting accelerations are filtered and integrated to calculate vertical space curve, acting as a simplified IMS (Figure 30).
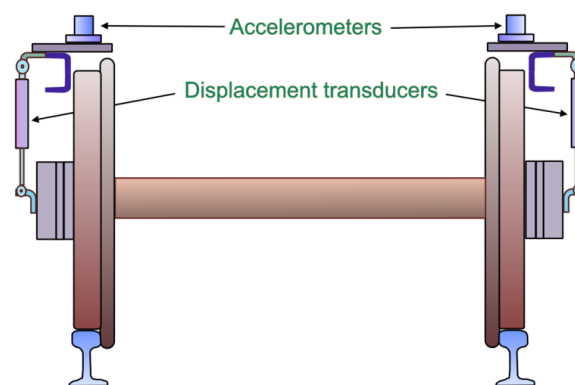
Figure 30. A simplified system for measurement of vertical irregularities (Lewis, 2011)

Accurate calculation of lateral track irregularities (i.e., alignment) with such methods is not feasible, because wheelset and track are relatively weakly coupled in the lateral direction due to the clearance between the wheel flanges and rails. Weston et al. (2015) review the methods of track

geometry measurements from in-service vehicles; Al-Nazer (2014) describes FRA research on this topic; Karis (2018) gives an overview of methods used on Japanese high-speed railways.

5. Processing of TGMS Outputs

The principle behind the space curve is the separation of track design elements from irregularities and their presentation in a track-centered coordinate system. Some of the steps of this process are similar, whether track geometry is measured by a traditional (i.e., inertial or chordal) TGMS or a surveying system. These steps are described in Section 5.2. For surveying systems, additional steps are required to transition from global reference system to track-based coordinate system. These steps are described in Section 5.1.

5.1 Conversion of Absolute Track Geometry into Space Curve

The process of conversion of absolute track geometry into space curve simultaneously achieves two goals:

1. Transition from the absolute coordinate system into a track-centered curvilinear coordinate system
2. Separation of track layout from track irregularities

When a reference track trajectory is known, space curve is easy to calculate.

To calculate alignment:

1. A global coordinate system xyz is defined such that xy is the horizontal plane and z is elevation.
2. Measured track centerline $<x, y>$ trajectory is calculated by averaging northings and eastings of left and right rail.
3. Reference track trajectory $<x_R, y_R>$ is aligned with the measured track centerline trajectory.
4. Distance between the measured and reference centerline is calculated (Figure 10). At each given point along the trajectory, it can be approximated as the magnitude of the cross-product of track heading vector and the vector pointing from a point on the reference trajectory to the nearest point on the measured trajectory. This distance is interpreted as the track centerline alignment.
5. Reference track curvature with respect to reference trajectory chainage s is calculated from the coordinates of the reference trajectory (Weisstein, 2018):

$$\kappa_R(s) = \frac{\frac{dx_R}{ds}\frac{d^2y_R}{ds^2} - \frac{dy_R}{ds}\frac{d^2x_R}{ds^2}}{\left(\left(\frac{dx_R}{ds}\right)^2 + \left(\frac{dy_R}{ds}\right)^2\right)^{\frac{3}{2}}} \tag{13}$$

For profile, the procedure is similar. Vertical distance between the reference trajectory and the measured trajectory is interpreted as track centerline profile, and the derivative of the reference trajectory's elevation with respect to chainage is interpreted as track grade (Figure 11).

Left and right rail alignment and profiles then can be calculated from centerline alignment, centerline profile, gauge, and cross level (Equations (9)-(10)). Caution must be exercised to ensure that the calculations are consistently performed in the appropriate (i.e., tilting or non-tilting) local reference frame (Figure 14).

In many cases the reference trajectory is not readily available. There are several ways to calculate it.

Regression and curve-fitting. For tangent track, the reference track centerline trajectory can be easily calculated by linear regression. In curves, various circle fitting methods can be used. In particular, Pratt's least squares algorithm (Pratt, 1987; Chernov, 2009) is quite efficient and robust for a wide range of curvatures and signal-to-noise ratios. Davis (1999) describes a least squares fitting method for spiral curves.

If the measured trajectory consists of multiple elements (i.e., tangents, curves, and spirals) it can be segmented into these elements, which can be a complex iterative process. Although determining the breakpoints and estimating the parameters of each given segment (e.g., radius of curvature, heading of tangent, etc.) for railroad track and highways is a well-researched problem (Trehag et al., 2008; McCrae and Singh, 2008; Stratakos et al., 2009; Di Mascio et al., 2012; Garach et al., 2014), these parameters may need to be optimized to ensure continuity of endpoint coordinates, bearing, and curvature between all the segments, while still minimizing the error between the measured trajectory and its fitted spline (Tong and Ding, 2010). Computationally, this involves fitting a spline consisting of linear, circular, and clothoid segments to the data, while making a trade-off between error minimization and avoiding an excessive number of segments. Commercial software products aimed at rail track design, such as Bentley OpenRail Designer (Bentley Systems, Inc., 2018) and Leica Geosystems ATrack (Leica Geosystems AG, 2018), can perform this type of analysis.

Filtering and smoothing. A simpler solution is to smooth the measured trajectory using appropriate digital filters and use the result as the reference trajectory. This will separate long-wavelength features of the track from short-wavelength features. Empirically, satisfactory results can be achieved when eastings, northings, and elevations of measured centerline trajectory are resampled at equal chainage intervals and then filtered independently with a second or fourth-order Butterworth filter. To eliminate phase distortion, a filter is applied in forward and then in reverse; signal padding and/or initial state determination method (Gustaffson, 1996; The MathWorks, Inc., 2019b) can be used to minimize end effects.

5.2   Separation of Track Irregularities from Track Layout

In inertial TGMS, data from transducers (e.g., accelerometers, angular velocity sensors, laser transducers, etc.) is integrated and combined into raw space curve data (i.e., vertical and lateral rail positions). This data already is in a track-based coordinate system, but track layout elements, such as curves and spirals, may still be mixed with track irregularities. Similarly, in chord-based TGMS, mid-chord offset due to track curvature is mixed with the offset due to track irregularities.

This process of separating track irregularities from track design elements is generally performed by a computer inside the TGMS; most of the details of this process are proprietary to TGMS manufacturers. The end user of the TGMS rarely has any control of it and may only see the processed space curve, with track irregularities and layout already separated into different variables (e.g., curvature, alignment, etc.).

Except for surveying systems, which measure absolute track geometry, using regression is usually not an option. Instead, track layout is separated by applying digital filters to transducer signals or to raw space curve variables. An example of such separation is shown in Table 2. The variables λ_y, $\lambda_{\Delta z}$, and λ_z designate cutoff wavelengths used to separate, respectively, curvature from alignment, superelevation from cross level, and grade from profile irregularities. Note that

this may vary significantly between TGMS systems. Some wavelength content may be discarded altogether, and some may be duplicated in multiple variables. However, regardless of the filtering and processing it employs, almost every TGMS will output, among other things, raw gauge and superelevation channels, which are unfiltered and contain all measured changes in gauge and superelevation, both design and irregularities.

Table 2. The relationship between space curve variables and filter cutoff wavelengths

Variable	Lateral Rail Position				Vertical Rail Position			
	L&R in Phase		L&R out of Phase		L&R in Phase		L&R out of Phase	
	$\lambda < \lambda_y$	$\lambda > \lambda_y$	$\lambda < \lambda_{\Delta y}$	$\lambda > \lambda_{\Delta y}$	$\lambda < \lambda_z$	$\lambda > \lambda_z$	$\lambda < \lambda_{\Delta z}$	$\lambda > \lambda_{\Delta z}$
Curvature		x						
Superelevation							x	x
Grade						x		
Cross level							x	
Gauge			x	x				
Centerline Alignment	x							
Centerline Surface					x			
L Rail Alignment	x		x	x				
R Rail Alignment	x		x	x				
L Rail Profile/Surface					x		x	
R Rail Profile/Surface					x		x	

Filter type. If space curve data is being extracted to be used as an input for MBD simulations, and if the MBD software uses the track geometry in its entirety, including track gradient, curvature, gauge, superelevation, and vertical and lateral alignment, then the choice of filter is not critical. For example, it has little relevance which wavelength (e.g., 20 ft of 200 ft) is being used as a cutoff between curvature and lateral alignment, because both curvature and alignment data will be used as inputs for the simulation. The key is to avoid missing or redundant data (see Section 5.4 and Section 8.1).

However, if space curve is being used to identify track defects or as an input in MBD software which does not use one of the components of track geometry (e.g., grade), then proper filter design becomes critical.

The most common approach is to use a finite impulse response (FIR) filter. It has a favorable frequency response curve, a linear phase response, and can be applied either in real time or in post-processing.

Infinite impulse response (IIR) filters have reasonably good frequency response characteristics, but they distort the signal due to a non-linear phase response. Some TGMS use them despite the distortion, but this approach generally is not recommended. To overcome phase distortion, IIR filters can be applied in post-processing, cascaded in forward and then in reverse.

Finally, a moving average filter can be used (Section 2.5). It has a linear phase response and can be implemented easily in either real time or in post-processing. However, its frequency response characteristics (i.e., roll-off rate and passband ripple) are not ideal.

International Union of Railways (UIC) Leaflet 518 specifies a 4-pole Butterworth filter with precision ±1 dB in the passband and attenuation of 24 dB/octave. The current Euronorm EN 13848 (as of 2018) does not specify filter type. The draft (prEN 13848-1; August 2016 version)

specifies upper and lower boundaries for filter transfer function and recommends FIR filter for real-time processing and FIR or IIR (second order Butterworth) filters for post-processing.

Filter cutoff wavelength. The choice of a cutoff wavelength for a filter is far from straightforward. Recall that the main goal of filtering is to separate track layout from track irregularities. The difficulty is twofold.

1. Some track irregularities can be longer than some track design elements. Therefore, a shorter cutoff wavelength may filter out some track irregularities, while a longer cutoff will make track design elements look like track irregularities.

2. Track design elements usually do not have a sinusoidal shape. In fact, design curvature and superelevation are usually not smooth functions, causing the transitions between design elements to seem like irregularities.

This problem is most severe in turnouts and in curves which have no spirals or short spirals. In these cases, excessively long cutoff wavelengths will result in transitions between curves and tangents being interpreted as large alignment deviations. If measured track geometry data shows excessively large alignment deviations near the beginning and the ends of the curves, but not in the body of the curve or on tangent track, filter cutoff wavelength may be too small for the short transition curves in the particular track. In addition, a turnout's entry angle may manifest itself as a cusp-shaped alignment anomaly.

Figure 31 and Figure 32 show the space curve calculated from absolute track geometry measurements made by a track surveying trolley.
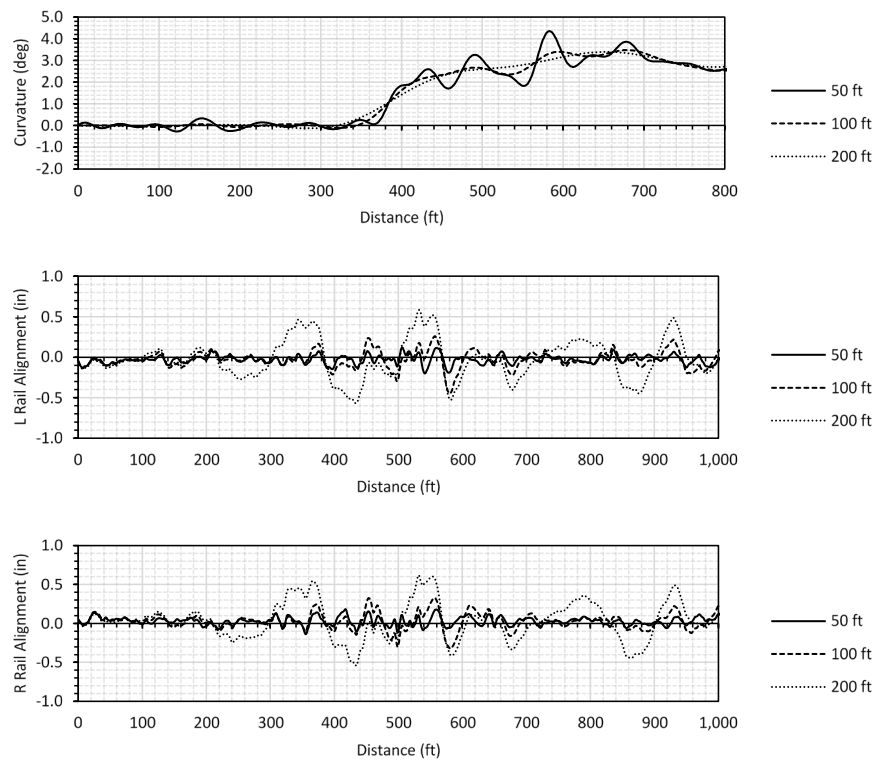
Figure 31. Curvature and alignment as functions of filter cutoff wavelength (data courtesy of Trimble GmbH)
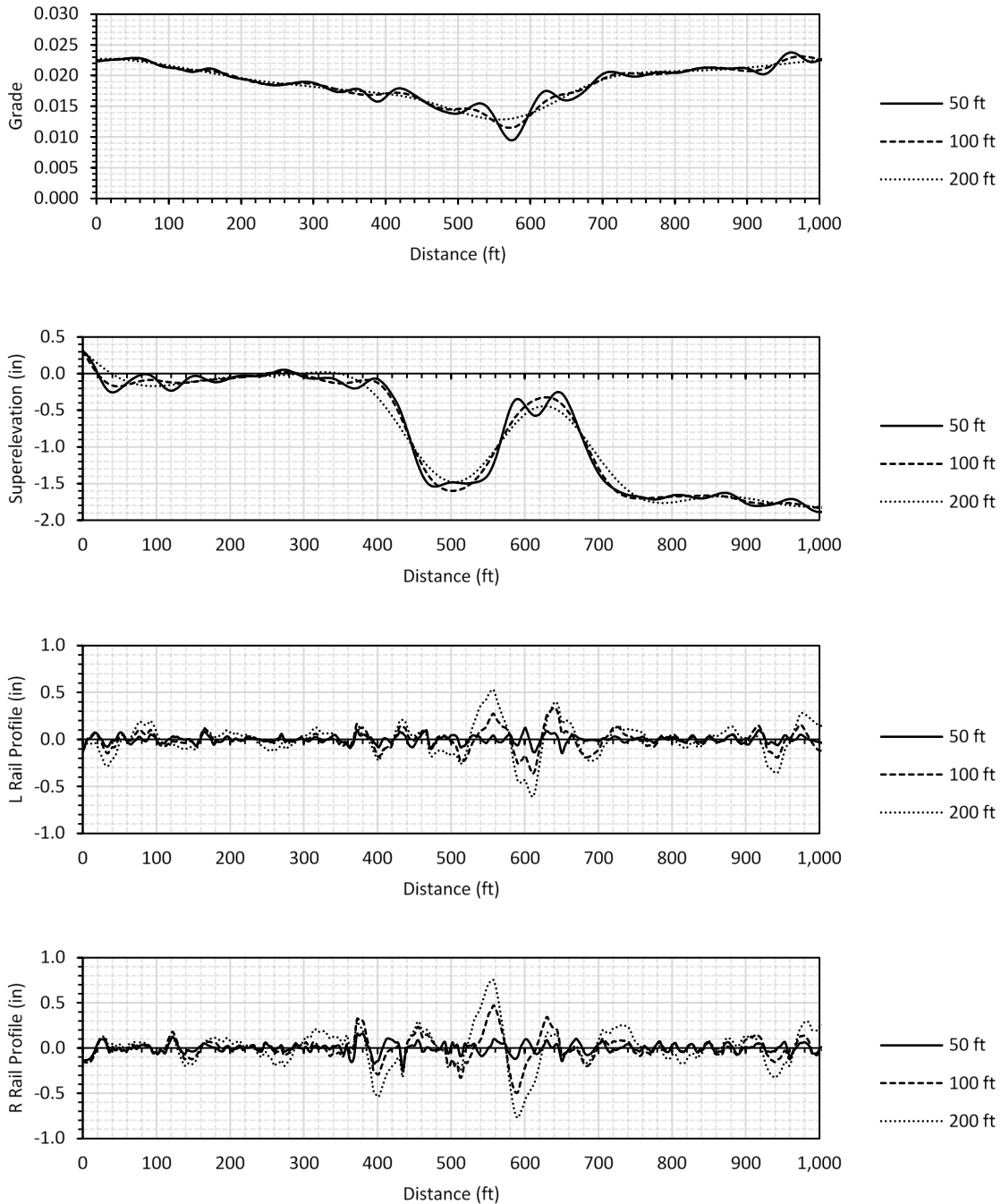
Figure 32. Grade, superelevation, and profile as functions of filter cutoff wavelength (data courtesy of Trimble GmbH)

Note the effect of filter parameters on the shape of the space curve. Longer cutoff wavelength results in smoother curvature, superelevation, and grade plots, but larger amplitudes of alignment and profile deviations. For these reasons, when space curve data is used to evaluate a track's compliance with safety standards or for calculations of TQI, the filter characteristics should be specified in detail.

Figure 33 illustrates the same concept. It shows the space curve corresponding to the dip in a track measured by a track surveying trolley and processed with the linear regression method and with different filters. The apparent depth of the dip changes significantly depending on the processing method.
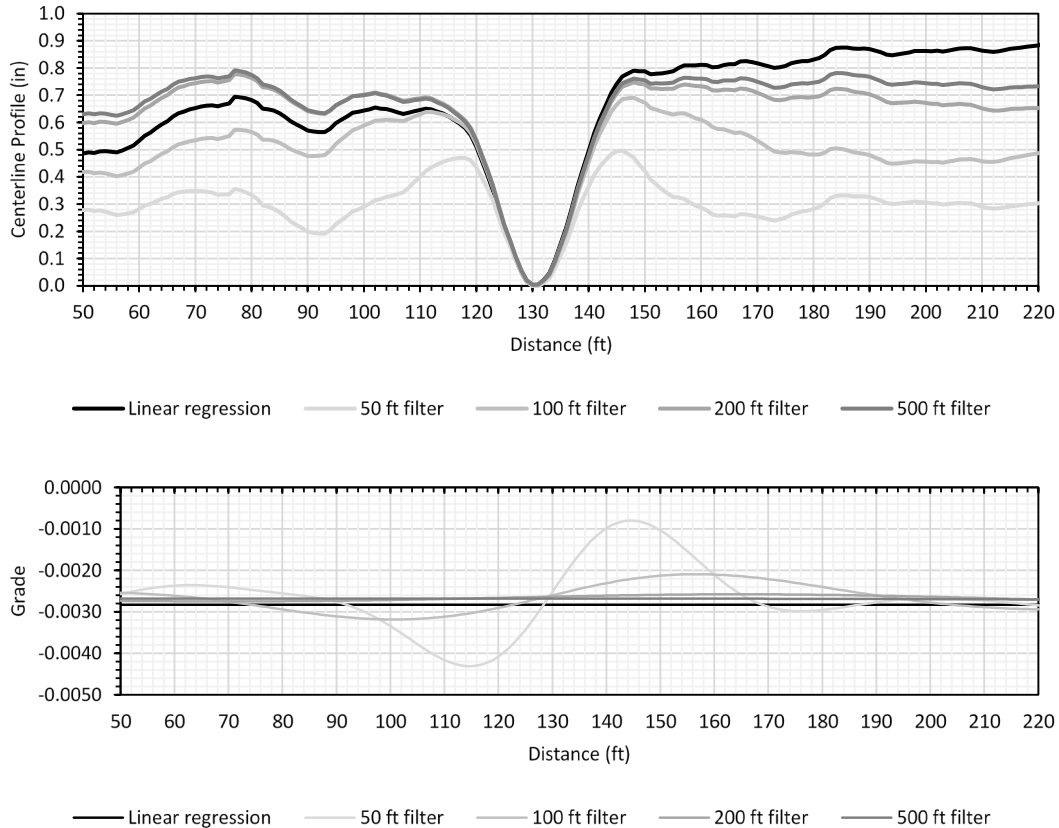
Figure 33. Track centerline profile (top) and grade (bottom) as functions of filter cutoff wavelength

Another issue to consider is the operating speed limit on the track and the expected vehicle response at that speed. For example, on an FRA Class 1 track (speed of 15 mph for passenger vehicles and 10 mph for freight vehicles), it may not be practical to measure 300 ft (100 m) track irregularities, because their effect on vehicles at Class 1 track speeds would be insignificant. Furthermore, most inertial TGMS systems would not even be able to repeatedly measure such long wavelength irregularities at such low speeds. At the same time, Class 6 track is unlikely to have sharp curves and short spirals, so a longer cutoff wavelength is appropriate.

In the United States there is currently no regulation or standard for the filter cutoff length for space curve, and the decision is left to the individual railroads and TGMS manufacturers. For high-speed operations in the Northeast Corridor, Amtrak uses upper a cutoff wavelength of 400 ft (122 m), noting these larger wavelengths are mainly measured for ride quality rather that safety reasons (Li et al., 2016); North American freight and transit operators who choose to measure space curve generally use an upper cutoff wavelength between 70 to 100 ft (20-30 m), and FRA ATIP track geometry vehicles use an upper cutoff wavelength of 400 ft. European

standards and regulations use a tiered approach. Euronorm EN 13848 specifies four wavelength domains:

- D1 domain, which includes alignment and profile wavelengths between 3 and 25 m (10 and 82 ft); the lower cutoff can be adjusted down to 1 m (3 ft.). Irregularities in D1 domain are measured for all track classes.

- D2 domain, which includes alignment and profile wavelengths between 25 and 70 m (82 and 230 ft). D2 domain irregularities are measured for track with speed limit >160 km/h (99 mph).

- D3 domain, which includes alignment wavelengths between 70 and 200 m (230 and 656 ft) and profile wavelengths between 70 and 150 m (230 and 492 ft). D3 domain irregularities are measured for track with speed limit >250 km/h (155 mph).

- The optional D0 domain, described in the recent draft of Euronorm prEN 13848-1:2016, includes wavelengths between 1 and 5 m (3 and 16 ft). Other than the minimum sampling distance (0.1 m, or 0.3 ft), no requirements for this domain are currently defined.

This approach offers multiple benefits:

- It offers some flexibility in separating track design elements from track irregularities. As previously noted, rail tracks with higher speed limits tend to have shallower curves and longer spirals, allowing for longer cutoff wavelengths.

- Short-wavelength irregularities (i.e., D1 domain) and long-wavelength irregularities (i.e., D2 and D3 domains) can be assessed separately using different acceptance criteria. This is beneficial because long irregularities tend to have larger amplitudes and would dominate space curve if they were lumped together with short irregularities, and because shorter defects usually produce more severe vehicle reactions for the same amplitudes (Haigermoser et al., 2015).

- As vehicle speed increases, it becomes more sensitive to long irregularities, as can be illustrated by speed-wavelength-frequency relationship:

$$v = \lambda f \tag{14}$$

A similar tiered approach is used in the United Kingdom, but the cutoff wavelength lengths between the tiers of irregularities are different from EN 13848 (Lewis, 2011).

Figure 34 illustrates the relationship between track irregularity wavelengths, vehicle speed, and resonant frequencies that are typical for rail vehicle suspension. The relationship suggests that the EN 13848 wavelength ranges may not be wide enough to capture irregularities that may excite some of the lower resonant frequencies (i.e., carbody roll); however, roll mode is mainly excited by cross level irregularities, which are not supposed to be filtered.
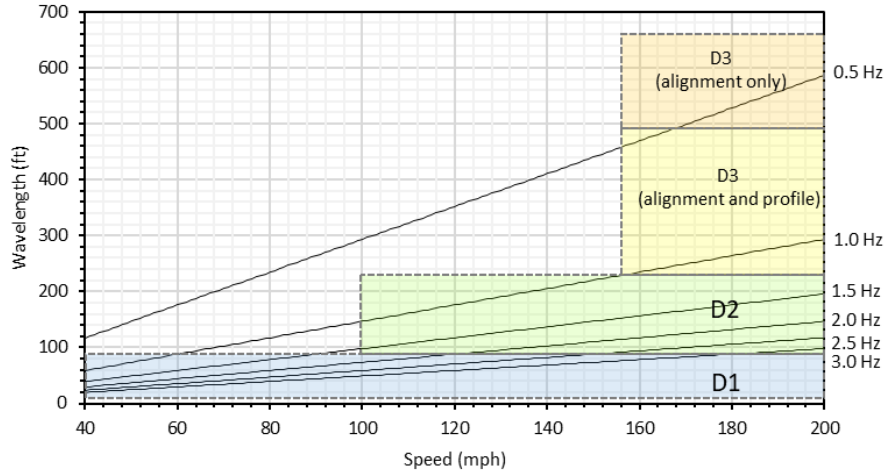
Figure 34. The relationship between wavelengths, vehicle speeds, and resonant frequencies; EN 13848 wavelength ranges are highlighted (Adapted from (Lewis, 2011))

For a detailed discussion of wavelength range as function of vehicle type, speed, and other considerations, see (Lewis, 2011).

5.3 Restoration of Space Curve from Chordal Measurements

Calculating chordal offset from measured space curve is simple; the inverse process (i.e., decoloring) is far more complicated. It is possible to partially restore space curve from chordal offset measurements (Cohen and Hutchens, 1970; Mauer, 1995; Grassie, 1996; Aknin and Chollet, 1999; Chung and Ham, 2004; Glaus, 2006; Naganuma and Yada, 2016; Wang et al., 2018a), or to extrapolate long chord offset data from shorter chord lengths (Carr et al., 2002), but a complete restoration of space curve data from MCO measurements alone is impossible. Track defects whose wavelength are close to even submultiples of chord length are irreversibly lost, and restoring perturbations with large wavelengths is difficult due to low signal to noise ratio. The process is further complicated by the effects of filters used to average MCO values over a distance.

Figure 35 shows a FFT magnitude illustrating an attempt to restore a space curve from MCO data. The first data series is the space curve measured by the TGMS aboard a vehicle; the second data series is a 62 ft MCO data recorded by the same TGMS; the third data series represents the space curve restored from the chordal measurements.
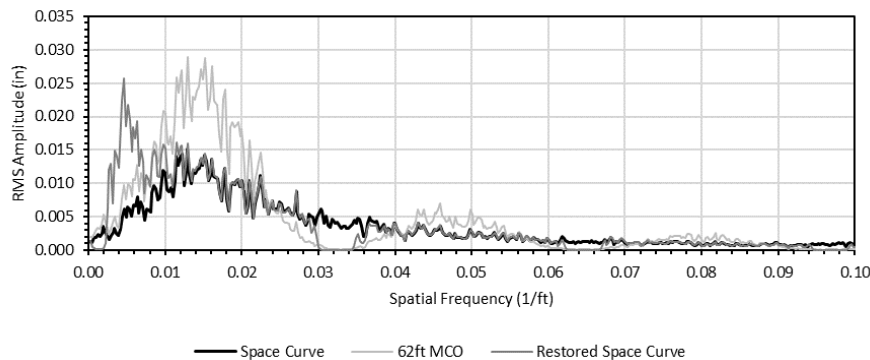
Figure 35. Space curve restoration from MCO measurements

42

In this example, track geometry data is restored remarkably well for wavelengths below ~85 feet (which is the cutoff wavelength used by this TGMS for computing the space curve). However:

1. Inevitably, there are holes in the restored space curve corresponding to the submultiples of chord length.

2. The restored space curve overestimates the amplitudes of long-wavelength perturbations (see Figure 22 and the accompanying discussion).

The quality of restoration may be improved by making asymmetric chordal measurements (Figure 20), or by combining chordal measurements with different chord lengths. With any restoration method, users must understand the range of wavelengths they are interested in measuring and the limitations of the restorative method. Frequency analysis can be a valuable tool in evaluating the quality of restoration (Haigermoser et al., 2013; Grabner, 2013a and 2013b).

5.4   Verification of TGMS Outputs

As discussed earlier, TGMS generally outputs alignments and profiles for left and right rails separately instead of centerline alignment and profile. Since TGMS also measure gauge and cross level, there is some redundancy between different measurement channels (see Table 2 and Equations (9)-(10)). If cross level and profile or gauge and alignment are measured with different sensors, this redundancy can be used to cross check the accuracy of data collected by the TGMS (see EN 13848-2:2006, Section A.3.2). This cross-check can be done in distance domain or wavelength domain by calculating cross-power spectral density, coherence, or transfer function (see Figure 36 and Section 7.2). Note that not only the magnitude and power but also the phase relationship between two outputs is important. Therefore, coherence or cross-power spectral density by itself is not a sufficient check.
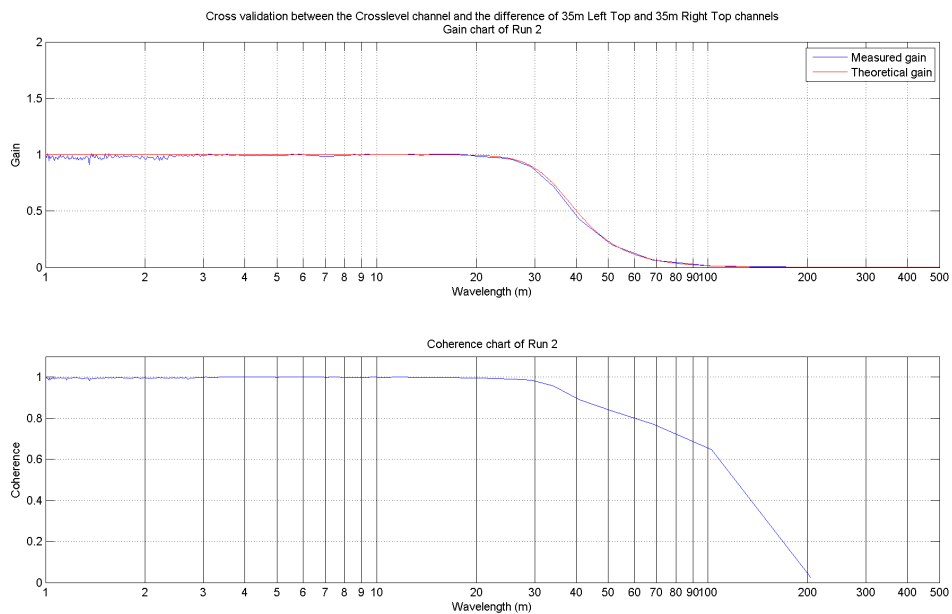
Figure 36. Example of a cross-check of TGMS measurements: transfer function gain (top) and coherence function (bottom) (Lewis, 2011)

Duplicate data in various channels can be a concern if the track geometry data is being collected for MBD simulation. For instance, a lateral track defect of a certain wavelength may be recorded in both curvature and alignment channels, which will cause the simulated vehicle's response to be overestimated. To avoid this, users of track recording vehicles must have a solid understanding of the given TGMS and its operating settings. For example, the software aboard a track recording vehicle may allow the operator to change the cutoff wavelength for alignment, but the measured track curvature may retain the same frequency content, leading to either redundant or missing alignment data. Choice of cutoff wavelength and methods of averaging MCO values have additional important implications (see Section 5.2).

6. Characterization of Track Geometry in the Distance Domain

In most cases, track geometry is assessed in the distance domain.

During this process, the outputs of a TGMS are being pre-processed and usually divided into shorter track segments. These segments are then analyzed using **statistical**, **parametrization**, or **vehicle response-based** methods.

With **statistical methods**, simple mathematic manipulations may need to be performed first (for example, track centerline alignment may be calculated from left and right rail alignment). For each track segment, statistical features are calculated. These features fall into one of two broad categories:

1. Features characterizing **isolated defects**, such as minima, maxima, and peak-to-peak values of track geometry variables (e.g., alignment, cross level, etc.), are used to characterize isolated defects, identify safety-critical defects, help determine maximum safe speed, and identify a need for immediate repairs.

2. Features characterizing the **overall track quality** of a segment, such as standard deviation of alignment and profile, are used to characterize the overall track roughness as a proxy for ride quality, or to prioritize track maintenance. Sometimes multiple statistical features are combined into parameters (i.e., **TQIs**).

The division between the two types of features is often blurred. The number and severity of isolated defects tends to correlate with overall track quality (Scanlan et al., 2016; Haigermoser et al., 2013), although this correlation is far from perfect. Furthermore, TQIs may be based on counting the number of defects in a track segment.

Parametrization methods involve describing individual track irregularities using deterministic functions, wavelets, and triangles (Section 6.5).

Vehicle response-based methods of various complexity attempt to describe track irregularities in terms of predicted vehicle reaction forces (Section 6.6).

Finally, features from many track segments can be aggregated and analyzed; for example, probability distribution of standard deviations among track segments may be calculated.

6.1 Pre-Processing

Data cleanup. Raw track geometry measurements often contain artifacts and other invalid data which must be removed or overwritten before further processing. This data includes:

- Segments of data where alignment and profile measurements are unreliable because the speed of the track geometry vehicle was too low for an accurate measurement

- Dropouts and spikes in signal due to:
  - Bolted joints and special track work, such as guardrails, frogs, and diamond crossings, where laser sensors fail to properly measure rail position
  - Obstruction of sensors by dust, debris, sun glare, rain, snow, etc.
  - Other malfunctions

Removal of signal artifacts and other invalid data is a challenging process. Ideally, an observer should be present aboard a track geometry measuring vehicle to identify and mark locations with unreliable measurements. When this information is unavailable, some artifacts can be detected and removed automatically in post-processing, e.g., by setting a threshold for rate of change of signal (Jia et al., 2014). For example, a 2-inch increase in gauge over a 1-ft distance is likely an artifact and not a real defect, since the track geometry vehicle did not derail or was otherwise damaged.

Position synchronization. A challenge arises when track geometry data from two or more measurement runs needs to be overlaid to assess repeatability of measurements or degradation of track geometry over time. Imperfections in measuring distance along the track (e.g., wheel tachometer error, lack of GNSS data) make this process quite complicated. Several solutions to this problem have been proposed (Hanreich et al., 2002; Jia et al., 2014; Xu et al., 2014; Wang et al., 2018b; Weston et al., 2015). A closely related problem is matching the location of defects to the correct milepost locations (Xu et al., 2016; Pedanekar, 2006).

Filtering. Pre-processing of track irregularity data may require additional filtering. For example, EN 13848 specifies different acceptance criteria for different irregularity wavelength ranges (e.g., D1, D2, D3). If the space curve has not already been broken into these ranges by the software aboard the TGMS, this step must be performed separately. Some railroads and regulatory bodies apply band-pass filters designed to detect certain irregularities which are likely to cause vehicle resonance (Figure 37).
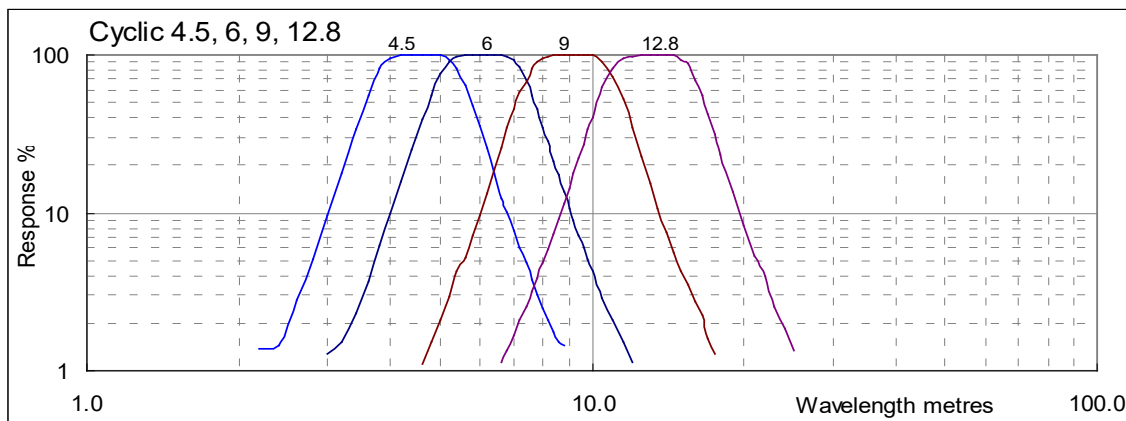
Figure 37. Band-pass filters used to isolate cyclic profile irregularities associated with submultiples of rail length (Lewis, 2011)

6.2 Track Segmentation

It is often necessary to break down data from long track sections into shorter sections to characterize each section separately. The sections can be of fixed length. EN 13848-5:2017 gives a typical value of 200 m (656 ft) for calculating standard deviation; most European railway operators use this interval (Haigermoser et al., 2013). In Japan, track quality index is calculated over 100 m (329 ft) and 500 m (1,640 ft) segments (Liu et al., 2015). In China, 200 m and 500 m segments are used (the latter is used for high-speed track). The 200 m length was proposed for calculating TQI in the Beijing Metro system (Liu et al., 2015). Sadeghi et al. (2017) used 1 km (3,280 ft) segment lengths. In Sweden, Q-Value is calculated over 1 km (3,280 ft) (Berawi,

46

2013) or 200 m sections (Arasteh Khouy et al., 2016). The 200 m segments are used in India (Berawi, 2013) and the Netherlands (Liu et al., 2015). Union Pacific Railroad uses 1-mile track segments (Brown and Ashmore, 2018). Network Rail (UK) uses 1/8-mile sections (Lewis, 2011). TTCI's experience with correlating track geometry with vehicle response statistics based on NN analysis suggests an optimum segment length of about 0.1 mile (Meddah, 2018).

In some cases, track may be segmented by layout type. For example, the length-based TQI developed by ENSCO and FRA (El-Sibaie and Zhang, 2004; Zhang et al., 2004) is calculated from 0.1-mile fixed length segments in tangent track; in curves and spirals, section length is tailored to the length of a spiral or a curve but does not exceed 0.1 mile. For switches, sections are 250 ft long; for crossings, 300 ft; and for bridges and tunnels, 400 ft. Jovanovic (2004) advises against fixed length segmentation and recommends segmenting the track in such a way to allow each segment to be as uniform as possible in terms of its degradation behavior; this requires knowledge of track layout, operational characteristics, track component types, presence of turnouts, bridges, culverts, grade crossings, etc.

6.3   Exploratory Data Analysis

Exploratory data analysis is an approach to data analysis that uses a variety of methods to provide insight into a data set (e.g., to determine the type of statistical distribution of a variable). Although it is not routinely performed when assessing track geometry quality, it may be a necessary step when deciding between different track geometry characterization methods (Sections 6.4 – Section 6.7). For example, if a track geometry variable shows an extremely skewed distribution, then track quality indices based on standard deviation should not be relied upon to predict maximum irregularity values.

Care must be taken not to generalize results from exploratory analysis of a track segment onto the entire rail system. Lasisi and Attoh-Okine (2018) show examples of the relationship between track geometry variables changing dramatically depending on which section of track is being analyzed.

Visual methods. Histograms provide a qualitative assessment of distribution of track geometry variables, although they should not be relied upon to determine if a variable is normally distributed. Other visual methods include box plots, Probability-Probability (P-P) plots, Quantile-Quantile (Q-Q) plots, and steam-and-leaf plots (Ghasemi and Zahediasl, 2012).

Normality tests provide quantitative evidence of normality of variable distribution. Some of the most common methods are the Kolmogorov-Smirnov test and the Shapiro-Wilk test (Ghasemi and Zahediasl, 2012). For example, Iyenger and Jaiswal (1995) used the Kolmogorov-Smirnov test to assess the normality of track profile measurements data, and Krug and Madejski (2018) used the Anderson-Darling method for the same purpose. Generally, different normality tests performed on the same data set give similar results, except in some borderline cases.

Covariance and correlation matrices. A covariance matrix is a matrix in which each member represents the covariance between two variables (e.g., left and right rail alignment). A closely related concept is a correlation matrix. If a linear least-square fit is calculated for a scatter diagram of two variables, the correlation coefficient (*R*-value) of 0 indicates no linear correlation between the variables, –1 indicates total negative linear correlation, and +1 indicates total positive linear correlation (Lasisi and Attoh-Okine, 2018). Performing this analysis on multiple combinations of track geometry variables results in a correlation matrix, in which each member

represents a correlation coefficient between two variables. For a linear regression model with a single input and a single output variable, a square of correlation coefficient (R^2 value) represents the amount of variation of the output variable that is explained by the regression.

Cross-correlation functions. Because track geometry variables can be treated as continuous functions of distance, their cross-correlation functions can be calculated. A cross-correlation function provides more information than a correlation coefficient; for example, it can identify time delay between two signals. The counterpart to a cross-correlation function in the wavelength domain is a cross-power spectral density function (see Section 7.2).

6.4 Irregularity Analysis: Statistical Approach

The opinions in the literature vary regarding the appropriate statistical treatment of track geometry in general. Iyengar and Jaiswal (1995) performed exploratory analysis of profile data from Indian Railways and concluded that the vertical track irregularity is well-approximated by a stationary Gaussian random model, and the peak amplitudes of vertical irregularities can be sufficiently well predicted accordingly.

On the other hand, the FRA-sponsored study of track irregularity data collected in the United States in 1970s and 1980s (Corbin, 1980; Hamid et al., 1983; Fazio and Corbin, 1986) concluded that track irregularities are best described by a combination of three processes:

1. A **continuous stationary random (Gaussian) process**. In the distance domain, it can be well described by a single roughness parameter (e.g., standard deviation) that is strongly related to track class.

2. A **periodic deterministic process** that describes uniform track irregularities, usually due to bolted rail joints. Welded joints may also show this effect, although less noticeably; analysis of European track geometry data shows other periodic irregularities, which are not apparently related to rail length (see Section 7.3). The periodic deterministic process and continuous stationary random process collectively constitute a **periodically modulated random process**.

3. **Track geometry anomalies**, which are defined as obvious physical interruptions in track structure. These anomalies define peak geometry values and are responsible for the majority of track Class exceptions.

Krug and Madejski (2018) cite studies with differing views on the mathematical nature of track irregularity distribution. After analyzing a large track geometry data set, they conclude that track irregularities, as a rule, are not normally distributed, consistent with the conclusions of the FRA study.

Many of the statistical features and indices described in Section 6.4.1 – Section 6.4.4, such as standard deviation and its functions, are good descriptors of a continuous stationary random process but not of a periodic deterministic process or anomalies. The latter especially may benefit from approaches described in Section 6.5.

6.4.1 Combining Track Geometry Variables

Before extracting statistical features, such as local maxima or standard deviation, track geometry variables may need to be combined, usually in a form of a linear combination. For example, EN

13848-6:2014 defines variables "combination of alignment" $\bar{y}$ (average of left and right rail alignment) and "sum of cross level and alignments:"

$$\bar{y} = \frac{y_L + y_R}{2} \tag{15}$$

$$s = \bar{y} + \Delta z \tag{16}$$

Other combined variables involve a combination of derivatives of irregularities in distance domain. For example, in Austria, a TQI called MDZ is used, which is based on calculating a change of acceleration from changes in lateral and vertical alignment. Although it is designed for use with chordal data, it can be modified for use with space curve data (Schubert, 1970, as cited in Haigermoser et al., 2015):

$$MDZ = c\frac{1}{L}v^{0.65}\sum_{i=1}^{L/\Delta x}\sqrt{\Delta z_i^2 + (\Delta y_i + \Delta cl_i)^2} \tag{17}$$

where Δy_i, Δz_i, and Δcl_i are, respectively, alignment surface, and cross level difference between two successive points (mm), v is train speed (km/h), c is scaling coefficient, L is measurement distance (m) and Δ_x is sampling interval (m).

Combined alignment and profile deviations. FRA regulations specify limits for combined track alignment and profile deviations. The following limit applies to outside rail in a curve for all track classes, as well as for any rail on Class 9 track (tangent or curved):

$$\frac{3}{4} \times \left|\frac{y_{MCO}}{y_0} + \frac{z_{MCO}}{z_0}\right| \leq 1 \tag{18}$$

where y_{MCO} and y_0 are, respectively, measured alignment MCO and the limit for the MCO at the same chord length specified in Appendix A; similarly, z_{MCO} and z_0 are measured profile MCO and the limit specified in Appendix A. Note the sign convention. 49 CFR §213.332 defines outward alignment deviation as positive and inward deviation as negative; for profile deviation, downward is positive and upward is negative.

6.4.2 Feature Extraction

Although the same feature extraction techniques can be used on space curve and chordal data, the results are obviously not directly comparable.

The most common features extracted from track irregularity signals are minimum and maximum values, mean, standard deviation (usually calculated over defined length – see Section 6.2), and percentiles.

Minima and maxima. FRA Track Safety Standards are based on minimum and maximum values of gauge, cross level, left and right rail alignment, and left and right rail profile, expressed in MCO format (see Appendix A). Chord lengths of 31 and 62 ft are used for all track classes, and a 124-ft chord is additionally used for track Class 6–9. The variable "31-ft runoff at the end of a raise" is generally interpreted as the peak-to-peak value of the rail profile space curve within a 31-ft window. A similar approach, albeit with different exception limits, is used by the U.S. Federal Transit Administration (FTA), by regulatory bodies in many countries, by individual railroads, and by transit agencies.

49

European standard EN 13848-5 defines three exception limits, from least to most severe: action limits, intervention limits, and immediate action limits. These are based on minima, maxima, and the rolling 100-m average of space curve variables. Immediate action limits are prescribed by EN 13848-5, while action limits and intervention limits are left up to the individual railroad operators to decide, although EN 13848-5:2017 lists typical values as a guideline.

Average square deviation is a statistic which was used by Amtrak (Ebersöhn and Conrad, 2003, as cited in Sadeghi, 2010; Craft, 2018):

$$R^2 = \sum_{i=1}^{n} \frac{d_i^2}{n} \tag{19}$$

where d_i is a deviation from nominal value at each measurement point, and n is number of data points in a given track segment. R^2 values, referred to as roughness index, are calculated separately for profile and alignment (MCO format), gauge, and cross level.

Standard deviations (SD) of track geometry variables are often used to characterize track quality and monitor its deterioration; several models (Esveld et al., 1988; Muinde, 2018; Soleimanmeigouni et al., 2018b; Andrews et al., 2014) assume that SD of alignment and profile increases linearly with time or gross tonnage. Some models describe a "sawtooth" pattern, where SD increases linearly after a brief period of higher increase rate (Berawi, 2013; Karttunen, 2015). EN 13848-6:2014 proposes the use of SDs of alignment, profile, and sum of cross level and alignment (Equations (15), (16)) to characterize track geometry quality. The same standard also proposes a combined standard deviation parameter (see Section 6.4.3).

Spatial derivatives. It has been suggested based on analysis and MBD simulations that vehicle response correlates better with second-order spatial derivatives of track irregularities than with their amplitudes (Li et al., 2012), although comparison with measured vehicle reaction does not always show a benefit (Haigermoser et al., 2015). Nevertheless, several derivative-based methods have been proposed.

EN 13848-6:2014 describes a point mass acceleration (PMA) method, based on calculating lateral, vertical, and combined acceleration of a point mass moving at a height z_{cg} above the track centerline:

$$\begin{aligned}
\Psi &= \frac{z_L - z_R}{W} \\
a_y &= cv^n(\ddot{y} + z_{cg}(\ddot{z} - \ddot{\Psi})) \\
a_z &= cv^n \ddot{z} \\
a_{yz} &= \sqrt{a_y^2 + a_z^2}
\end{aligned} \tag{20}$$

where a_y, a_z, and a_{yz} are, respectively, lateral, vertical, and combined accelerations of the point mass, v is maximum line speed, c and n are scaling constants, W is nominal track width ("cant base"), and other variables are as previously defined. The derivatives are with respect to distance along the track.

Fraction of non-conforming points is another statistic which can be used in conjunction with other statistical features. In Japan, P-index is defined as the fraction of sampling points within a given track segment whose parameter measurements fall outside a ±3mm limit value (Liu et al., 2015). A similar approach is used in Poland with w_5-index (see Section 6.4.4) and in Sweden

with K-index, defined as a percentage of track length where none of the standard deviation parameters exceed a limit (Anderson, 2002, as cited in Berawi, 2013).

Number of exceedances per track length. In India, Composite Track Record (CTR) is defined as (Talukdar et al., 2006):

$$CTR = 100 - (UA + TA + GA + AB) \tag{21}$$

where *UA*, *TA*, *GA*, and *AB* are, respectively, number of profile, twist, gauge, and alignment peak values exceeding safety limit per 1 km of track. In the United States, certain profile and exception limits are specified in terms of several non-overlapping deviations within a certain distance (49 CFR §213).

Other statistical variables, such as skewness and kurtosis (i.e., measures of asymmetry and sharpness of the peak of the probability distribution function) have been studied but are not widely used (Haigermoser et al., 2015).

Distribution functions. Krug and Madejski (2015 and 2018) analyzed a large volume of track geometry measurements and concluded that track irregularities, in general, are not normally distributed, and standard deviations space curve variables cannot accurately predict extreme values of irregularities (see Section 7.3 for more on this topic) They concluded that standard deviations are not appropriate indicators of track quality, and instead proposed describing each track segment by its distribution function or by a Quasi Cumulative Distribution Function (QCDF), $\ell_\Sigma(s)$, defined as a "cumulative length of the track irregularity with the size equal or larger than the threshold s" (Krug and Madejski, 2018). The value of QCDF varies from 0 for infinitely large irregularities ($\ell_\Sigma(\infty) = 0$) to value equal to track length for infinitely small irregularities ($\ell_\Sigma(0) = L$).

Length-based indices. A length-based TQI has been developed in the United States under the guidance of FRA (El-Sibaie and Y. Zhang, 2004; Zhang et al., 2004). It is based on the fact that the rougher the space curve is, the larger the ratio between the length of the space curve stretched in a straight line (L_s) to its "unstretched" length (L_0):

$$TQI = \left(\frac{L_s}{L_0} - 1\right) \times 10^6 \tag{22}$$

A separate TQI is calculated for profile, alignment, cross level, and gauge over each 0.1-mile long track segment. The stretched space curve length is estimated as the sum of distances between two consecutive points:

$$L_s = \sum_{i=1}^{n} \sqrt{\Delta y_i^2 + \Delta x_i^2} \tag{23}$$

where Δx is sampling spacing, Δy is the difference in measurements between two consecutive data points, and n is the number of data points in the segment.

A possibility of using fractal analysis as a means of deriving a TQI by characterizing a roughness of a space curve has been explored (Hyslip et al., 2002). From the various methods to perform this task, Hyslip et al. chose a divider method, which approximates the shape of a line by a piecewise linear function with increasingly smaller steps. They proposed quantifying the

roughness of chordal measurements (e.g., vertical profile, alignment, etc.) with 1st and 2nd order fractal dimensions, D_{R1} and D_{R2}, the first of which characterizes large-scale roughness and the second of which characterizes small-scale roughness. Fractal analysis of vertical irregularities has recently been used by Austrian Federal Railways (Landgraf, 2016).

6.4.3 Combining Extracted Features

Extracted features (e.g., minima and maxima, SD, etc.) are often combined into a single parameter. Note that this is not the same as combining track geometry variables and extracting features from these combinations (see previous sections). When variables are combined first, the effects of their interaction (i.e., alignment defect occurring simultaneously with profile defect) are considered, whereas combining features extracted from separate variables does not differentiate whether defects occur simultaneously or not. Another important note is that the quality of track alignment, profile, etc., often degrades at different rates (Berawi et al., 2010), and this information is lost when different statistics are combined into one.

Many TQIs are based on combinations of the standard deviations of key track geometry parameters (e.g., alignment, profile, cross level, and gauge) calculated over a specified track length.

Euronorm TQIs. Euronorm EN 13848-6:2014 defines Track Quality Classes (TQCs) based on combining standard deviations of left and right rail alignment and left and right rail profile in space curve format:

$$\overline{\sigma_y} = \frac{1}{2}(\sigma_{yL} + \sigma_{yR}) \tag{24}$$

$$\overline{\sigma_z} = \frac{1}{2}(\sigma_{zL} + \sigma_{zR}) \tag{25}$$

For each of the six speed ranges, five TQCs are defined, where TQI thresholds for each class are based on measurements of European rail network. Within each speed range, class A represents the best 10th percentile of European track of that speed range, class B represents 10th to 30th percentile, class C represents 30th to 70th percentile, class D represents 70th to 90th percentile, and class E represents 90th percentile (i.e., the worst 10 percent of European track).

The same standard also proposes combining weighted standard deviations of centerline alignment, gauge, cross level, and centerline profile into a "combined standard deviation" (CoSD) parameter:

$$CoSD = \sqrt{w_{\overline{y}}\sigma_{\overline{y}}^2 + w_{\Delta y}\sigma_{\Delta y}^2 + w_{\Delta z}\sigma_{\Delta z}^2 + w_{\overline{z}}\sigma_{\overline{z}}^2} \tag{26}$$

Weighing factors and limits for the combined parameter are left up for the individual railroad to determine based on specific purpose (for example, $w_{\Delta y}$ for planning of tamping operations should be 0, since tamping does not correct gauge deviation).

China. In China, TQI is an average of the SDs of seven different track geometry variables (i.e., left and right alignment, left and right profile, cross level, gauge, and twist) (Li and Xiao, 2014; Liu et al., 2015; Higgins and Liu, 2018). The recently proposed Generalized Energy Index (Section 7.5) uses the same approach, except SDs are replaced with energy indices corresponding to the seven track geometry variables.

J-coefficient. In Poland, synthetic track quality coefficient J is used (Sadeghi, 2010; Madejski and Grabozyk, 2002; Haigermoser et al., 2015):

$$J = \frac{\sigma_y + \sigma_z + \sigma_{tw} + 0.5\sigma_{\Delta y}}{3.5} \tag{27}$$

where σ_{tw} is the standard deviation of twist on a 5-meter base, and alignment and profile are in 10-m chord MCO format.

Track Geometry Index (TGI). In India, a TGI based on standard deviations has been proposed (Talukdar et al., 2006; Berawi, 2013). The TGI is calculated for each 200-m track segment and then five segments inside each 1 km are averaged.

$$TGI = \frac{2UI + TI + GI + 6ALI}{10} \tag{28}$$

where *UI*, *TI*, *GI*, and *ALI* are (vertical) unevenness index, twist index, gauge index, and alignment index, defined as follows:

$$UI = 100 \times \exp\left(-\frac{\sigma_{z,m} - \sigma_{z,n}}{\sigma_{z,u} - \sigma_{z,n}}\right) \tag{29}$$

$$TI = 100 \times \exp\left(-\frac{\sigma_{tw,m} - \sigma_{tw,n}}{\sigma_{tw,u} - \sigma_{tw,n}}\right) \tag{30}$$

$$GI = 100 \times \exp\left(-\frac{\sigma_{g,m} - \sigma_{g,n}}{\sigma_{g,u} - \sigma_{g,n}}\right) \tag{31}$$

$$ALI = 100 \times \exp\left(-\frac{\sigma_{y,m} - \sigma_{y,n}}{\sigma_{y,u} - \sigma_{y,n}}\right) \tag{32}$$

In these definitions, subscript "m" is measured value, "u" is value prescribed for urgent maintenance, and "n" is value prescribed for new track. Profile is in the format of MCO with 9.6-m (31-ft) chord length, alignment is in the format of MCO with 7.2-m (24-ft) chord length, and twist is in 3.6-m (12-ft) base. $\sigma_{y,m}$ and $\sigma_{z,m}$ are measured by averaging standard deviations of left and right rail alignment and profile, respectively:

$$\sigma_{y,m} = \frac{\sigma_{y,L} + \sigma_{y,R}}{2} \tag{33}$$

$$\sigma_{z,m} = \frac{\sigma_{z,L} + \sigma_{z,R}}{2} \tag{34}$$

Sadeghi et al. (2017) adjusted the weighing coefficients in the Indian TGI method based on correlation coefficients between the ISO Ride Comfort Index calculated from vehicle accelerations (ISO 2631-1:1997) and track geometry variables.

Q-Value. In Sweden, a "Q-value" TQI is used (Anderson, 2002, as cited in Sadeghi, 2010; Haigermoser et al., 2015):

$$Q = 150 - \frac{100}{3}\left(\frac{\sigma_H}{\sigma_{H,\text{lim}}} + 2\frac{\sigma_S}{\sigma_{S,\text{lim}}}\right) \tag{35}$$

where σ_H is the mean of SDs of left and right rail profile, σ_S is mean of SDs of alignment, gauge, and crosslevel, and $\sigma_{H,\text{lim}}$ and $\sigma_{S,\text{lim}}$ are maximum permissible values for a given track class. The

index is designed to be used with track geometry measurements in a format of MCO with 12-m (39-ft) chord length.

Overall Track Geometry Index. Sadeghi (2010) proposed an Overall Track Geometry Index (OTGI), which is based on mean (μ) and standard deviation (σ) values of space curve variables in a given track segment:

$$OTGI = \frac{\frac{w_{g+}}{2}p_g^+ + \frac{w_{g-}}{2}p_g^- + w_y p_y + w_z p_z + w_{tw} p_{tw}}{\frac{w_{g+} + w_{g-}}{2} + w_y + w_z + w_{tw}} \tag{36}$$

where w_{g+}, w_{g-}, w_y, w_z, and w_{tw} are weighting factors corresponding to wide gauge, narrow gauge, alignment, profile, and twist irregularity, respectively, and p_g^+, p_g^-, p_y, p_z, and p_{tw} are quality indexes corresponding to these parameters:

$$p_g^+ = |\bar{\mu}_g + 3\sigma_g| \tag{37}$$

$$p_g^- = |\bar{\mu}_g - 3\sigma_g| \tag{38}$$

$$p_y = \frac{1}{2}\left(|\bar{\mu}_{yL}| + 3\sigma_{yL} + |\bar{\mu}_{yR}| + 3\sigma_{yR}\right) \tag{39}$$

$$p_z = \frac{1}{2}\left(|\bar{\mu}_{zL}| + 3\sigma_{zL} + |\bar{\mu}_{zR}| + 3\sigma_{zR}\right) \tag{40}$$

$$p_{tw} = |\bar{\mu}_{tw}| + 3\sigma_{tw} \tag{41}$$

The weighting factors and OTGI ranges for each track class are calculated from the tolerance intervals for track geometry defects in a given class.

Combined TQI (CN, Canada). Canadian National Railway Company (CN) calculates a combined TQI by averaging the TQIs of six parameters (i.e., gauge, cross level, left and right profile, and left and light alignment) over a track segment (Liu et al., 2015). Partial TQI for each parameter is defined as:

$$TQI_i = 1000 - C\,\sigma_i^2 \tag{42}$$

where σ_i is standard deviation for a given parameter, and C is a constant whose value is 700 for mainline track.

UPRR TQI (Union Pacific RR, USA). Union Pacific Railroad (UPRR) calculates a TQI for each 1-mile track segment. The TQI is defined as an average of Surface Quality Index (SQI) and Gauge Quality Index (GQI) (Brown and Ashmore, 2018).

The SQI is a weighted sum of standard deviations of left and right profile and alignment (62-ft MCO format):

$$SQI = \frac{0.5\left(\sigma_{yL,MCO62} + \sigma_{yR,MCO62}\right) + 1.0\left(\sigma_{zL,MCO62} + \sigma_{zR,MCO62}\right)}{3} \tag{43}$$

The GQI is based on gauge deviation within the curved and tangent sections of a track segment:

$$GQI = \frac{n_T \sigma_{\Delta y,T} + n_C \sigma_{\Delta y,C}}{n_T + n_C} \tag{44}$$

where $\sigma_{\Delta y,T}$ and $\sigma_{\Delta y,C}$ are SDs of gauge deviation within the tangent and curved sections, and n_T and n_C are numbers of data points within the segment corresponding to tangent track and curves, respectively.

Track Geometry Interaction Map. Liu and Magel (2007) used multi-body dynamic simulations to correlate the peak-to-peak amplitudes of track geometry defects and the resulting wheel unloading and lateral-to-vertical (L/V) wheel force ratios. The results were presented as Track Geometry Interaction Maps (TGIM) showing the combinations of simultaneously occurring alignment and surface defects producing unsafe wheel loads. Based on these maps, Liu and Magel (2007) derived an empirical index called Track Geometry Interaction Map Parameter (TGIMP):

$$TGIMP = \left[\left(\frac{y}{y_0} \right)^m + \left(\frac{z}{z_0} \right)^m \right]^{\frac{1}{m}} \tag{45}$$

where y and z are peak-to-peak magnitudes of alignment and surface irregularities in the space curve format, y_0 and z_0 are their prescribed safety limits, and m is a parameter which can be adjusted based on the assumed strength of lateral-vertical interaction. TGIMP values below 1 are considered safe. Based on the results of the simulations, Liu and Magel proposed $y_0 = 50\ mm$, $z_0 = 50\ mm$, and $m = 2$ for the particular vehicle and conditions simulated.

Principal Component Analysis. Lasisi and Attoh-Okine (2018) describe a methodology for creating a combined TQI based on standard deviations and weighing factors. The latter are calculated using a rather complicated method based on Principal Component Analysis (PCA) and machine learning.

6.4.4 Aggregation and Statistical Analysis of Features

For peak values, the simplest aggregation method is a count of defects per track segment length (Roghani et al., 2015).

Another method is calculating the percentage of track conforming to a certain quality limit. For example, in Poland a five-parameter index (w_5) based on MCO data collected with 18.9-m (62-ft) chord length is used (Madejski and Grabozyk, 2002). The index w associated with each measured parameter (i.e., gauge, crosslevel, twist, alignment, and profile) is defined as a ratio of sum of length of defects (ΣL_i) to the total length of a track section (L):

$$w = \frac{\Sigma L_i}{L} \tag{46}$$

The combined index w_5 is a ratio of length of defect-free track segments to the total length of sections, calculated under the assumption that different irregularity types are independent of each other:

$$w_5 = 1 - (1 - w_g)(1 - w_{xlv})(1 - w_{tw})(1 - w_y)(1 - w_z) \tag{47}$$

In the Netherlands, Q-index is used to normalize σ_i the standard deviation of a given track geometry parameter over a 200-meter section of track, against σ_{i80}, the 80th percentile of standard deviations for 200-m (656 ft) segments within a maintenance section, ranging from 5 to 10 km (3.1–6.2 miles) in length (Liu et al., 2015):

55

$$Q = 10 \times 0.675^{\left(\sigma_i / \sigma_{i,80}\right)} \tag{48}$$

Euronorm EN 13848-6:2014 proposes the following ways to aggregate standard deviations or other TQIs from small track segments to determine the track quality class of the entire system: maximum TQI, mean TQI, percentiles of distribution of TQI, and percentage of track length conforming to a minimum track class. Maximum and mean values of TQIs are recommended for acceptance of track works and development of detailed working plans for track maintenance. Percentile of a distribution of TQIs is more appropriate as a key performance indicator in a high-level maintenance strategy, design of vehicles according to track quality requirements, and selection of track sections for vehicle acceptance testing. The same Euronorm also proposes a method of converting various non-standard TQIs into a standardized TQI used in the Euronorm (Equations (24)-(25)) based on their cumulative frequency distributions.

Liu et al. (2015) recommended using 80th percentile statistics for TQI distribution on the Beijing Metro system to plan for track maintenance since the Metro could perform mechanized maintenance on no more than 20 percent of its tracks annually.

Sharma (2016) normalized the value of TQI for each track segment (using El-Sibae and Zhang's length-based TQI) against the 95th percentile of its distribution over multiple inspection dates.

6.5   Irregularity Analysis: Parametrization Methods

Parametrization methods may help identify periodic irregularities and anomalies and separate them from stochastic irregularities. However, information on the specifics of these methods is relatively sparse, and their advantages over traditional statistical methods are unclear (see Section 6.7).

6.5.1 Analytical Descriptions

The FRA-sponsored study of track geometry in the 1970s/1980s (Corbin, 1980; Hamid et al., 1983; Fazio and Corbin, 1986) proposed a procedure for describing certain track irregularities as deterministic functions. No automated procedure has been proposed for identifying these irregularities and separating them from other irregularities, which makes it difficult to implement for processing large volumes of data.

The following function was proposed for describing rail joints as cusp of a shape:

$$y(x) = C e^{-k} |x| \tag{49}$$

where $y(x)$ is rail profile or alignment, C is joint cusp amplitude, and k is decay rate. Amplitude values are described by a stationary random process suggestive of Γ-distribution whose probability density function is described by:

$$P(C) = \left(\frac{4}{\bar{C}}\right)^4 \frac{C^3 e^{-\frac{4C}{\bar{C}}}}{6} \tag{50}$$

where $\bar{C}$ is mean amplitude. The study suggested $\bar{C}$ values for various FRA track classes.

Other functions were proposed for description of track anomalies (see Table 3 and Appendix B).

Table 3. Description of track anomalies (adapted from Hamid et al., 1983)

Name	Occurrence	Possibility of Existence					
		Δy	y_L, y_R	$\bar{y}$	z_L, z_R	$\bar{z}$	Δz
Cusp	Joints, turnouts, interlockings, sun kinks, buffer rail, insulated joints in CWR, splice bar joints in CWR, piers at bridges	**High**	Medium	Medium	Medium	Low	**High**
Bump	Soft spots, washouts, mud spots, fouled ballast, joints, spirals, grade crossings, bridges, overpasses, loose bolts, turnouts, interlockings	**High**	Medium	**High**	Medium	**High**	Low
Jog	Spirals, bridges, crossings, interlockings, fill-cut transitions	None	Low	**High**	None	**High**	Low
Plateau	Bridges, grade crossings, areas of spot maintenance	Medium	Low	Medium	Low	**High**	Low
Trough	Soft spots, soft and unstable subgrades, spirals	Low	Low	Medium	Low	Medium	None
Sinusoid	Spirals, soft spots, bridges	None	Low	**High**	Low	Medium	None
Damped Sinusoid	Spirals, turnouts, localized soft spots	Low	None	Low	Low	Low	Low
sin(x)/x	Localized soft spots, insulated joints	None	None	None	None	Low	None

6.5.2 Clustering and Wavelet Analysis

Kraft et al. (2015 and 2018) describe using multiple methods of **clustering** to identify track defects with repeated shapes. Clustering is a process whose purpose is "*to form groups of signals which have maximum similarity with other signals in this group and minimum similarity with signals in other groups*" (Kraft et al., 2015). Clustering can be shape-based (i.e., signals are stretched or contracted and then compared directly), feature-based (i.e., features are extracted from the signal, combined into a feature-vector, and then clustered), or model-based (i.e., model of the data is identified first).

A study by the European Rail Research Institute (ERRI, 1999) suggested a procedure for separating stationary components of irregularities from anomalies and proposed using wavelet analysis to describe anomalies.

6.5.3 Triangular Elements

The DYNOTRAIN project investigated parametrization of isolated track defects using triangular elements. Peaks of the space curve signal can be identified, using a certain minimum threshold for peak-to-peak distance. Each peak is then approximated with a triangular shape, whose height, base, area, height-to-base ratio, etc., can be used to parametrize the defect (Haigermoser et al., 2013).

6.6 Irregularity Analysis: Vehicle Response Methods

Several methods, collectively known as Vehicle Response Analysis (VRA), offer a compromise between calculating TQIs from track geometry described in the previous sections, and a vehicle-

specific analysis (e.g., MBD simulations or vehicle response measurements). These methods use track geometry measurements as input and attempt to predict the vehicle's response using analytical or empirical functions (Haigermoser et al., 2015). The complexity of these methods varies widely. For example, a series of MBD simulations may be performed in advance on a model of a specific vehicle, and the results are then used to derive a linear system of equations that ties track geometry variables to vehicle response. Features extracted from measured track geometry data can then be input into this linear system to yield outputs describing the vehicle's response to the measured track geometry.

EN 13848-6 VRA Method. The vehicle response analysis method described in EN 13848-6:2014 relies on detailed and well-validated MBD models of a vehicle to simulate the vehicle's response to a large variety of sinusoidal-shaped track irregularities of various amplitudes and wavelengths. Simulations are conducted at various speeds, track curvature, and superelevation values. The minimum and maximum lateral and vertical wheel forces and body accelerations are extracted from simulation results and normalized with respect to the safety limits in EN 14363. These vehicle reaction statistics are then related to the amplitudes and mean gradients of the track irregularities via a set of linear equations, which are solved to obtain a series of coefficients. To analyze measured track geometry, the space curve is broken into a series of individual irregularities. Amplitudes and gradients of these irregularities are combined with the coefficients calculated from MBD simulations to yield predicted vehicle reactions.

Neural Networks. Neural network (NN) approaches have been developed by the ERRI (ERRI, 1999, as cited in Haigermoser et al., 2015) and TTCI (Li et al., 2006). These approaches segment the track into sections, extract track geometry features from each section, and relate them to vehicle response parameters, such as percentiles of vertical and lateral wheel forces, via neural networks. The weights in the NN, which describe the relationships between inputs and outputs, are refined in an iterative procedure called NN training, which involves measured track geometry and measured vehicle response data. Once the NN is trained, it can be used to predict vehicle response from measured track geometry (Haigermoser et al., 2015; Karis, 2018).

Methods based on filters and transfer functions. Haigermoser et al. (2015) and Karis (2018) describe a number of other vehicle response analysis methods, including the VRA and Pupil method used in the Netherlands, Empirical Transfer Functions (ETF) methods developed in Austria, system identification methods developed in Japan, and a number of system identification methods developed in Europe under the DYNOTRAIN program. Some of these methods operate in the distance domain, others in the frequency or wavelength domain (see Section 7).

6.7 Comparative Assessment of Distance Domain Track Geometry Characterization Methods

FRA-sponsored TQI study, 1980s. In the early 1980s, several TQIs were studied as a part of an FRA-sponsored program (Hamid and Gross, 1981). The following TQIs were investigated:

- Gauge: mean, SD, 99th percentile, third moment of gauge in in^3, fourth moment of gauge in in^4

- Cross level: SD of cross level after subtraction of moving mean

- Warp: SD and 99th percentile of 20-ft warp

- Profile: SD of space curve, SD of 3-ft MCO, 99th percentile of 16-ft MCO

- Superelevation: RMS value of cross level deviation from balanced superelevation

- Alignment: SD of space curve, SD of 2-ft MCO, SD of 10-ft MCO, and SD of 16-ft MCO

The study concluded that there was a strong correlation between SD-based TQIs for alignment, gauge, profile, and cross level and the posted track class. Furthermore, each TQI generally correlated well with other TQIs of the same variable. However, the following final set of TQIs were recommended based on their ability to quantify track's ability to carry out its functional requirements, sensitivity to track degradation, computational complexity, and ease of interpretation: SD of gauge, 99th percentile of gauge, SD of 20-ft warp, SD of 10-ft alignment MCO, and SD of unbalanced superelevation.

DYNOTRAIN study, 2010s. In 2009-2013, track geometry and vehicle reaction measurements from approximately 1,500 km (900 miles) of track were studied under the European DYNOTRAIN research program. The results of the study are described in detail in (Haigermoser et al., 2013); a summary is given in (Haigermoser et al., 2014) and (Haigermoser et al., 2015). For each track segment, vehicle reaction statistics (i.e., minimum and maximum of body accelerations, vertical and lateral wheel forces, and L/V ratios) and various track geometry features (e.g., minimum, maximum, maximum of absolute value, standard deviation, outputs of VRA, PMA models, etc.) were measured and/or calculated. Multiple regression analysis was used to approximate vehicle response statistics as linear combinations of track geometry statistics, while controlling for the effects of vehicle speed, curvature, and cant deficiency. The end results were the R^2 values showing the correlations between track irregularity statistics and vehicle reaction statistics. Depending on a vehicle, type of track (i.e., tangent or curve), track geometry statistic, and vehicle response statistic, R^2 varied from very small (<0.1) to very large (>0.9) values.

For example, for measured values for maximum net axle lateral force (ΣY) the following regression equation was used by default:

$$\Sigma Y = \beta_0 + \beta_1 \kappa + \beta_2 a_y + \beta_3 \sigma_{\bar{y},D1} \tag{51}$$

where $\beta_{0,1,2,3}$ are regression coefficients, κ is track curvature, a_y is lateral acceleration due to cant deficiency, and $\sigma_{\bar{y},D1}$ is SD of track centerline alignment in D1 wavelength range.

Some of the key conclusions of DYNOTRAIN data analysis were:

- Overall, the method of track quality characterization described in EN 13848-6 (i.e., SDs of space curve variables filtered with D1/D2/D3 band-pass filters; see Section 5.2) is appropriate for track irregularity characterization. Alternative methods investigated do not offer significant, consistent benefits.

- All vehicles in the study (i.e., locomotive, passenger car, empty and loaded 4-axle freight cars, and empty 2-axle car) showed similar trends in terms of correlation between track geometry variables and vehicle responses.

- Unexpectedly, the correlations between SDs of irregularities and min/max vehicle reaction forces were slightly higher than between min/max of track geometry variables and min/max of vehicle reactions. Adding min/max of track geometry variables as an additional variable to the regression model did not result in significant improvements.

59

- Also, unexpectedly, statistics (i.e., min/max or SD) of first and second spatial derivatives did not offer a consistent improvement over standard method in terms of predicting vehicle reaction forces.

- Standard deviations of alignment and profile in D1 wavelength domain (3–25 m), e.g., $\sigma_{\bar{y},D1,}$ were better predictors of vehicle response that SD of the same variables in D1+D2 domain (3–70 m), e.g., $\bar{\sigma}_{y,D1+D2}$. However, adding SDs of D1 and D2 as separate variables in the regression model, e.g., $\beta_3\,\bar{\sigma}_{y,D1} + \beta_4\,\bar{\sigma}_{y,D2}$, improved results compared to using SD of D1 variables alone. This is consistent with the expectation that irregularities in different wavelength ranges have different effects on the vehicle.

- Compared to the standard method (i.e., SD values of individual space curve variables), the CoSD parameter (EN 13848-6:2014) improved correlation for some variables but reduced it for others.

- Compared to the standard method, using a combination of SD of alignment and SD of cross level to predict lateral reactions ($\beta_3\,\bar{\sigma}_{y,D2} + \beta_4\,\bar{\sigma}_{\Delta z}$) improved the results. The same was true, to a lesser extent, for a combination of SD of profile and SD of crosslevel to predict vertical reactions.

- Interestingly, correlations between vehicle response and statistics (peak-to-peak values and standard deviations) derived from asymmetric chord measurements were similar to the standard method.

- Parametrization of all track irregularities (not just anomalies) by Triangles and Mexican Hat wavelets did not improve the results compared to the standard method.

- The results from vehicle response modeling methods were mixed:

  - In most cases, the VRA method of EN 13848-6:2014 led to worse results than the standard method.

  - The PMA method as defined in EN 13848-6 led to worse results than the standard method.

  - Methods using adaptive filters and transfer functions based on MBD simulations showed better results than standard method in tangent track, but worse results in curves. However, if instead of actual measurements, vehicle reaction data from MBD simulations is used, these methods show superior results to standard methods. The authors of the study concluded these methods may have a potential to improve track geometry characterization and that more research is needed.

Other studies. Scanlan et al. (2016) analyzed track geometry data from 335 km of a mainline rail track. Three TQIs were compared: Polish J-Coefficient (Equation (27)), Sadeghi's OTGI (Equation (36)), and Swedish Q-value (Equation (35)). The authors of the study correlated these indices to the number of Class 5 exceptions (Transport Canada's Class 5 is similar to FRA Class 5). The study showed that Swedish Q-value as well as OTGI index both correlate well with the number of exceedances. Furthermore, the study found that OTGI index "may be able to provide additional information identifying track geometry irregularities independent of length of track used to define the standard deviation and mean" and Q-value "appears capable of providing additional track geometry condition information at bin sizes less than 100 m in length".

El-Sibaie and Zhang (2004) analyzed a large volume of data collected under FRA's ATIP program in the late 1990s and concluded that length-based TQIs (Equations (22)-(23)) differentiate between FRA track Classes better than standard deviations; for example, length-based gauge TQI of Class 4 track was 95 percent higher than of Class 5 track, whereas the difference between SDs of Class 4 and Class 5 track was only 35 percent.

Sharma (2016) used logistical regression to correlate the length-based TQI of a track segment with the probability of FRA track Class defects being present in the segment. The logistic regression generated from the data had a form:

$$P_d = \frac{\exp(\beta_0 + \beta_1 \cdot TQI)}{1 + \exp(\beta_0 + \beta_1 \cdot TQI)} \tag{52}$$

where P_d is the probability of track defects and $\beta_0 = -3.3457$ and $\beta_1 = -0.7490$ are constants calculated from the studied data set.

Camacho et al. (2016) assessed the track geometry quality of two short (600 m and 460 m) light rail tracks using the Euronorm SD method and Indian Railways' TGI method; they concluded that the Euronorm method seemed to be more appropriate for identifying short wavelength irregularities than TGI.

Krug and Madejski (2015; 2018) analyzed data from 466 track segments (200 m each) and concluded that standard deviations of track irregularities should not be used for track maintenance planning, because track irregularities, as a rule, are not normally distributed; instead, they recommended describing track segments in terms of cumulative probability distributions (see Section 6.3). The observation on non-normality is consistent with the findings of the FRA-sponsored study in the late 1970s (Corbin, 1980; Hamid et al., 1983; Fazio and Corbin, 1986).

For statistics based on spatial derivatives of space curves, different studies give conflicting results (Karis, 2018):

- The DYNOTRAIN project, as discussed above, showed that statistics bases on spatial derivatives do not show a consistent improvement over standard method (i.e., SDs of space curve) in terms of predicting vehicle response (Haigermoser et al., 2013).

- Another study based on DYNOTRAIN data showed inconclusive results (Lönnbark, 2012).

- A study on simple (i.e., 1 and 3 degrees of freedom) MBD simulations showed high correlations between second-order space curve derivatives and vehicle response (Li et al., 2012).

- A study based on the DYNOTRAIN and Green Train projects (Karis, 2018; Karis et al., 2018) found a similar correlation between vertical irregularities and vertical axle box acceleration and between second-order derivative of vertical irregularities and vertical axle box acceleration.

The general trend is that statistics based on second spatial derivative, at least for profile/surface, show good correlation with vehicle reaction forces and accelerations in simulations, but not in measured data. Karis (2018) suggests that this may be at least in part due to the failure to account

for variability in vertical track stiffness along the distance of the track and that more research on the use of second derivatives is needed.

7. Characterization of Track Geometry in the Wavelength Domain

The first steps in wavelength domain characterization are similar to distance domain characterization (see Section 6.1 – Section 6.2), but there are some differences:

1. Wavelength characterization almost always is performed on space curve data and rarely on MCO data.

2. Signal artifacts (e.g., spikes, small dropouts, etc.) may not need to be removed, because rare, isolated defects, depending on their frequency of occurrence, may not distort PSD plots as much as they distort TQIs and other distance domain statistics.

3. If the data is divided into track segments, they are usually longer that those used for distance domain analysis (EN 13848-6:2014 recommends a segment length of about 5 km for frequency analysis, noting that shorter segments can be analyzed with Short Time Fourier Transform (STFT) techniques). With spectrograms, sliding distance windows can be used (Figure 9).

4. Characterization of track curvature in the wavelength domain requires additional steps to be directly comparable to track centerline alignment data. One possible method is:

    4.1. Convert track curvature into inverse units of distance (i.e., from degrees to ft^{-1}) using Equation (2).

    4.2. Apply a high-pass filter with cutoff wavelength of about 500 to 1,000 ft (the numbers may need to be adjusted based on the given TGMS settings). This will eliminate the components of the curvature that are due to design elements (i.e., curves and spirals) and will leave the curvature changes associated with lateral track irregularities,

    4.3. Integrate the result twice with respect to distance to convert it into track centerline alignment.

    4.4. Convert the result into the units of space curve variables (i.e., inches). Multiply by (–1) if appropriate for the sign convention of the given TGMS.

The result can be now converted into wavelength domain and compared to the track centerline alignment to determine which lateral track irregularities are duplicated in curvature and alignment variables.

After pre-processing and segmentation, track geometry data is converted from distance domain into wavelength domain and, in some cases, parametrized. The next sections describe this process.

7.1 Fourier Transform and Power Spectral Density Estimation

The most common way to transform the signal from the distance domain into the wavelength domain is using **non-parametric methods**, which explicitly calculate the spectral content of the signal (**parametric methods**, which use auto-regressive or moving average models, are far less common). Non-parametric methods are generally based on Fourier Transform, which presents a signal as a sum of a series of sinusoidal functions (Berawi, 2013; Haigermoser et al., 2013; Heinzel et al., 2002; Smith, 1997). For a continuous signal $f(x)$, the Fourier transform is given:

$$F(k) = \int_{-\infty}^{\infty} f(x)e^{-2\pi jkx}dx \tag{53}$$

where k is wavenumber (spatial frequency):

$$k = 1/\lambda \tag{54}$$

For a discrete signal with N data points, the **Discrete Fourier Transform (DFT)** can be calculated, where the output corresponding to each wavenumber is:

$$F(m) = \sum_{n=0}^{N-1} f(n) \cdot e^{-2\pi j\frac{1}{N}nm} = \sum_{n=0}^{N-1} f(n)\cos\left(\frac{2\pi nm}{N}\right) - j\sum_{n=0}^{N-1}(n)\sin\left(\frac{2\pi nm}{N}\right)$$

$$(m = 0, ..., N-1) \tag{55}$$

where n is index of the input datapoint, m is the index of the waveform number, $f(n)$ is the input sequence (signal), and $F(m)$ is the output corresponding to the waveform index m. The index m can be converted into wavenumber $1/\lambda_m$ by:

$$\frac{1}{\lambda_m} = \frac{m}{N\lambda_s}, (m = 0, ..., N-1) \tag{56}$$

where λ_s is sampling distance.

The number of samples in the original signal N is also the number of frequency bins in the DFT. The factor $1/(N\lambda_s)$ is the frequency bin width, also called the frequency resolution.

The DFT of the signal sequence can be presented in magnitude and phase plots, where zero-to-peak magnitude A and phase angle ϕ corresponding to each waveform number are:

$$A(m) = |F(m)|, \Phi(m) = \angle\big(F(m)\big) \tag{57}$$

Zero-to-peak magnitude can be converted into root-mean-square (RMS) magnitude by dividing by $\sqrt{2}$. The units of DFT magnitude are the units of the signal (for most track irregularities, inches or mm).

DFT magnitude depends on the width of the frequency bin, $1/(N\lambda_s)$, which makes it difficult to compare DFT magnitudes of sections of track with different length or sampled at different distance intervals. One way to solve this problem is by calculating the **Power Spectral Density (PSD)** of the signal, which is approximated as a square of the DFT amplitude normalized by the frequency bin width:

$$P(m) = \frac{\lambda_s}{N}\left|\sum_{n=0}^{N-1} f(n) \cdot e^{-2\pi j\frac{1}{N}nm}\right|^2, (m = 0, ..., N-1) \tag{58}$$

PSD derives its name from the fact that in many cases, such as electrical circuits, physical power of the signal is proportional to the square of amplitude of the signal (Cusumano, 2005). The PSD measures signal "power" per wavenumber, which, in the case of track geometry data has units of $in^2 \cdot ft$ or mm^2/m. Unlike the magnitude of DFT, PSD does not depend on sampling rate or signal length. A PSD obtained with DFT is called a **periodogram**.

A PSD can also be described as a Fourier Transform of autocorrelation of the signal, i.e., of its correlation with a time-delayed version of itself. If a signal has a strong periodic component, then it will show a high autocorrelation for a corresponding time period and a corresponding peak in its PSD.

DFT works well as a method of PSD estimation when the signal length that is being processed contains an integer number of periods of sinusoidal waveforms, which is almost never the case. The fact that at least some of the frequencies will have a non-integer number of periods leads the spectral content of those frequencies to leak into neighboring frequency bins. This effect is called "spectral leakage." One way to combat it is by using an approach called **windowing**. The input in a time domain, signal $f(n)$, is multiplied by a function whose amplitude is maximum at the center of the input signal and minimum at the edges; DFT is then performed, and the resulting output sequence, $F(m)$, is scaled according to the window shape. While windowing reduces the effects of spectral leakage, it introduces other distortions, and those two effects should be balanced. There are many different types of window shapes, such as rectangular (which is equivalent to no windowing), flattop, triangular, Hamming, Hanning, Blackman-Harris, Kaiser-Bessel, and others. The choice of the windowing method depends on the nature of input signal. The Hanning window is generally considered appropriate for signals which have both periodic and random (i.e., noise) components, such as track irregularities (Cerna and Harvey, 2000; Wickramarachi, 2003). A PSD obtained with windowing is called a **modified periodogram**.

In software, DFT is usually implemented using a **FFT**, a family of algorithms relying on symmetric properties of the Fourier Transform to speed up execution. Some, but not all, FFT algorithms require the input sequence length N to be a power of 2 (256, 512, 1024, etc.) samples.

DFT is the most common method of PSD estimation, but not necessarily the most accurate, and it tends to result in a noisy output; the longer the track segment analyzed and the shorter the sampling distance, the noisier the output will be, which can make reading and interpreting PSDs difficult. While this noise can be reduced by down sampling the signal, thus reducing the number of bins, this effectively discards a large amount of data.

One of the solutions to the problem is Bartlett's method, which breaks the input signal into smaller segments, performs DFT on each segment, computes a PSD from the DFT amplitude, and then averages the PSDs of all segments. An improved variation of Bartlett's method, called Welch's method (The MathWorks, Inc., 2019a), uses overlapping segments and applies one of the windowing methods (see previous section) to each segment. The greater the number of segments, the smoother the resulting outputs. However, an excessive number of segments can cause the resulting PSD to significantly deviate from the original noisy shape, especially in signals with wide bandwidth content, such as gauge and cross level (Figure 38) (Haigermoser et al., 2013).
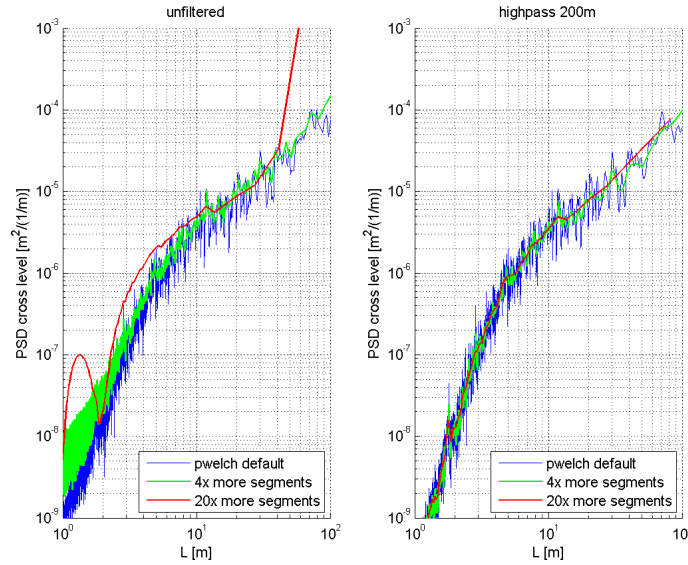
Figure 38. PSD of unfiltered cross level signal (left) and PSD of cross level signal pre-filtered with a 200-meter high-pass filter (right), both calculated with Welch's method (note the distorting effect of excessive number of segments) (Data from DYNOTRAIN project (Haigermoser et al., 2013))

7.2 Cross Power Spectral Density, Coherence, and Transfer Functions

PSD plots are used to examine the wavelength content of a standalone variable, such as gauge or left rail alignment. The relationship between two variables in the wavelength domain can be examined using mathematical methods that are closely related to PSD: **Cross Power Spectral Density**, **Coherence**, and **Transfer Functions**.

Cross Power Spectral Density (CPSD) shows the power density of the signal that is shared between two signals. The higher the CPSD value for a wavelength λ, the more similar the power of the two signals is at that wavelength (note that the two signals may not be in phase). CPSD is also described as a Fourier Transform of the cross-correlation function between two signals (recall that a PSD is the Fourier Transform of the autocorrelation of a signal). The CPSD of discrete signals is calculated by:

$$S_{xy} = \frac{\lambda_s}{N}(X \times \bar{Y}), X = \sum_{n=0}^{N-1} x(n) \cdot e^{-2\pi j \frac{1}{N}nm}, Y = \sum_{n=0}^{N-1} y(n) \cdot e^{-2\pi j \frac{1}{N}nm} \tag{59}$$

where S_{xy} is the CPSD of the two signals, $x(n)$ and $y(n)$ are their sequences in distance domain, X and Y are their Fourier transforms, and other variables are as previously defined.

Coherence is a way to normalize a CSPD by power density of the two individual signals. It can be calculated as follows (EN 13848-2:2006, Appendix A):

66

$$\Gamma = \frac{|S_{xy}|^2}{S_{xx} \times S_{yy}}, S_{xx} = \frac{\lambda_s}{N}\left|\sum_{n=0}^{N-1} x(n)\cdot e^{-2\pi j\frac{1}{N}nm}\right|^2, S_{yy}$$

$$= \frac{\lambda_s}{N}\left|\sum_{n=0}^{N-1} y(n)\cdot e^{-2\pi j\frac{1}{N}nm}\right|^2 \tag{60}$$

where Γ is (magnitude-squared) coherence of two signals, S_{xy} is their CPSD, and S_{xx} and S_{yy} are PSDs of each signal. Coherence is always between 0 and 1; $\Gamma = 0$ implies that the two signals are unrelated at that wavelength, and $\Gamma = 1$ implies that they are linearly related (though not necessarily in phase).

Coherence has been used to study the relationship between track geometry variables. Left and right rail alignment signals tend to have high coherence, especially at long wavelengths; the same is true of left and right profile signals. On the other hand, mean alignment, mean profile, gauge, and cross level signals have low coherence, i.e., are more or less independent (Corbin, 1980; Hamid et al., 1983; Haigermoser et al., 2015). An example of a coherence plot is shown in Figure 39.
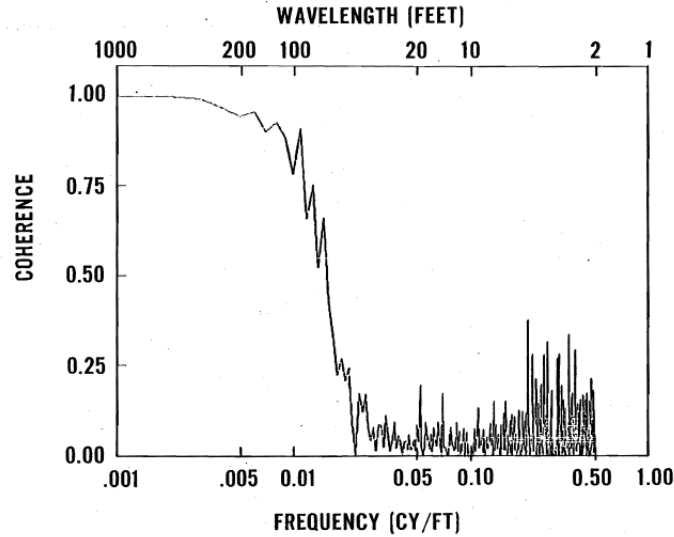
Figure 39. An example of coherence between left and right rail alignment (Hamid et al., 1983)

Transfer Function (TF) between two signals is an expression of distortions between the two signals in the wavelength domain, with one of them assumed to be an input and the other one an output. TF is the CPSD of the two signals normalized against the PSD of the input signal (EN 13848-2:2006):

$$H_{xy} = \frac{S_{xy}}{S_{xx}} = \frac{X\times\bar{Y}}{X\times\bar{X}}, \ X = \sum_{n=0}^{N-1} x(n)\cdot e^{-2\pi j\frac{1}{N}nm}, Y = \sum_{n=0}^{N-1} y(n)\cdot e^{-2\pi j\frac{1}{N}nm} \tag{61}$$

Transfer functions are usually displayed as magnitude and phase plots. If the phase plot shows significant noise, this should be viewed with caution; this noise may be a mere consequence of low amplitudes of two signals at that frequency (Smith, 1997).

FFT, PSD, TF and coherence functions are often used to verify outputs from TGMS (see Section 5.4). In some cases, frequency analysis of alignment data can reveal missing wavelengths and reveal if restoration of space curve data from MCO measurements has not been performed correctly (Haigermoser et al., 2013; Grabner, 2013a and 2013b).

7.3 Interpretation and Limitations of PSD

During the transformation from space curve to PSD, data from a large length is averaged and phase information is lost. Thus, the PSD does not fully describe the shape of the space curve. For example, a PSD of a signal consisting of large discrete random amplitude pulses may be identical to a PSD of a signal with small overlapping pulses (Corbin, 1980).

The extent to which a PSD describes track irregularity depends, to a large extent, on their statistical nature (see Section 6.4). If, as some studies suggest, track irregularity is well approximated by a stationary Gaussian random model, then the peak amplitudes of irregularities (and therefore track Class defects) can be sufficiently well predicted from the PSD. If, on the other hand, track irregularities are a combination of a continuous stationary random process, a periodic deterministic process, and track anomalies, like other studies suggest, then peak amplitudes cannot be predicted from the PSD alone.

A continuous stationary random process is adequately described by the PSD continuum (i.e., overall shape of the PSD curve). A periodic deterministic process describes uniform track irregularities, such as bolted rail joints. This process contributes to both PSD continuum and pronounced peaks in the PSD plot; such peaks are located at wavelengths corresponding to rail length and its submultiples, i.e., L, L/2, L/3, etc. (see Figure 40 and Figure 41). Track geometry anomalies represent isolated events that are not properly characterized by PSDs due to the averaging and phase suppression properties of PSDs. The PSD of track with anomalies looks similar to the PSD of the same track with anomalies removed (Corbin, 1980).
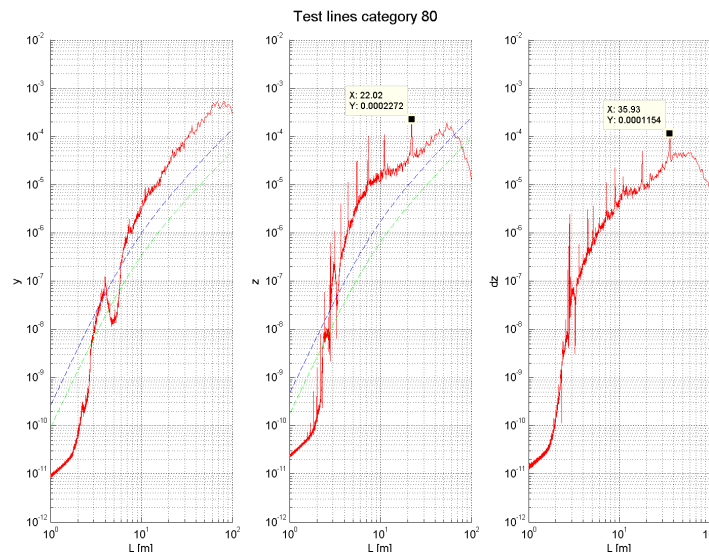
Figure 40. PSD of alignment, profile, and cross level, showing the effects of continuous stationary random process and a periodic deterministic process (Data from the DYNOTRAIN project (Haigermoser et al., 2013))
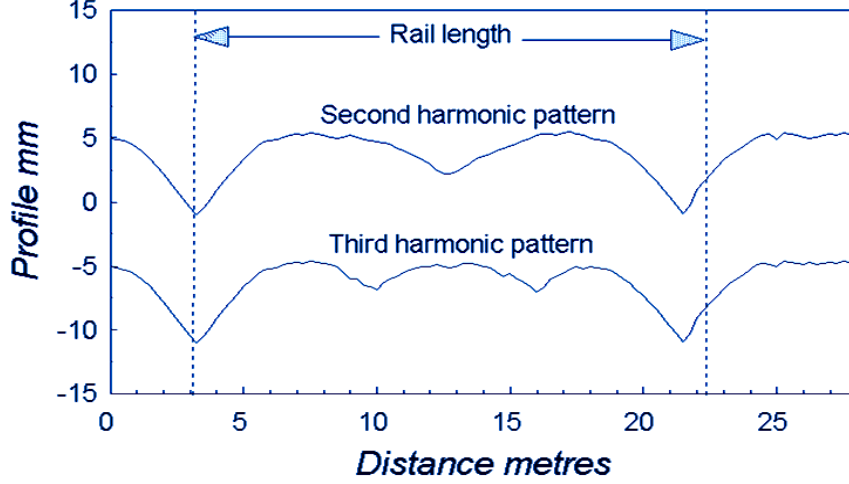
Figure 41. Harmonic patterns as submultiples of rail length (Lewis, 2011)

7.4 Parametrization of PSDs

PSD plots can be parametrized, i.e., described in a condensed form with a small number of parameters. This helps store PSD data for synthesis of track irregularities, establishing standards for PSD, and quantitative comparisons between PSDs of different track sections (or track classes, railroad systems, etc.).

The simplest parametrization of a PSD is by straight line on a log-log plot:

$$S(\Omega) = S_0 \left(\frac{\Omega}{\Omega_0}\right)^{-w}, \Omega = \frac{2\pi}{\lambda} \tag{62}$$

where Ω_0 is a standardized spatial circular frequency in rad/m or rad/ft, $S_0 = S(\Omega_0)$ is roughness at frequency Ω, and w is waviness parameter, usually between 2 and 4, corresponding to the slope of a log-log PSD plot. For a better approximation, a piecewise linear fit with 2-4 segments is sometimes used (Corbin, 1980; Haigermoser, 2015; Iyengar and Jaiswal, 1995).

This type of parametrization has the problem of overestimating the PSD of small wavelength irregularities (when $w > 0$ and $\Omega \to \infty$, $S(\Omega) \to \infty$). To avoid this, various polynomial approximations based on extended roughness models have been proposed (Berawi, 2013; Haigermoser, 2015). The general form of polynomial equations proposed by the FRA study (Corbin, 1980; Hamid et al., 1983; Fazio and Corbin, 1986) is related to the piecewise linear approximation:

$$S_{\bar{y},\bar{z}}(\Omega) = \frac{A\Omega_B^2(\Omega^2+\Omega_A^2)}{\Omega^4(\Omega^2+\Omega_B^2)}, \; S_{\Delta y,\Delta z}(\Omega) = \frac{A\Omega_B^2}{(\Omega^2+\Omega_A^2)(\Omega^2+\Omega_B^2)} \tag{63}$$

where Ω_A and Ω_B correspond to the break frequencies, i.e., breakpoints of a piecewise linear approximation, and parameter A is a measure of roughness, proportional to the square of standard deviation of a track geometry variable.

ERRI (ERRI, 1989, as cited in Haigermoser et al., 2015, and Berawi et al., 2013) has developed another form, which is now widely used in European countries:

$$S_{\bar{y},\bar{z}}(\Omega) = \frac{A_i \Omega_c^2}{(\Omega^2+\Omega_r^2)(\Omega^2+\Omega_c^2)}, S_{\Delta y,\Delta z} = \frac{A_j \Omega^2}{(\Omega^2+\Omega_r^2)(\Omega^2+\Omega_c^2)} \frac{\Omega^2}{b(\Omega^2+\Omega_s^2)} \tag{64}$$

China Academy of Railway Sciences (CARS) proposed the following polynomial to describe alignment, profile, gauge, and cross level PSDs of different track classes (Chen et al., 2008, as cited in Berawi, 2013, and Haigermoser et al., 2015):

$$S_{\bar{y},\bar{z},\Delta y,\Delta z}(\Omega) = \frac{a\Omega^2+b}{c\Omega^6+d\Omega^4+e\Omega^2+\Omega} \tag{65}$$

French National Railway Company (SNCF) proposed a polynomial approximation for profile PSD (Berawi, 2013; Haigermoser et al., 2015):

$$S_z(\Omega) = \frac{A}{\left(1+\frac{\Omega}{\Omega_0}\right)^8} \tag{66}$$

It has been suggested (Hamid et al., 1983; Iyengar and Jaiswal, 1995) that the overall shape of the PSD curve as characterized by breakpoints does not significantly change with track class. Rather, the difference between track classes is characterized by a roughness parameter. In other words, PSD plots of different track classes are curves of similar shape, shifted vertically (Figure 42). On the other hand, data collected in the DYNOTRAIN project shows differences in the shape of PSD curves not only between track classes but also between different railway networks (Figure 43).
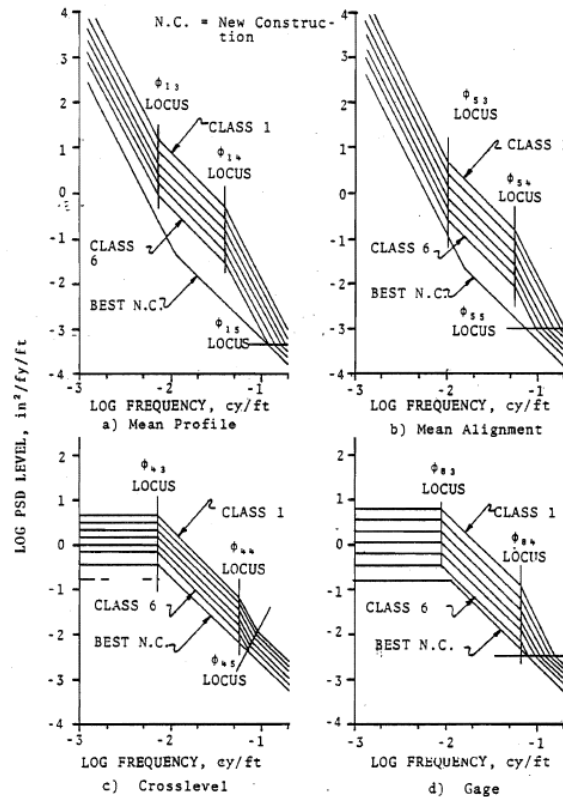
Figure 42. Proposed parametrization for PSD curves corresponding to different track classes (Hamid et al., 1983)
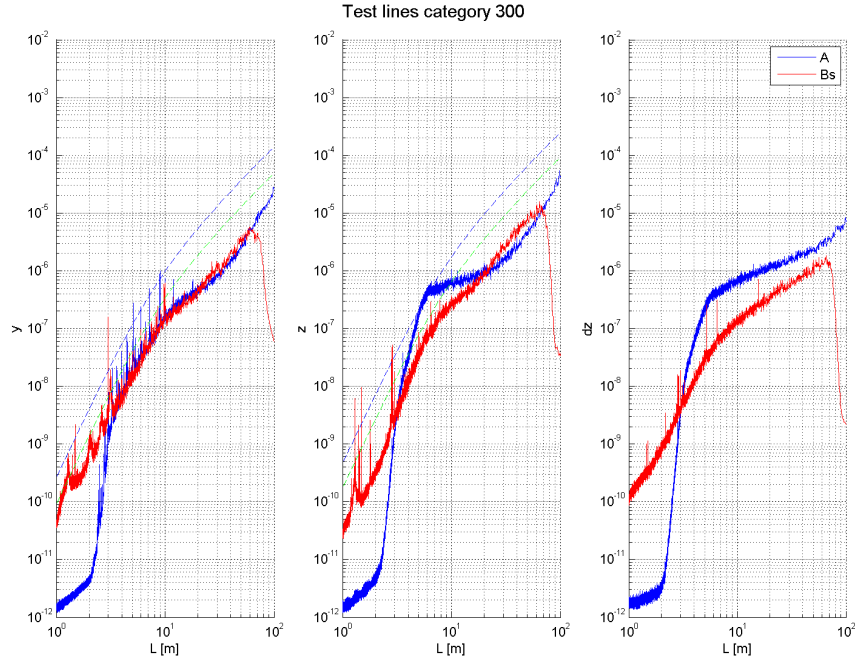
Figure 43. PSD of alignment, profile, and cross level irregularities from two European railways – dashed lines correspond to the theoretical PSD shapes described by the ERRI formulae (Data from DYNOTRAIN project (Haigermoser et al., 2013))

7.5 Generalized Energy Index

In China, a metric called Generalized Energy Index (GEI) has been proposed (Li and Xiao, 2013). It relies on PSD calculation by DFT for each track segment. GEI is designed to reflect the effects of track irregularities of various wavelengths on a vehicle.

GEI is defined as:

$$GEI = \sum_{i=1}^{7} \alpha_i \sqrt{\frac{1}{N-1} \sum_{m=0}^{N-1} w(\lambda_m) E(\lambda_m)} \qquad (67)$$

where $i = 1, ... 7$ is the index of the track geometry variable (left and right alignment, left and right profile, cross level, gauge, and twist), α_i is the weighting factor for this variable, $m = 0,1, ... (N-1)$ is the index of the waveform number λ_m, N is the number of data points in the segment and consequently the number of frequency bins in DFT, $E(\lambda_m)$ is the energy of waveform λ_m calculated by DFT, and $w(\lambda_m)$ is a weighting factor for the given wavelength, which is normalized such that $\sum_{m=0}^{N-1} w(\lambda_m) = 1$.

In other words, the GEI of each track geometry variable is a total power of signal weighted by a function $w(\lambda_m)$, which varies by vehicle and its speed. It can be considered a type of a vehicle-response based method (Section 6.5).

71

8. Processing of Track Geometry Data for Vehicle Dynamic Simulations

One of the uses of measured track geometry is to generate inputs for MBD simulation of rail vehicles. Some of the governmental regulations (49 CFR §213 Appendix D) and industry standards for vehicle qualification (EN 14363:2016; AAR MSRP Ch. 11, 2015; AAR M-976, 2013; AAR S-2043, 2009) prescribe certain requirements for track geometry inputs into MBD simulations, such as deterministic track defect shapes (Figure 44), frequency content of track irregularities, or standardized track geometry files representing different track classes.
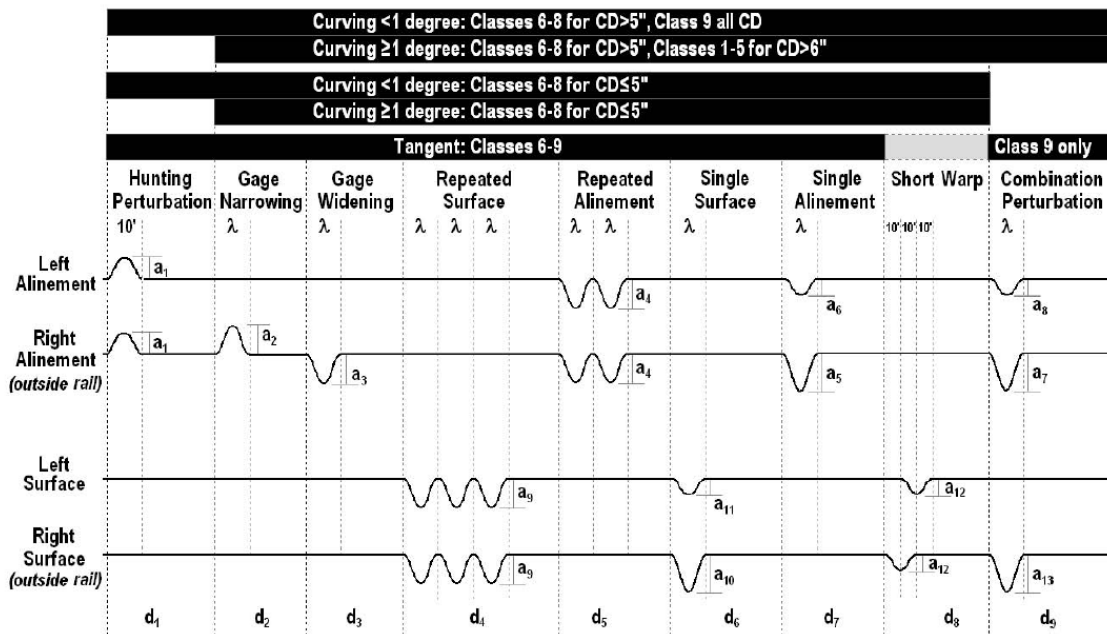
Figure 44. Basic layout of Minimally Compliant Analytical Track (MCAT) (49 CFR §213 Appendix D)

Because many details of this processing depend on the MBD software, the procedures described below are meant as general guidelines.

8.1   Use of Measured Irregularities

Measured track irregularities are most often used when MBD simulation is used to calibrate a vehicle model or to predict the vehicle's response to a known track segment.

Track geometry data for MBD software must be in a space curve format. If only MCO data is available, it must be decolored (Section 5.3), and the user must understand which wavelengths cannot be restored and how they may affect vehicle behavior. At a minimum, MBD software requires information on track curvature, centerline alignment (i.e., mean alignment), track centerline profile (i.e., mean profile/surface), gauge, and superelevation. Alternatively, it may require track curvature, left rail alignment, right rail alignment, left rail surface, and right rail surface (which is the format usually outputted by TGMS). The conversion between the two formats is shown in Equations (8) – (10).

Below are some of the guidelines to follow when processing measured track geometry data for use in MBD software:

- When track geometry is measured to evaluate track quality, it should be measured in a loaded condition, whenever possible (see Section 4.2). However, MBD software usually calculates dynamic deflection of track based on vehicle weight, speed, track stiffness, and other parameters; combined with track geometry that is already measured under load, this may lead to overestimation of the effects of track irregularities. On the other hand, using an artificially high track stiffness in MBD simulations to compensate for this effect may lead to unwanted side effects. An ideal solution would involve using loaded track geometry measurements for track quality analysis and unloaded measurements, along with a realistic track stiffness for MBD simulations, but this is rarely an option.

- Appropriate sign convention/polarity must be observed. Sign convention of TGMS output often differs from that of MBD software.

- Variables which have a noticeable stepwise shape due to quantization error may need to be filtered.

- Track geometry data prepared for MBD software must be in the appropriate (i.e., tilting or non-tilting) coordinate system (see Figure 14).

- Appropriate filters should be used to separate track layout from track irregularity data. These may not be the same filters that are ideal for track geometry characterization (see Section 5.2). In some cases, the filters used by the software aboard the TGMS vehicle may result in missing wavelengths that are important for MBD simulations; for example, space curve in the D1 wavelength domain excludes wavelengths shorter than 3 m (10 ft). Depending on the available data and the goal of the MBD simulation, it may be appropriate to synthesize track irregularities in the missing wavelength range (Haigermoser et al., 2015).

- There must be no duplication of data between different input variables and no missing wavelengths whenever possible (see Section 5.4 and Table 2). For example:

  - If the MBD software requires superelevation and left and right rail surface as separate variables, it may require the superelevation variable to include only vertical irregularities (and design elements) with long wavelengths; irregularities with short wavelength must be included in left profile and right profile variables instead. In contrast, the superelevation variable outputs of most TGMS vehicles includes both long and short wavelengths. The solution is to calculate synthetic cross level from left and right rail surface ($z_L - z_R$) and subtract it from the superelevation. The resulting smooth superelevation, Δz_s, will be the superelevation input for the MBD software. If the MBD software requires left profile and right profile input but no superelevation input, then the smooth superelevation must be distributed between the two rail surface variables:
  $$(z_{L,New} = z_L + \frac{1}{2}\Delta z_s; \; z_{R,New} = z_R - \frac{1}{2}\Delta z_s)$$

  - MBD software may require left alignment and right alignment variables, but no separate gauge variable. In this case synthetic gauge must be calculated from left and right rail alignment ($y_L - y_R$) and subtracted from the raw gauge deviation

measured by TGMS. The resulting smooth gauge, $\Delta y_s = (\Delta y - (y_L - y_R))$, must be distributed between the two rail alignment variables

$$(y_{L,New} = y_L + \frac{1}{2}\Delta y_s; \; y_{R,New} = y_R - \frac{1}{2}\Delta y_s)$$.

In practice, gauge deviation may not be distributed equally between left and right rail, so this will be only an approximation of actual rail positions; the same problem applies to the superelevation input described above.

- o The separation between curvature and alignment can be especially challenging. The wavelength content of alignment channels usually is known or can be easily determined by PSD, FFT, etc. However, the wavelength content of a curvature channel may be more difficult to define (Section 7). The TGMS manufacturer may need to be consulted.

Designers of TGMS can make the outputs of their systems more user-friendly for multi-body simulations by following these guidelines:

- Clearly specifying sign convention, coordinate system, and filter characteristics (i.e., type, cutoff wavelength, and roll-off rate) for all outputs (see prEN 13848-1, August 2016 version)

- For chordal outputs, specifying the method of removing chordal offset component due to curvature (e.g., moving average filter with a 62-foot window width)

- Accommodating the need for different filter settings as functions of track class by:

  - o Allowing the operator of TGMS system to adjust cutoff wavelengths depending on track class, or

  - o Outputting multiple sets of space curve variables with different cutoff wavelengths (e.g., 100 ft for low-speed track and 400 ft for high-speed track) and allowing the user to choose which set to use

- Whenever possible, using filter settings for curvature and grade/gradient outputs that are consistent with space curve filter settings, i.e., ensuring that there are no wavelength bands that are duplicated or missing in both curvature and alignment, or in both profile and grade variables (for example, 200-ft low-pass filter for curvature and 200-ft high-pass filter for alignment)

8.2   Synthesis of Track Geometry Data

Synthesis of track geometry data consists of design of track layout (e.g., curves, spirals, superelevation, etc.) and synthesis of track irregularities. In many cases, such as for simulations comparing different turnout designs, only track layout is necessary.

Track irregularities can by synthesized by deterministic models, stochastic models, or their combinations. For deterministic irregularities, distance-domain functions such as those suggested by characterization studies (Table 6) or prescribed in standards and regulations (Figure 44) are used.

Stochastic approach is usually based on PSDs of irregularities that are parametrized in piecewise linear of polynomial form (Section 7.4). The synthesis of space curve from these parametrized

PSDs can be based on inverse Fourier Transforms, wavelets, or linear dynamic systems; see (Haigermoser et al., 2015; Klöckner et al., 2017; Panunzio et al., 2017) for an overview of synthesis methods.

If a combined stochastic-deterministic approach is used, shapes of irregularities are deterministic (e.g., Equation (49)), but their amplitudes and/or wavelengths are determined stochastically (e.g., Equation (50)).

9. Summary and Conclusions

Track geometry measurement is a rapidly developing field. In the last four decades, track geometry measurement systems became more affordable, modular, autonomous, and accurate over wider ranges of irregularity wavelengths and vehicle speeds.

Track geometry almost always is measured and recorded in the distance domain, with variables such as track curvature, alignment, surface, gauge, and cross level plotted against the distance along the track (i.e., chainage). This format helps separate track design elements, such as curves and spirals, from track irregularities. In the United States track geometry nomenclature is not fully standardized, with different agencies sometimes using conflicting or ambiguous terms (e.g., cross level vs. superelevation, warp vs. twist).

Alignment and surface can be recorded in the format of space curve or chordal offsets. Chordal offsets are widely used because they easily can be verified with hand measurements. Space curve is more difficult to measure but, unlike chordal offsets, it does not hide certain defects, does not depend on arbitrary values (i.e., chord lengths and versine ratios), and is more directly related to the vehicle's response; thus, it is a more objective method of recording and assessing track irregularity data.

One of the difficulties in measuring and processing track geometry data is that different conditions call for different processing settings. For example, filter settings that are appropriate for FRA Class 1 track may not be appropriate for FRA Class 8 track. European standard EN 13848 shows an example of a flexible approach in which high-speed tracks require measuring track irregularities over wider bandwidth than low-speed tracks.

Another challenge is separation of track irregularities from artifacts caused by special trackwork and various environmental conditions. This process is difficult to automate; manual input may be required to achieve good sensitivity and specificity.

Track irregularities are characterized in terms of maximum and minimum values of track irregularity variables. When these maxima exceed permissible limits for a given track class, they are called defects or exceptions. Track irregularities also can be characterized by calculating TQIs, which do not only consider the extreme values but also the overall variation of track geometry. Many different TQIs have been proposed; most of them are based on standard deviations of track irregularity variables and their weighted combinations. Other TQIs based on percentiles, first and second derivatives, fractal dimensions, etc., also have been proposed. Some agencies use a single index characterizing vertical and lateral irregularities. Studies comparing different TQIs in terms of their correlation with vehicle reactions (i.e., accelerations and wheel-rail forces) show results that are often contradictory and/or inconclusive.

Which TQI is preferable over others is a difficult question. Several comparative studies emphasize the correlation between TQI and FRA Track Class. Indeed, there is some value in being able to predict the extreme values of track irregularities from a single TQI value. On the other hand, it can be argued that a TQI that is tailored to predict Track Class would be redundant, and a better approach is to separate Track Class (as characterized by extreme values of irregularities) from track quality (as characterized by SD or other TQIs). This view appears to be reflected in the Euronorms, which use maximum irregularity values to define track speed range (equivalent to FRA Track Class) and SD values to determine track quality class. For example, a

track with alignment SD below 0.5 mm is defined as Track Quality Class A if the maximum applicable speed is 120 km/h, but the same SD corresponds to Track Quality Class C if the maximum applicable speed is 300 km/h (EN 13848–6:2014).

Characterization of track geometry in wavelength/frequency domain is useful for making general conclusions about large sections of track and when validating data from track geometry measurement systems. The transition from the distance domain to the wavelength domain is usually done with FFT, with results presented as magnitude and phase or PSD plots, which can be approximated by piecewise linear functions or polynomials. The relationship between different track geometry variables can be explored with CPSD plots, coherence plots, and transfer functions. Left and right rail alignment signals tend to have high coherence, especially at long wavelengths; the same is true of left and right profile signals. On the other hand, mean alignment, mean profile, gauge, and cross level signals have low coherence, i.e., are more or less independent.

Methods for processing measured track geometry into inputs for MBD simulations are well established, as are the methods for synthesizing artificial track geometry data.

10. Recommendations for Track Geometry Characterization Study

Based on the results of this literature review, the following approach is recommended for characterization of U.S. track geometry data collected within FRA's ATIP:

1. Space curve data, rather than chordal data, should be used for characterization. This creates a challenge for data collected at Track Classes 1-2 (and a high percentage of Class 3 track), where space curve is unavailable due to slow vehicle speed. This leads to two options:

    a. Forfeiting the characterization of alignment and profile on Track Classes 1-3, and only characterizing gauge and superelevation for these Track Classes

    b. Restoring space curve from chordal data, while being aware of the limitations of this process and using caution when comparing the statistics based on restored data from Track Class 1-3 with statistics based on the original space curve data from higher Track Classes

2. Data should be pre-screened for:

    a. Artifacts due to special trackwork and other causes, determined based on first spatial derivative exceeding certain threshold (to be determined)

    b. Sections where alignment and surface measurements are unreliable due to low speed

    c. Sections where alignment and surface measurements are inconsistent with gauge and superelevation measurements

    Data from these sections should not be used in the analysis. Depending on the length of the section, data can be either overwritten by interpolating between edge values, or the section may be cut out entirely. Additional smoothing or filtering may need to be applied to avoid discontinuities.

3. The following variables should be analyzed: curvature, gauge, superelevation/cross level, left alignment, right alignment, centerline alignment, left profile, right profile, centerline profile, twist, and warp.

4. Alignment and profile data should be pre-filtered. FIR or cascaded forward-reverse 2nd or 4th order Butterworth filters appear to be the most likely candidates. Several filters should be designed, with exact settings to be determined during analysis:

    a. High-pass filter with ~80 ft cutoff wavelength, to be used for lower classes of track (similar to D1 domain in Euronorms)

    b. High-pass filter with ~200 ft cutoff wavelength, to be used for higher classes of track (similar to a combination of D1 and D2 domains)

    c. Band-pass filter with ~80 ft high cutoff and ~200 ft low cutoff (similar to D2 domain)

    d. Low-pass filter with ~200 ft cutoff (similar to D3 domain)

Cutoff wavelength should be refined such that the magnitudes of the filter artefacts in spirals are smaller than typical irregularities in the same track classes.

5. Exploratory data analysis should be performed on each space curve variable to determine the characteristics of its statistical distribution.

6. Track data should be segmented by track type (i.e., tangent, curve, spiral). When segment length exceeds 0.1 mile, it should be segmented into 0.1-mile segments. If locations of turnouts and bridges are known, they should be separated into special segments.

7. In the distance domain, the following statistical features should be extracted from the space curve variables in each segment:

    a. Minimum, maximum, mean, standard deviation, 1st, 5th, 50th, 95th and 99th percentiles

    b. Same statistics of absolute values of space curve variables

    c. Minimum, maximum, mean, standard deviation, 1st, 5th, 50th, 95th and 99th percentiles of first and second spatial derivatives of space curve variables

    d. Same statistics of absolute values of derivatives of space curve variables

    e. Number of FRA Track Class exceptions in a segment

    f. Ratio of combined length of FRA Track Class exceptions to the total segment length

    g. Length-based TQI (based on the method by Zhang and El-Sibaie)

    h. Other TQIs calculated from these values, if desired

    i. Actual FRA Track Class based on exceptions

8. Statistical features from different track segments should be aggregated by track category (e.g., FRA Class 4, primarily freight, tangent track). For each track category, distribution of previously discussed statistical features (e.g., standard deviations, TQIs, etc.) should be presented in terms of probability density distribution and/or cumulative probability distribution.

9. Segmentation of track used for wavelength domain is to be determined. Track segment lengths should likely be longer than what is used for distance domain analysis. At the same time, calculating one single PSD function based on the entire track category may mask meaningful differences (Figure 43). Segment lengths of approximately 0.3-3 miles may be ideal for wavelength analysis.

10. In the frequency/wavelength domain, the following should be calculated:

    a. PSD of (unfiltered) space curve variables. The exact method is to be determined in the process of analysis. FFT or Welch's method with Hanning windowing are the most likely candidates.

    b. Coherence between space curve variables (e.g., left and right rail alignment, centerline alignment and gauge, gauge and cross level, etc.)

11. Parametrization of PSD data should be attempted using piecewise linear functions or polynomial expressions.

This approach may need to be modified based on the results of the exploratory data analysis and other findings throughout the characterization process.

11. References

1.   Ahmadian, M. (1999). Filtering effects of mid-chord offset measurements of track geometry data. *Proceedings of the 1999 ASME/IEEE Joint Railroad Conference, April 15, 1999.*

2.   Aknin, P. & Chollet, H. (1999). A new approach for the modelling of track geometry recording vehicles and the deconvolution of versine measurements. *IAVSD Conference, Pretoria, 1999.*

3.   Al-Nazer, L. (2014). Track Profile Approximation Using Railcar Body Acceleration Data (Report No. DOT/FRA/ORD-14/42). Federal Railroad Administration.

4.   Andani, M. T. (2016). The application of Doppler LIDAR technology for rail inspection and track geometry assessment. PhD Dissertation, Virginia Tech, Blacksburg, Virginia.

5.   Andani, M.T., Peterson, A., Munoz, J., & Ahmadian, M. (2018). Railway track irregularity and curvature estimation using doppler LIDAR fiber optics. *Journal of Rail and Rapid Transit, 232*(1), 63–72.

6.   Anderson, M. (2002). Strategic planning of track maintenance. *Department of Infrastructure, Borlänge.*

7.   Andrews, J., Prescott, D., & De Rozieres, F. (2014). A Stochastic Model for Railway Track Asset Management. *Reliability Engineering & System Safety, 130*(10), 76–84.

8.   Arasteh Khouy, I., Larsson-Kråik, P.O., Nissen, A., & Kumar, U. (2016). Cost-effective track geometry maintenance limits. *Journal of Rail and Rapid Transit, 230*(2), 611–622.

9.   Association of American Railroads, Manual of Standards and Recommended Practices, Section C, Part II, Chapter 11: Service-Worthiness Tests and Analyses for New Freight Cars, Washington, DC, 2015.

10.   Association of American Railroads, Manual of Standards and Recommended Practices, Specification M-976: Truck Performance for Rail Cars, Washington, DC, 2013.

11.   Association of American Railroads, Manual of Standards and Recommended Practices, Standard S-2043: Performance Specification for Trains Used to Carry High-Level Radioactive Material, DC, 2009.

12.   Bentley Systems, Inc. OpenRail Designer: rail Track and Electrification Design and Analysis Software. Accessed January 2, 2019.

13.   Berawi, A.R.B. (2013). Improving Railway Track Maintenance Using Power Spectral Density. PhD Dissertation, University of Porto.

14.   Bracciali, A., Piccioli, F., & De Cicco, T. (2009). Measurement and analysis of mid wavelength rail irregularity. *Proceedings of Railway Engineering 2009 Conference, London, June 2009.*

15.   Broquetas, A., Comerón, A., Gelonch, A., Fuertes, J.M., Castro, J. A., Felip, D., López, M. A., & Pulido, J.A. (2012). Track Detection in Railway Sidings Based on MEMS Gyroscope Sensors. *Sensors.*

16.   Brown, A.B. & Ashmore, S.J. (2018). Union Pacific Railroad. Personal communication. December 4, 2018.

17.   Burton, T. (2018). RILA Train Mounted Survey System, Opportunities & Constraints.

18.   Camacho, D., Lee, T.H., Rapp, S., & Martin, U. (2016). Light rail ballasted track geometry quality evaluation using track recording car data. *Proceedings of the 15th International Conference on Railway Engineering Design and Operation (CR 2016)*.

19.   Carr, G., Diaz, C., & Martin, G. (2002). Determining profile and alignment using an optical technique with extrapolations. *Proceedings of ASME/IEEE Joint Rail Conference, Washington, DC, April 23-25, 2002*.

20.   Cerna, M. & Harvey, A.F. (2000). The Fundamentals of FFT-Based Signal Analysis and Measurement. National Instruments, Application Note 041, 2000. Accessed: Dec. 17, 2018.

21.   Chen, Q., Niu, X., Zhang, Q. & Cheng, Y. (2015). Railway track irregularity measuring by GNSS/INS integration. *Navigation, 62*(1), 83-93.

22.   Chen, Q., Niu, X., Zuo, L., Zhang, T., Xiao, F., Liu, Y., & Liu, J. (2018). A railway track geometry measuring trolley system based on aided INS. *Sensors, 2018*(18).

23.   Chen, X., Wang, L., Tao, X., Cui, G., Yang, F., Chai, X., & Wu, W. (2008). Study on the judgement method for track irregularity of the main railway lines in China. *Journal of China Railway Science, 9*(4), 22–27.

24.   Chernov, N. (2009). Circle Fit (Pratt Method). Accessed: March 22, 2019.

25.   Chung, W. & Ham, Y. (2004). Investigation of the track irregularities reconstruction methods. *Key Engineering Materials, 270-273*, 1659-1664.

26.   Ciobanu, C. (2016). The versine formulae. Accessed: December 12, 2018.

27.   Clouse, A. (2018). Federal Railroad Administration. Personal communication. April 6, 2018.

28.   Cohen A. & Hutchens, W. (1970). Methods for the reconstruction of rail geometry from mid-chord offset data. *Joint Transportation Engineering Conference, Chicago, IL, USA, October 11-14, 1970*.

29.   Corbin, J.C. (1980). Statistical Representations of Track Geometry. Volume I – Main Text (Report. No. FRA/ORD-80/22.1). Federal Railroad Administration.

30.   Craft, M. (2018). Amtrak. Personal communication. November 29, 2018.

31.   Cusumano, J.P. (2005). The Power Spectral Density and the Autocorrrelation. Experimental Nonlinear Dynamics: Supplemental Handout.

32.   Davis, T.G. (1999). Total least-squares spiral curve fitting. *Journal of Surveying Engineering, 125*(4).

33.   Ebersöhn, W. & Conrad, J.R. (2003). Implementing a railway infrastructure maintenance system. Amtrak, Washington, DC.

34.   Elkhoury, N., Hitihamillage, L., Moridpour, S., & Robert, D. (2018). Degradation Prediction of Rail Tracks: A Review of the Existing Literature. *The Open Transportation Journal, 2018*(12), 88–104.

35.   El-Sibaie, M. & Zhang, Y. (2004). Objective track quality indices. *Journal of the Transportation Research Board No. 1863*, 81-87.

36.   Engstrand, A. (2011). Railway Surveying – A Case Study of the GRP 5000. MS Thesis, Royal Institute of Technology, Stockholm.

37.   Esveld, C., Jourdain, A., Kaess, G., & Shenton, M.J. (1988). Historic data on track geometry in relation to maintenance. *Rail Engineering International, Issue 2*.

38.   European Committee for Standardization (CEN) (2016). EN 14363:2016, Railway applications – Testing for the acceptance of running characteristics of railway vehicles – Testing of running behaviour and stationary tests.

39.   European Committee for Standardization (CEN) (2008). EN 13848-1:2003+A1: Railway applications – Track – Track geometry quality – Part 1: Characterization of track geometry.

40.   European Committee for Standardization (CEN) (2016). PrEN 13848-1: Railway applications – Track – Track geometry quality – Part 1: Characterization of track geometry.

41.   European Committee for Standardization (CEN) (2006). EN 13848-2:2006: Railway applications – Track – Track geometry quality – Part 2: Measuring systems – Track recording vehicles.

42.   European Committee for Standardization (CEN) (2017). EN 13848-5:2017: Railway applications – Track – Track geometry quality – Part 5: Geometric quality levels - plain line, switches and crossings.

43.   European Committee for Standardization (CEN) (2014). EN 13848-6:2014: Railway applications – Track – Track geometry quality – Part 6: Characterisation of track geometry quality.

44.   European Rail Research Institute (1989). ERRI Question B 176. Bogies with steered or steering wheelsets (Report No. 1).

45.   European Rail Research Institute (1999). ERRI Question C210. Development of methods to describe geometric track quality, with the aim of analysing dynamic vehicle behavior (Report No. 1: Summary Report). Utrecht, 1999.

46.   Fazio, A.E. & Corbin, J.L. (1986). Track quality index for high speed track. *Journal of Transportation Engineering, 112*(1), 46–61.

47.   Federal Railroad Administration Office of Railroad Safety (2017). Track and rail & infrastructure integrity compliance manual; Volume I, Chapter 3: Track safety standards. Automated Track Inspection Program (ATIP) Geometry Car Operation.

48.   Federal Railroad Administration Office of Railroad Safety (2017). Track and rail & infrastructure integrity compliance manual; Volume II, Chapter 1: Track safety standards. Track safety standards Classes 1 through 5.

49.   Federal Railroad Administration Office of Safety (2019). Track Geometry Car System Capabilities (Report No. FRA DOTX 217).

50.   Gabara, G. & Sawicki, P. (2018). A New Approach for Inspection of Selected Geometric Parameters of a Railway Track Using Image-Based Point Clouds. *Sensors, 18*(3).

51.   Garach, L., de Oña, J., & Pasadas, M. (2014). Mathematical formulation and preliminary testing of a spline approximation algorithm for the extraction of road alignments. *Automation in Construction, 47*(2014), 1-9.

52.   Ghasemi, A. & Zahediasl, S. (2012). Normality Tests for Statistical Analysis: A Guide for Non-Statisticians. *International Jounral of Endocrinology and Metabolism, 10*(2).

53.   Glaus, R. (2006). The Swiss Trolley – a modular system for track surveying. *Siebzigster Brand, 70*.

54.   Grabner, G. (2013). TrioTRAIN: Track geometry analysis. Frankfurt, Germany.

55.   Grabner, G. (2013). TrioTRAIN: Methods for describing and assessing track geometry. Frankfurt, Germany.

56.   Grassie, S. (1996). Measurement of railhead longitudinal profiles: a comparison of different techniques. *Wear, 191*(1996), 245-251.

57.   Gustaffson, F. (1996). Determining the initial states in forward-backward filtering. *IEEE Transactions on Signal Processing, 44*(4), 988–992.

58.   Haigermoser, A., Bezin, Y., Coudert, F., Eickhoff, B., Grabner, G., Kraft, S., Thomas, D., & Wolter, U. (2013). DynoTRAIN WP2 Deliverable D2.6 – Final Report on Track Geometry.

59.   Haigermoser, A., Eickhoff, B., Thomas, D., Coudert, F., Grabner, G., Zacher, M., Kraft, S., & Bezin, Y. (2014). Describing and assessing track geometry quality. *Vehicle System Dynamics, 52*(Supplement 1).

60.   Haigermoser, A., Luber, B., Rauh, J., & Grafe, G. (2015). Road and track irregularities: measurement, assessment and simulation. *Vehicle System Dynamics, 53*(7).

61.   Hamid & Gross, A. (1981). Track-Quality Indices and Track-Degradation Models for Maintenance-of-Way Planning. *60th Annual Meeting of the Transportation Research Board, Washington, DC, January 12–16, 1981.*

62.   Hamid, Rasmussen, K., Baluja, M., & Yang, T.-L. (1983). Analytical Descriptions of Track Geometry Variations. Volume I – Main Text (Report No. DOT/FRA/ORD-83/03.1). Federal Railroad Administration.

63.   Hanreich, W., Mittermayr, P., & Presle, G. (2002). Track Geometry Measurement Database and Calculation of Equivalent Conicities of the OBB Network. *Proceedings of 2002 AREMA Conference.*

64.   Hay, W. (1982). Railroad engineering, 2nd Edition. John Wiley & Sons, New York.

65.   Heinzel, G., Rudiger, A., & Schilling, R. (2002). Spectrum and spectral density estimation by the Discrete Fourier Transform (DFT), including a comprehensive list of window functions and some new flat-top windows.

66.   Higgins, C. & Liu, X. (2018). Modeling of track geometry degradation and decisions on safety and maintenance: A literature review and possible future research directions. *Journal of Rail and Rapid Transit, 232*(5), 1385–1397.

67.   Hyslip, J., Trosino, M., & Selig, E. (2002). Fractal Analysis of Track Geometry Data. *Proceedings of the 2002 AREMA Conference.*

68.   International Organization for Standardization (1997). Mechanical vibration and shock – Evaluation of human exposure to whole-body vibration – Part 1: General requirements (ISO 2631-1:1997).

69.   Iyengar, R.N. & Jaiswal, O.R. (1995). Random Field Modeling of Railway Track Irregularities. *Journal of Transportation Engineering. 121*(4).

70.   International Union of Railways (UIC) (2005). Leaftet 518: Testing and approval of railway vehicles from the point of view of their dynamic behavior – safety – track fatigue – ride quality, 3rd Edition.

71.   Jia, C., Xu, W., Wei, L., & Wang, H. (2013). Study of Railway Track Irregularity Standard Deviation Time Series Based on Data Mining and Linear Model (Article ID 486738). *Mathematical Problems in Engineering*.

72.   Jia, C., Wei, L., Wang, H., & Yang, J. (2014). Study of Track Irregularity Time Series Calibration and Variation Pattern at Unit Section (Article ID 727948). *Computational Intelligence and Neuroscience*.

73.   Jiang, Q., Wu, W., Li, Y., & Jiang, M. (2017). Millimeter Scale Track Irregularity Surveying Based on ZUPT-Aided INS with Sub-Decimeter Scale Landmarks. *Sensors, 2017*(17).

74.   Jovanovic, S. (2004). Railway Track Quality Assessment and Related Decision Making. *2004 IEEE International Conference on Systems, Man and Cybernetics, The Hague, Netherlands, October 10–13, 2004*.

75.   Karttunen, K. (2015). Influence of rail, wheel and track geometries on wheel and rail degradation. Ph.D. Thesis, Chalmers University of Technology, Göteborg, Sweden, 2015.

76.   Karis, T. (2018). Correlation between Track Irregularities and Vehicle Dynamic Response Based on Measurements and Simulations. Licentiate Thesis, Royal Institute of Technology, Stockholm, Sweden.

77.   Karis, T., Berg, M., Stichel, S., Li, M., Tomas, D., & Dirks, B. (2018). Correlation of track irregularities and vehicle responses based on measured data. *Vehicle System Dynamics; 56*(6), 967–981.

78.   Klöckner, A., Knoblach, A., & Heckmann, A. (2017). How to shape noise spectra for continuous system simulation. *Mathematical and Computer Modelling of Dynamical Systems, 23*(3), 284–300.

79.   Kraft, S., Causse, J., & Coudert, F. (2015). An approach for the classification of track geometry defects. *Proceedings of the 24th Symposium of the International Association for Vehicle System Dynamics (IAVSD 2015), Graz, Austria, 17–21 August 2015*.

80.   Kraft, S., Causse, J., & Coudert, F. (2018). Vehicle response-based track geometry assessment using multi-body simulation. *Vehicle System Dynamics, 56*(2), 190–220.

81.   Kreye, C., Eissfeller, B., & Ameres, G. (2004). [Architectures of GNSS/INS Integrations Theoretical Approach and Practical Tests](). Institute of Geodesy and Navigation, University FAF Munich, Neubiberg, Germany. Accessed Dec. 12, 2018.

82.   Krug, G.A. & Madejski, J. (2015). Track maintenance strategies optimization problem. *Railway Engineering 2015 – 13th International Conference & Exhibition, Edinburgh, UK, 2015*.

83.   Krug, G.A. & Madejski, J. (2018). Improving track condition by application of quasi cumulative distribution function (QCDF). *5th International Conference on Road and Rail Infrastructure, Zadar, Croatia, May 17-19, 2018*.

84.   Landgraf, M. (2016). Railway Track Condition: Assessment – Aggregation – Asset Management. *11th World Congress on Railway Research, Milan, Italy, May 29 – June 2, 2016*.

85.   Lasisi, A. & Attoh-Okine, N. (2018). Principal components analysis and track quality index: a machine learning approach. *Transportation Research Part C: Emerging Technologies, 91*, 230–248.

86.   Lewis, R. (2011). Track geometry recording and usage: Notes for a lecture to Network Rail.

87. Lee, S. (2005). Development of Objective Track Quality Indices (Report No. RR05-01). Federal Railroad Administration.

88. Leica Geosystems AG (2018). ATrack Suite by Leica Geosystems: Automated Track As-Built Engineering & Optimization Software. Accessed January 2, 2019.

89. Li, D., Hyslip, J., Sussman, T., & Chrismer, S. (2016). Railway geotechnics. CRC Press, Boca Raton, FL.

90. Li, D., Meddah, A., Haas, K., & Kalay, S. (2006). Relating track geometry to vehicle performance using neural network approach. *Proceedings of the Institution of Mechanical Engineers, Part F: Journal of Rail and Rapid Transit 220 p. 273–281*.

91. Li, M., Persson, I., Spannar, J., & Berg, M. (2012). On the quality of second-order derivatives of track irregularity for assessing vertical track geometry quality. *Vehicle System Dynamics, 50*(Supplement).

92. Li, H. & Xiao, T. (2014). Improved generalized energy index method for comprehensive evaluation and prediction of track irregularity. *Journal of Statistical Computation and Simulation, 84*(60), 1213–1231.

93. Lindahl, M. (2001). Track geometry for high-speed railways: A literature survey and simulation of dynamic vehicle response. Royal Institute of Technology, Stockholm.

94. Liu, R., Xu, O., Sun, Z., Zou, C., & Sun, Q. (2015). Establishment of track quality index standard recommendations for Beijing Metro (Article ID 473830). *Discrete Dynamics in Nature and Society*.

95. Liu, X., Saat, M., & Barkan, C. (2012). Analysis of causes of major train derailments and their effect on accident rates. *Journal of the Transportation Research Board, 2289*, 154–163.

96. Liu, Y. & Magel, E. (2007). Performance based track geometry and the track geometry interaction map. *Proceedings of International Heavy Haul Conference, Specialist Technical Session, Kiruna, Sweden, June 11-13, 2007*.

97. Lönnbark, G. (2012). Characterization of Track Irregularities with Respect to Vehicle Response. Royal Institute of Technology, Stockholm, Sweden.

98. Luck, T., Eissfeller, B., Kreye C., & Meinke, P. (2001). Measurement of Line Characteristics and of Track Irregularities by Means of DGPS and INS. *International Symposium on Kinematic Systems in Geodesy, Geomatics and Navigation, Banff, Alberta, Canada, June 5-8, 2001*.

99. Madejski, J. & Grabczyk, J. (2002). Continuous geometry measurement for diagnostics of tracks and switches. *Proceedings of the International Conference of Switches, Delft, Netherlands, 2002*.

100. Mahalakshmi, V. & Joseph, K.O. (2013). GPS Based Railway Track Survey System. *International Journal of Computer Applications in Engineering Sciences, Volume III, Special Issue on National Conference on Information and Communication (NCIC'13)*.

101. Malone, J. (2007). Performace and testing requirements for portable track geometry inspection systems. *TCRP Research Results Digest, 83*.

102. Mandal, N.K., Dhanasekar, M., & Sun, Y.Q. (2016). Impact Forces at Dipped Rail Joints. *Proceedings of the Institution of Mechanical Engineers, Part F: Journal of Rail and Rapid Transit, 230*(1), 271–282.

103.   Marquis, LeBlanc, J., & Tajaddini, A. (2014). Vehicle Track Interaction Safety Standards. *Proceedings of the 2014 Joint Rail Conference (JRC2014), Colorado Springs, CO, April 2-4, 2014.*

104.   Di Mascio, P., Di Vito, M., Loprencipe, G., & Ragnoli, A. (2012). Procedure to determine the geometry of road alignment using GPS data. *Procedia – Social and Behavioral Sciences, 53,* 1204–1217,.

105.   The MathWorks, Inc. Welch's Power Spectral Density Estimate. Accessed: March 22, 2019.

106.   The MathWorks, Inc. Zero-Phase Digital Filtering. Accessed: March 22, 2019.

107.   Mauer, L. (1995). Determination of Track Irregularities and Stiffness Parameters with Inverse Transfer Functions of Track Recording Vehicles. *Vehicle System Dynamics Supplement, 24*(1995), 117–132.

108.   McCrae, J. & Singh, K. (2008). Sketching Piecewise Clothoid Curves. EUROGRAPHICS: Workshop on Sketch-Based Interfaces and Modeling.

109.   Meddah, A. (2018). TTCI. Personal communication. November 2018.

110.   Moskal, A. & Pastucha, E. (2016). Track and gauge geometry measurements – the present and future. *Measurement Automation Monitoring, 62*(2), 66-71.

111.   Morant, S. (2016). Automating geometry measurement offers real-time benefits. International Railway Journal.

112.   Morell, J. (2017). Evaluation of the Federal Railroad Administration's Autonomous Track Geometry Measurement System Research and Development Program (Report No. DOT/FRA/ORD-17/05). Federal Railroad Administration.

113.   Muinde, M.S. (2018). Railway track geometry inspection optimization. M.S. Thesis, Luleå University of Technology.

114.   Naganuma, Y. & Yada, T. (2016). Development of truly portable track geometry recording trolley and accompanying new measurement principle. *Proceedings of the 15th International Conference on Railway Engineering Design and Operation (CR 2016), 2016.*

115.   Nielsen, J., Berggren, E., Lölgen, T., Müller, R., Stallaert, B., & Pesqueux, L. (2013). RIVAS Deliverable D2.5: Overview of Methods for Measurement of Track Irregularities Important for Ground-Borne Vibration. International Union of Railways.

116.   Panunzio, A.M., Puel, G., Cottereau, R., Simon, S., & Quost, X. (2017). Construction of a stochastic model of track geometry irregularities and validation through experimental measurements of dynamic loading. *Vehicle System Dynamics, 55*(3), 399–426.

117.   Pedanekar, N.R. (2006). Methods for aligning measured data taken from specific rail track sections of a railroad with the correct geographic location of the sections. US Patent No. US 7,130,753 B2.

118.   Pinter, O. (2012). Using of Trimble® GEDO CE system for absolute track positioning. [in Czech], Diploma Thesis, Czech Technical University in Prague, Prague.

119.   Pratt, V. (1987). Direct least-squares fitting of algebraic surfaces. *SIGGRAPH '87: Proceedings of the 14th annual conference on computer graphics and interactive techniques, ACM, New York, NY, USA, 1987.*

120.   Puzavac, L., Popović, Z., Lazarević, L. (2012). Influence of Track Stiffness on Track Behaviour under Vertical Load. *Promet – Traffic & Transportation, 24*(5), 405–412.

121.   Rail Accident Investigation Board (RAIB) (2014). Rail Accident Report: Class investigation into rail breaks on the East Coast Main Line (Report No. 24/2014).

122.   Reedman, M. (2014). Kinky Tracks. *Conference on Railway Excellence (CORE-2014), Adelaide, Australia, May 5–7, 2014*.

123.   Roghani, A., Macciotta, R., & Hendry, M. (2015). Combining track quality and performance measures to assess track maintenance requirements. *Proceedings of the 2015 Joint Rail Conference, San Jose, CA, USA, March 23–26, 2015*.

124.   Sadeghi, J. (2010). Development of railway track geometry indexes bases on statistical distribution of geometry data. *Journal of Transportation Engineering, 136*(8).

125.   Sadeghi, J., Heydari, H., & Doloei, E. A. (2017). Improvement of Railway Maintenance Approach by Development of a New Railway Condition Index. *J. Transportation Engineering, Part A: Systems, 143*(8).

126.   Scanlan, K.M., Hendry, M.T., & Martin, C.D. (2016). Evaluating the equivalency between track quality indices and minimum track geometry threshold exceedances along a Canadian freight railway. *Proceedings of the 2016 Joint Rail Conference, Columbia, SC, USA, April 12–15, 2016*.

127.   Schubert, E. (1970). Die Planung von Gleisdurcharbeitungen auf Grund von Oberbaumessungen. *Der Eisenbahningenieur, 21*,140–143.

128.   Sharma, S. (2016). Data-Driven Optimization of Railway Track Inspection and Maintenance Using Markov Decision Process. M.S. Thesis, State University of New York at Buffalo.

129.   Sherrock, E. (2018). ENSCO. Personal communication. Dec. 17, 2018.

130.   Smith, S.W. (1997). The Scientist and Engineer's Guide to Digital Signal Processing. California Technical Publishing, San Diego.

131.   Soleimanmeigouni, I., Ahmadi, A., & Kumar, U. (2018). Track geometry degradation and maintenance modelling: A review. *Journal of Rail and Rapid Transit, 232*(1), 73–102.

132.   Soleimanmeigouni, I., Ahmadi, A., Arasteh Khouy, I., & Letot, C. (2018). Evaluation of the effect of tamping on the track geometry condition: A case study. *Journal of Rail and Rapid Transit, 232*(2), 408–420.

133.   Stow, J. & Andersson, E. (2006). Field testing and instrumentation of railway vehicles. Handbook of railway vehicle dynamics, ed. S. Iwnicki, CRC Press, Boca Raton, FL.

134.   Stratakos, J., Gikas, V., & Fragos, K. (2009). A multi-scale curve matching technique for the assessment of road alignment using GPS/INS data. *6th International Symposium on Mobile Mapping Technology, Presidente Prudente, São Paulo, Brazil, July 21–24, 2009*.

135.   Stuart (2017). Autonomous track geometry measurement system: technical development and short line demonstration. *Rail Infrastructure and Vehicle Inspection Technology Conference, University of Illinois Urbana-Champaign, June 20-21, 2017*.

136.   Sun, Y.Q., Spiryagin, M., Cole, C., & Simson, S. (2013). Effect of Wheel-Rail Contacts and Track Gauge Variation on Hunting Behaviours of Australian Three-Piece Bogie Wagon.

Proceedings of the 23ʳᵈ International Symposium on Dynamics of Vehicles on Roads and on Tracks, Qingdao, China, 19–23 August, 2013.

137. Sundaram, N. & Wilson, R. (2016). Portable track geometry measurement system: a unique derailment investigation tool. *Presentation, 2016 APTA Rail Conference, 2016*.

138. Szwilski, T.B., Begley, R., Dailey, P., Sheng, Z., & Rahall, N.J. (2003). Determining rail track movement trajectories and alignment using HADGPS. *Proceedings of the AREMA Annual Conference, Chicago, Ill, USA, October 2003*.

139. Tong, X. & Ding, K. (2010). Estimating Geometric Parameters of Highways and Railways Using Least-Squares Adjustment. *Survey Review, 42*(318), 359–374.

140. Talukdar, K., Arulomozhi, U., Prrabhakar Reddy, K., & Satyanarayan (2006). Improvement of TGI Value by Computer Analysis. *Presentation, Indian Railway Institute of Civil Engineering*.

141. Transport Canada (2012). TC E-54: Rules Respecting Track Safety. Effective May 25, 2012.

142. Trehag, J., Handel, P., & Ogren, M. (2008). Onboard estimation and classification of railroad curvature. *IEEE Transactions on Instrumentation and Measurement, 59*(3).

143. Trimble Inc. (2017). Trimble adds inertial-based trolley solution to its track survey and scanning rail portfolio. Press Release.

144. United States Code of Federal Regulations. 49 CFR §213: Track Safety Standards, Subpart C. Track Geometry.

145. United States Code of Federal Regulations. 49 CFR §213: Track Safety Standards, Subpart G. Train Operations at Track Class 6 and Higher.

146. United States Code of Federal Regulations. 49 CFR §213 Appendix D: Minimally Compliant Analytical Track (MCAT) Simulations Used for Qualifying Vehicles to Operate at High Speeds and at High Cant Deficiencies.

147. Vogelaar, J. (2017). Absolute track geometry, what is it and how does it help me? *Rail Infrastructure and Vehicle inspection Technology Conference, University of Illinois Urbana-Champaign, June 20-21, 2017*.

148. Wang, P., Wang, Y., Tang, H., Gao, M., Chen, R., & Xu, J. (2018). Error theory of chord-based measurement system regarding track geometry and improvement by high frequency sampling. *Measurement, 115*, 204–216.

149. Wang, Y., Wang, P., Wang, X., & Liu, X. (2018). Position synchronization for track geometry inspection data via big-data fusion and incremental learning. *Transportation Research Part C: Emerging Technologies, 93*, 544–565.

150. Weisstein, E.W. Curvature. MathWorld – A Wolfram Web Resource. Accessed: December 12, 2018.

151. Weston, P., Roberts, C., Yeo, G., & Stewart, E. (2015). Perspectives on railway track geometry condition monitoring from in-service railway vehicles. *Vehicle System Dynamics, 53*(7), 1063–1091.

152. Wickramarachi, P. (2003). Effects of windowing on the spectral content of a signal. *Sound and Vibration, 37*(1), 10–13.

153.	Wolf, G. (2015). Principles of Track Geometry. *Presentation, WRI-2015, Principles Course, May 19, 2015.*

154.	Wrobel, S. (2013). Multi-function LIDAR sensors for non-contact speed and track geometry measurement in rail vehicles. M.S. Thesis, Virginia Polytechnic Institute and State University, Blacksburg, VA.

155.	Xu, P., Sun, Q., Liu, R., & Souleyrette, R.R. (2016). Optimal match method for milepoint postprocessing of track condition data from subway track geometry cars. *Journal of Transportation Engineering, 142*(8).

156.	Xu, P., Sun, Q., Liu, R., Souleyrette, R.R., & Wang, F. (2014). Optimizing the Alignment of Inspection Data from Track Geometry Cars. *Computer-Aided Civil and Infrastructure Engineering, 30*(1).

157.	Yada, T., Soda, Y., & Naganuma, Y. (2017). Improvement of the realignment performance for short wavelength track irregularity on a tamping machine. *WIT Transactions on Engineering Sciences, 118.*

158.	Yazawa, E. & Takeshita, K. (2002). Development of measurement device of track irregularity using inertial mid-chord offset method. *Quarterly Report of RTRI, 43*(3).

159.	Zarembski, A.M., Grissom, G.T., Euston, T.L., & Cronin, J.J. (2015). Relationship between missing ballast and development of track geometry defects. *Transportation Infrastructure Geotechnology, 2*, 167–176.

160.	Zhang, Y., El-Sibaie, M., & Lee, S. (2004). FRA track quality indices and distribution characteristics. *Proceedings of AREMA Annual Conference, Nashville, TN, September 19-22, 2004.*

Appendix A.
FRA Track Safety Limits (49 CFR §213)

Table 4. Alignment exception limits defined in United States Code of Federal Regulations (49 CFR §213)

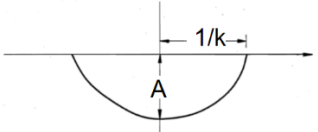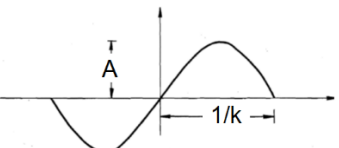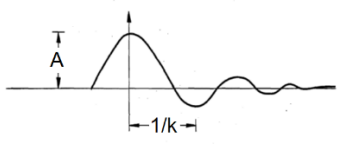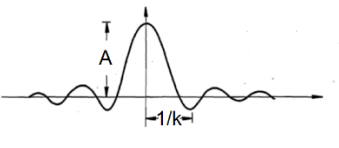| Parameter *(all exceptions in inches)*	Type of track	Additional qualifiers	Track Class									
			Exc.	1	2	3	4	5	6	7	8	9
Operating Speed Limit, Freight (mph)			10	10	25	40	60	80				
Operating Speed Limit, Passenger (mph)				15	30	60	80	90	110	125	160	220
Min. gauge				56	56	56	56	56	56	56	56	56¼
Max. gauge			58¼	58	57¾	57¾	57½	57½	57¼	57¼	57¼	57¼
Change of gauge within 31'									¾	½	½	½
31' MCO	Tangent								½	½	½	½
31' MCO	Curved					1¼	1	½	½	½	½	½
62' MCO	Tangent			5	3	1¾	1½	¾	¾	¾	¾	½
62' MCO	Curved			5	3	1¾	1½	⅝	⅝	½	½	½
124' MCO	Tangent								1½	1¼	1	¾
124' MCO	Curved								1½	1¼	¾	¾
31' MCO	Curved	**Outside rail** in operations at a qualified cant deficiency >5"				¾	¾	½	½	½	½	½
62' MCO	Curved			1¼	1¼	1¼	⅞	⅝	⅝	½	½	½
124' MCO	Curved								1¼	1	¾	¾
31' MCO		For ≥3 non-overlapping deviations within a distance 5x chord length, each of which exceeds these limits							⅜	⅜	⅜	⅜
62' MCO									½	⅜	⅜	⅜
124' MCO									1	⅞	½	½

Table 5. Profile exception limits defined in United States Code of Federal Regulations (49 CFR §213)

Parameter (all exceptions in inches)	Type of track	Additional qualifiers	Track Class								
			1	2	3	4	5	6	7	8	9
Operating Speed Limit, Freight (mph)			*10*	*25*	*40*	*60*	*80*				
Operating Speed Limit, Passenger (mph)			*15*	*30*	*60*	*80*	*90*	*110*	*125*	*160*	*220*
31' runoff at the end of a raise			3½	3	2	1½	1				
31' MCO								1	1	¾	½
62'MCO			3	2¾	2¼	2	1¼	1	1	1	¾
124' MCO								1¾	1½	1¼	1
Deviation from zero cross level	Tangent		3	2	1¾	1¼	1	1	1	1	1
Reverse elevation	Curved		3	2	1¾	1¼	1	½	½	½	½
Superelev.+cross level	Curved		8	8	7	7	7	7	7	7	7
62' warp		Except in some spirals designed prior to 1998	3	2¼	2	1¾	1½	1½	1½	1¼	1
62' warp		6 consecutive pairs of joints ≥10' apart		1¼	1¼	1¼	1¼	1	1	1	1
62' warp	Curved	Where elevation >6"	1½	1½	1½	1½	1½				
10' warp	Curved							1¼	1⅛	1	¾
31' warp	Spiral	Certain spirals designed prior to 1998	2	1¾	1¼	1	¾				
31' MCO		For operations at a qualified cant deficiency >5"			1	1	1				
62' MCO			2¼	2¼	1¾	1¼	1				
124' MCO								1½	1¼	1¼	1
10' warp	Curved		2	2	1¾	1¾	1½	1¼	1	1	¾
10' warp	Curved	For operations at a qualified cant deficiency >7"						1¼	1	¾	¾
31' MCO		For ≥3 non-overlapping deviations within a distance 5x chord length, each of which exceeds these limits						¾	¾	½	⅜
62' MCO								¾	¾	¾	½
124' MCO								1¼	1	⅞	⅝

Appendix B.
Proposed Descriptions of Deterministic Track Anomalies (Hamid et al., 1983)

Table 6. Proposed formulae and parameter values for track anomalies (adapted from Hamid et al., 1983)

Name	Shape	Formulae	Gage A (inch)	Gage k (ft⁻¹)	Alignment A (inch)	Alignment k (ft⁻¹)	Cross level A (inch)	Cross level k (ft⁻¹)	Profile A (inch)	Profile k (ft⁻¹)
Cusp		$y = Ae^{-k\lvert x\rvert}$ $y = A(1 - \lvert\sin(\pi kx)\rvert)$ $y = A(1 - 2k\lvert x\rvert)$	0.8–1.4	0.016–0.061	0.5–3.0	0.011–0.103	0.9–3.0	0.031–0.095	0.9–3.0	0.016–0.095
Bump		$y = A\,\mathrm{sech}(kx)$ $y = Ae^{-\frac{1}{2}(kx)^2}$ $y = \dfrac{A}{1 + k^2 x^2}$	0.8–1.4	0.031–0.040	0.5–2.8	0.009–0.083	1.0–3.0	0.017–0.031	0.5–4.0	0.013–0.065
Jog		$y = \dfrac{1}{2}A\tanh(2kx)$ $y = \dfrac{A}{\pi}\mathrm{atan}(\pi kx)$ $y = \dfrac{Akx}{\sqrt{1 + 4k^2 x^2}}$	N/A	N/A	0.5–3.3	0.006–0.025	1.6–2.8	0.020–0.050	0.5–5.0	0.008–0.045
Plateau		$y = \sqrt{\dfrac{A^2}{1 + (kx)^8}}$	0.8–1.3	0.029–0.08	1.2–1.6	0.025–0.027	0.6–1.0	0.026–0.04	0.9–3.0	0.009–0.033

93

Name	Shape	Formulae	Range of Values							
			Gage		Alignment		Cross level		Profile	
			A (inch)	k (ft⁻¹)	A (inch)	k (ft⁻¹)	A (inch)	k (ft⁻¹)	A (inch)	k (ft⁻¹)
Trough		$y = Ak\sqrt{\left(\frac{1}{k}\right)^2 - x^2}$	N/A	N/A	1.4–2.2	0.013–0.029	N/A	N/A	0.7–2.0	0.020–0.025
Sinusoid		$y = A\sin(\pi k x)$	N/A	N/A	0.8–1.2	0.033–0.020	N/A	N/A	1.0–1.5	0.020–0.025
Damped Sinusoid		$y = Ae^{-kx}\cos(\pi k x)$	0.5–1.0	N/A	1.0–2.2	0.013–0.015	0.9–1.2	0.051–0.061	N/A	N/A
sin(x)/x		$y = \dfrac{A\sin(kx)}{\pi k x}$	N/A	N/A	N/A	N/A	N/A	N/A	1.0–1.2	0.031–0.033

Abbreviations and Acronyms

ACRONYM	DEFINITION
AAR	Association of American Railroads
ATGMS	Autonomous Track Geometry Measurement System
ATIP	Automated Track Inspection Program
CFR	Code of Federal Regulations
CoSD	Combined Standard Deviation
CPSD	Cross Power Spectral Density
CTR	Composite Track Record
DFT	Digital Fourier Transform
EN	Euronorm
ERRI	European Rail Research Institute
ETF	Empirical Transfer Function
FFT	Fast Fourier Transform
FIR	Finite Impulse Response
FRA	Federal Railroad Administration
GEI	Generalized Energy Index
GNSS	Global Navigation Satellite System
GPS	Global Positioning System
GQI	Gauge Quality Index
IIR	Infinite impulse Response
IMS	Inertial Measurement System
ISO	International Organization for Standardization
LIDAR	Light Detection and Ranging
L/V	Lateral-to-Vertical
LVDT	Linear Variable Differential Transformer
MBD	Multi-Body Dynamics
MCO	Mid-Chord Offset
MSRP	Manual of Standards and recommended Practices
NN	Neural Network
OTGI	Overall Track Geometry Index

ACRONYM	DEFINITION
PCA	Principal Component Analysis
PMA	Point-Mass Acceleration
P-P	Probability-Probability
PSD	Power Spectral Density
QCDF	Quasi Cumulative Distribution Function
Q-Q	Quantile-Quantile
RFID	Radio-Frequency Identification
SD	Standard Deviation
SQI	Surface Quality Index
TF	Transfer Function
TGI	Track Geometry Index
TGIM	Track Geometry Interaction Map
TGIMP	Track Geometry Interaction Map Parameter
TGMS	Track Geometry Measurement System
TQC	Track Quality Class
TQI	Track Quality Index
TSI	Technical Specifications for Interoperability
TTCI	Transportation Technology Center, Inc.
UIC	International Union of Railways (Union Internationale des Chemins de fer)
UPRR	Union Pacific Railroad
VRA	Vehicle Response Analysis
VRMS	Vehicle Response Measurement System
VTI	Vehicle-Track Interaction